NASA CR-66792

LOW-TEMPERATURE HEAT PIPE RESEARCH PROGRAM

by

E. C. Phillips

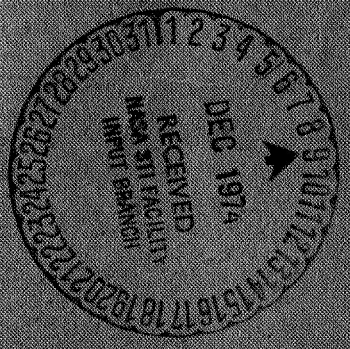

Prepared Under Contract No. NAS 1-8000

by

Donald W. Douglas Laboratories
McDonnell Douglas Astronautics Company — Western Division

for

NATIONAL AERONAUTICS AND SPACE ADMINISTRATION

DAC-63366

NASA CR-66792

LOW-TEMPERATURE HEAT PIPE RESEARCH PROGRAM

by

E. C. Phillips

Prepared under Contract No. NAS1-8000 by

Donald W. Douglas Laboratories

McDonnell Douglas Astronautics Company — Western Division

for

NATIONAL AERONAUTICS AND SPACE ADMINISTRATION

CONTENTS

FIGURES

TABLES

LOW TEMPERATURE HEAT PIPE RESEARCH PROGRAM

By E. C. Phillips*

SUMMARY

The need for low-temperature heat pipes--those which operate in the temperature range of -100° to +200°F--for thermal management of spacecraft has led to development of processing and fabricating techniques. However, generation of basic data for use in design and analysis has lagged. Of most importance are wick fluid flow and evaporator performance data.

Wick permeabilities and capillary pressures are dependent on the geometry and material of the wick structure as well as the surface tension, density, and viscosity of the wicks' working fluids. Permeabilities for thin wicks are also dependent on the menisci radii of the liquid/vapor interface. They were measured for wicks ranging in thickness from 0.005 to 0.100 in. and structures ranging from square mesh screen to metal foams and felts. Permeabilities were also measured as a function of the menisci radii in the liquid/vapor interface. Two measurement techniques were used: forced flow and gravity flow; results are presented in graphic form as a function of flow per unit area. Measured permeability data were found to deviate slightly from Darcy's law.

Evaporator performance was determined by measuring maximum evaporator heat fluxes for metal screen, felt, and foam wick structures with water, methanol, and butanol. Heat fluxes were measured in the vapor and at the vapor pressure of the working fluid. Maximum heat fluxes at operating temperatures of approximately 100° and 150°F in the vapor of the working fluid were found to be lower than those measured in air at atmospheric pressure.

This report outlines heat pipe design procedures, making use of the wick permeability and evaporator heat flux data. Figures of merit for various potential low-temperature heat pipe working fluids are presented.

---

*Program Manager, Energy Transport Applications
Donald W. Douglas Laboratories, Richland, Washington

INTRODUCTION

In 1964, the heat pipe was identified by Grover et al. (ref. 1) as a simple, efficient, heat-transfer device particularly suitable for applications in low-gravity space environments. Since that time, both Government and privately sponsored groups have spent considerable effort on the development of heat pipes. Initially, effort centered around high-temperature devices compatible with temperatures typically encountered in nuclear heat sources of various types. However, in the intervening period, the capability of heat pipes to solve difficult heat transfer and thermal management problems in all temperature ranges became evident. In particular, designers began to consider heat pipes for thermal management of spacecraft and associated experiments. Thus, interest in the lower temperature range between approximately -100° and +200°F increased rapidly.

Development of processing techniques, and fabrication of low-temperature heat pipes and heat pipe networks, has progressed considerably in recent years. But the understanding of heat pipe operation, and generation of basic data for use in analysis and design of low-temperature heat pipe systems, has not kept pace. It is this problem to which the work described in this report addresses itself; namely, to provide the necessary information to design and predict performance of low-temperature heat pipe systems. Specifically, wick fluid flow data (e. g. wick permeabilities and capillary pressures) and evaporator performance data (e. g. evaporator heat fluxes) were measured experimentally, and design procedures were developed.

Basic Heat Pipe Theory

Figure 1 is a heat pipe schematic. In the evaporator region, heat is absorbed and a phase-change from liquid to vapor takes place. Due to the rise in temperature, pressure increases; this causes vapor to flow to the condensor region of the pipe where the process is reversed and heat is rejected. Very small temperature drops are coupled with the transfer of large quantities of heat in the phase change from liquid to vapor to liquid. This property provides the capacity for transporting large quantities of thermal energy in a near-isothermal system. Following condensation, the cycle is completed with the return of the liquid to the evaporator region. In practice, a heat pipe designed for a specific application may bear little resemblance to the one shown in figure 1; however, all heat pipes operate on the same principle and have in common, (1) a container envelope, (2) a working fluid, and (3) a liquid-return mechanism. In general, the liquid-return mechanism is a wicking structure which relies on capillary action to provide the liquid pumping pressure. In some applications, a preferential gravity gradient can be used to return the liquid to the evaporator and no wicking structure may be required.

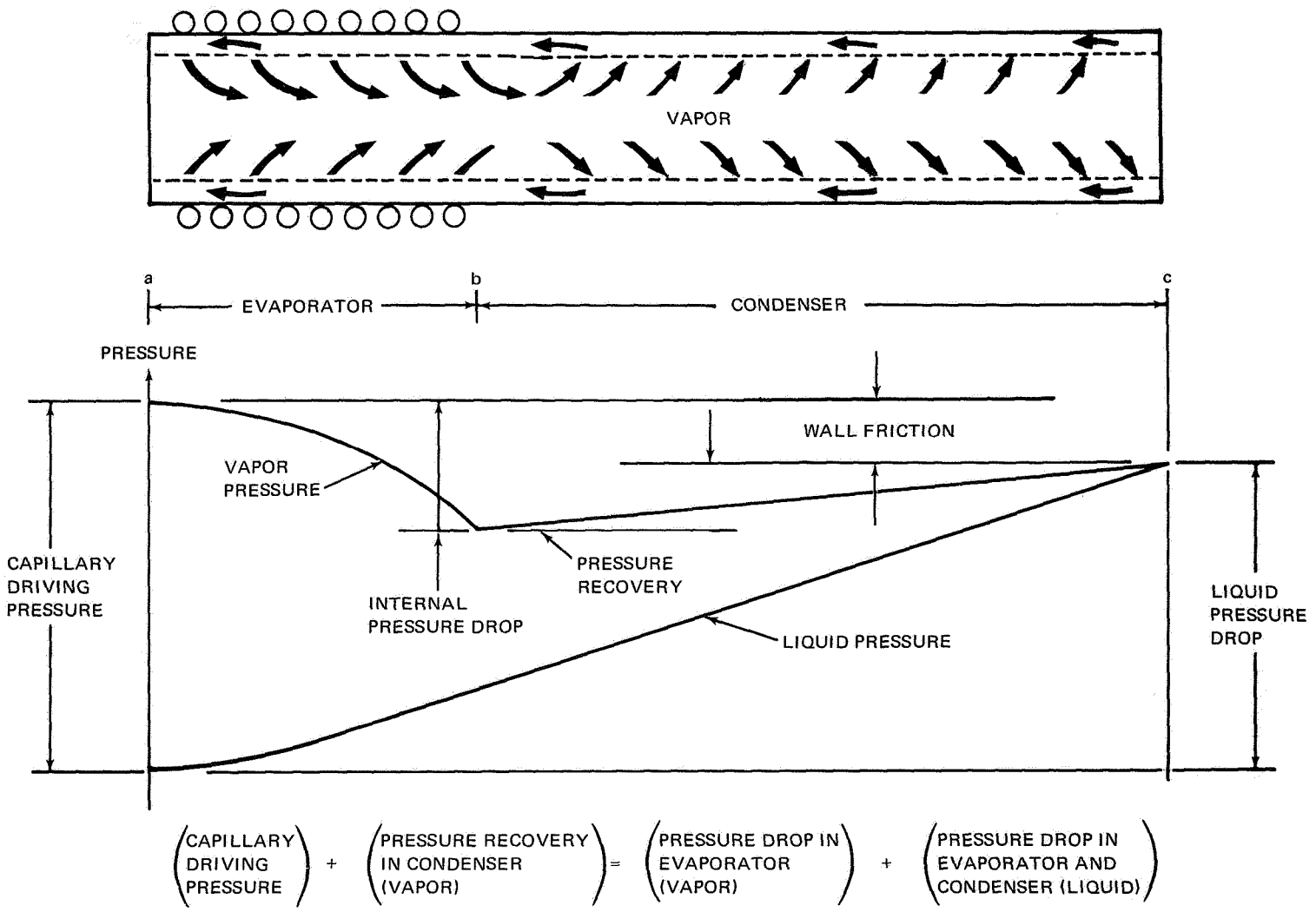

Figure 1. Heat Pipe Cross-Section

The basis for heat pipe design has primarily been a theory developed by Cotter (ref. 2) in 1965. This theory permits the calculation of the maximum heat transfer capability of a heat pipe by equating the sum of the pressure drops in the liquid phase (ΔP_L) and the vapor phase (ΔP_V) to the difference between maximum capillary pumping pressure (ΔP_C) and the pressure due to differences in elevation in a gravity field (ΔP_g):

$$\Delta P_L + \Delta P_V = \Delta P_C - \Delta P_g \tag{1}$$

The maximum possible value of the sum of $\Delta P_L + \Delta P_V$ occurs when ΔP_C is the maximum pumping pressure that the wick or, in general, the liquid-return mechanism can provide (sometimes called the blowthrough pressure). For this case, equation (1) represents a limit imposed by the pumping capability of the liquid-return mechanism on the maximum axial heat flux. The maximum heat transfer capability of the heat pipe can also be restricted by sonic choking of the vapor flow near the end of the evaporator (refs. 3 and 4) or by excessive entrainment of the liquid by high speed vapor flow, (refs. 5 and 6). In addition, there is a limit on the maximum evaporator heat flux that can be sustained without drying out the wick.

In high-temperature systems, vapor velocities can be high; ΔP_V and limits (such as sonic and entrainment) associated with the vapor flow must be carefully evaluated. However, in almost all low-temperature applications, vapor velocities are very low--on the order of 1 to 10 ft/sec--and essentially, they can be neglected. Design of low-temperature heat pipe systems, therefore, requires information relating to ΔP_L, ΔP_C, and maximum allowable evaporator heat fluxes. The maximum evaporator heat flux is an especially important limitation in low-temperature heat pipes. The radial evaporator heat flux for incipient nucleate boiling is much higher for liquid metals than for low temperature organic fluids due to the higher thermal conductivity of liquid metals. Thus, the evaporator heat flux is a much less important limitation in high-temperature heat pipes than in low-temperature systems. The expression for the pressure drop in the liquid is a function of the liquid-return mechanism.

One of two basic return-mechanism configurations is usually used in low-temperature heat pipes; isotropic wick configuration, or bypass flow configurations. In addition, composites and variations governed by available materials or the ingenuity of the designer can result in an almost infinite variety of flow mechanisms. The liquid pressure drop in an isotropic wick heat pipe, as a function of heat flow is given by Darcy's law (see, for example, ref. 2):

$$\Delta P_L = \frac{1}{K_p} \frac{\nu_L}{A_w g_c} \frac{Q}{h_{fg}} \left[\frac{\ell_e}{2} + \ell_a + \frac{\ell_c}{2} \right] \tag{2}$$

where

ΔP_L = liquid pressure drop ($lb_f - ft^{-2}$)
K_p = permeability constant (ft^2)
ν_L = kinematic viscosity of the liquid ($ft^2 - hr^{-1}$)
A_w = wick cross-section area (ft^2)

g_c = universal gravitation constant = 4.17 x 108 ft - lb_m - $lb_f^{-1} hr^{-2}$
Q = heat flow ($Btu\text{-}hr^{-1}$)
h_{fg} = latent heat of vaporization of working fluid ($Btu\text{-}lb_m^{-1}$)
ℓ_e = evaporator length (ft)
ℓ_a = adiabatic section length (ft)
ℓ_c = condenser length (ft)

Implicit in equation (2) is the assumption of uniform heat input in the evaporator region and uniform rejection in the condenser region. Similarly, ΔP_L for bypass wick heat pipes can be expressed as

$$\Delta P_L = \frac{8\pi \nu_L}{A_a^2 g_c} \frac{Q}{h_{fg}} \left[\frac{\ell_e}{2} + \ell_a + \frac{\ell_c}{2}\right] + \frac{\pi}{16} \frac{\nu_L}{K_p g_c} \frac{\left(r_v + r_w\right)^2}{r_v(r_w - r_v)} \frac{Q}{h_{fg}} \left(\frac{\ell_c + \ell_e}{\ell_c \quad \ell_e}\right) \tag{3}$$

where

A_a = cross-sectional area of the bypass flow tube
r_w = (inside diameter of pipe)/2
r_v = vapor channel radius

The first term in equation (3) is the pressure drop in a bypass (arterial) flow tube, while the second term is the pressure drop associated with the flow of liquid from and to the artery in the circumferential direction. Uniform heat input and rejection has been assumed here as in equation (2).

In equations (2) and (3), the only unknown is the permeability constant, K_p. All other parameters are either measurable physical dimensions or fluid properties which can generally be found in existing handbooks. Determining ΔP_L, therefore, depends on experimentally determining K_p, using laboratory test techniques described later in this report.

In theory, ΔP_C is given by

$$\Delta P_C = \frac{2 \sigma \cos \theta}{r_c} \tag{4}$$

where σ is surface tension θ is the contact angle of the working fluid with the wick material, and $1/r_c$ is the maximum possible curvature of the menisci in the surface openings. If there is complete wetting, θ has a value of 0 and the maximum pumping capability of the wick structure is $2\sigma/r_c$. It is not possible to predict ΔP_C for a given wick, however, because wick surfaces do not exhibit clearly defined uniform circular openings with measurable radii. In addition, wettability is a function of the working fluid and wick material, and values of $\theta = 0$ can not always be obtained. ΔP_C can, however, be determined experimentally by using wick capillary pressure tests described in this report.

The value of ΔP_g may be determined by the following expression:

$$\Delta P_g = \rho (g/g_c) \ell \cos \beta \qquad (5)$$

where ℓ is the length of a heat pipe and β is the inclination of a heat pipe with respect to a gravity vector. Equation (1) may not be applicable, however, if nucleate boiling is occurring in the wick.

The evolution of vapor can change the permeability of a particular wicking configuration by blocking the liquid-flow passages with vapor. A wick configuration that uses an artery as a liquid-return path is particularly susceptible to blockage by vapor evolution. For a given wick configuration, there is a maximum evaporator heat flux that can be applied without drying the wick. This maximum heat flux is, however, a complicated function of working fluid, wick and tubing materials, and wick configuration; thus, it does not lend itself to analytical prediction. Data obtained using equipment which is not limited by the pumping capability of the liquid delivery system will be helpful in assessing the effect of evaporative heat flux on low-temperature heat pipes.

Review of Applicable Literature

A number of investigators have obtained and reported data on wick permeability, capillary pumping pressure, and maximum evaporator heat flux. Costello and Redecker (ref. 7) and Costello and Frea (ref. 8) have investigated the burnout heat flux limit for wick-covered surfaces. However, the configuration and geometry of test apparatus was such that the question of evaporator burnout in a heat pipe liquid supply situation cannot be conclusively answered. A qualitative investigation of boiling burnout in a water-filled glass heat pipe was conducted by Bähr et al. (ref. 6). The progressive stages of wick dryout (as radial heat flux increased) were observed, but no quantitative data were reported. Reiss and Schretzmann (ref. 9) have observed that they were able to operate sodium heat pipes at higher radial heat fluxes than did other experimenters using sodium boiling on a non-wick-lined surface. Thus, presence of the wick, or some other facet of heat pipe operation, appears to enhance the capability of sodium to withstand a boiling burnout.

An extensive program undertaken by Kunz et al (ref. 10) has investigated capillary wicking height, permeability, and dryout radial heat fluxes for a number of different wicks. However, wick configurations tested represent porosities predominantly in the 70% to 85% range with very small and random pore sizes. There is an interest in wicks of higher porosity and larger pore size, because the optimum value of pore size and porosity for many low-temperature working fluids is larger than those for wicks previously tested. In addition, there is a need for performance data on thinner wicks that would facilitate near-isothermal operation.

In the literature, evaporative heat flux tests performed by Kunz et al. (ref. 10) were the only ones described that are designed to measure the effect

of radial heat flux on heat pipes. But there are several aspects of the testing procedure that limit the general applicability of the data.

In the first place, their tests were performed with the test chamber open to the atmosphere. This is not the condition that exists in a heat pipe; it will usually cause the radial heat flux at burnout to be higher than that which could be achieved in a heat pipe. Because the test chamber was open to the atmsophere, their tests were conducted with the liquid in a subcooled state. For some tests, as much as 20 000 Btu/hr-ft^2 out of a maximum heat flux of 70 000 Btu/hr-ft^2 was required to bring the water temperature to the boiling point. It has been observed (refs. 11 and 12) that increasing the amount of subcooling decreases the bubble size at departure. This should have an appreciable effect on the burnout heat flux because smaller bubbles would be less likely to block a wick. In addition, operation with the test chamber open to the atmosphere limits the test to only one value of saturation temperature; namely, the boiling point. The size of bubbles at departure is a very sensitive function of saturation temperature (ref. 12). The effect of temperature is discussed in the Evaporator Heat Flux Tests section of this report.

The second condition of their tests which is different from that which could exist in a heat pipe is the method of liquid supply. They tested wicks which were immersed in a liquid so that liquid could be supplied around the entire perimeter of the wick, and vapor could vent through the sides.

Permeability of screen wicks has been investigated by Schmidt (ref. 13) and he has derived a formula for the calculation of pressure drop in such wicks. Katzoff (ref. 14) has measured the wicking height for several screen wicks.

With the data contained in references previously cited, the designer is able to design certain heat pipes, but the choice of wicks and wick configurations is limited. The purpose of the present work is to extend the knowledge of heat pipe design parameters to allow a larger selection. This involves determining capillary wicking pressures, permeabilities, and evaporator heat fluxes for incipient burnout for a number of wicks and wick configurations.

Capillary wicking pressures were obtained for screens and porous metals (foam and felt) by determining the height of liquid which a particular wick could sustain. Values of capillary pressure with the liquid exposed to air and to its own vapor were determined by two test techniques. Initial testing indicated that these techniques yielded similar results, so the simpler method with the chamber open to air was used for subsequent tests.

Permeabilities of various wicks were measured by three techniques; (1) forced flow, (2) gravity flow, and (3) measurement of permeability in operating heat pipes. These tests involve measuring the flow and pressure drop through a porous medium. The wicks were of a higher porosity than any which had been previously tested. The forced flow permeability technique proved to be much easier to apply than either of the other techniques.

The maximum evaporator heat flux that various wicks supplied by an artery can sustain was measured both under the vapor pressure of the liquid and open to the atmosphere. A narrow wick with an arterial supply was used to minimize the variation of suction in the test wick. Heat pipes with an artery type of liquid return are particularly susceptible to vapor blockage, because a single bubble in the artery can grow and block the artery, and the radial heat flux at which such blockage occurs is a very important parameter. As expected, wick boiling characteristics were found to be a very sensitive function of the amount of subcooling and the operating temperature. Thus, it is essential that maximum evaporative heat flux data be obtained with the test apparatus operating only under its own vapor pressure.

The following sections of this report describe the wicks and fluids used in the program and provide a detailed description of each of the tests. A section is included on the use of the data for heat pipe design. Tables summarizing useful capillary pressure, permeability, and maximum evaporator heat flux data are included.

SYMBOLS

A = area (ft^2)

A_a = cross-sectional area of bypass flow tube (ft^2)

A_w = wick area (ft^2)

d_r = recession depth (ft)

D_c = $2r_c$ = capillary diameter (ft)

D_H = hydraulic diameter (ft)

D_p = 1.5 times screen diameter (ft)

$(FOM)_0$ = zero-g figure-of-merit ($Btu\text{-}lb_f\text{-}ft^{-2}\text{-}centipoise^{-1}$)

$(FOM)_1$ = 1-g figure-of-merit ($lb_f\text{-}ft^2\text{-}lb_m^{-1}$)

g = acceleration due to gravity ($ft\text{-}hr^{-2}$)

g_c = universal gravitation constant (4.17×10^8 $ft\text{-}lb_m\text{-}lb_f^{-1}\text{-}hr^{-2}$)

h = height of liquid column (ft)

h_{fg} = latent heat of vaporization of working fluid ($Btu\text{-}lb_m^{-1}$)

Δh = elevation of pressure measurement point in wick above transducer diaphragm (ft)

K_p = permeability constant (ft^2)

ℓ = length (ft)

ℓ_a = adiabatic section length (ft)

ℓ_c = condenser length (ft)

ℓ_e = evaporator length (ft)

$\dot{m} = \frac{Q}{h_{fg}}$ = mass flow (ft)

p = pressure ($lb_f\text{-}ft^{-2}$)

P = wetted perimeter (ft)

P_a = atmospheric pressure (lb_f-ft^{-2})

ΔP_C = capillary pumping pressure (lb_f-ft^{-2})

ΔP_g = pressure due to differences in elevation in gravity field (lb_f-ft^{-2})

ΔP_G = pressure in excess of atmospheric pressure (lb_f-ft^{-2})

ΔP_L = pressure drop in liquid phase (lb_f-ft^{-2})

ΔP_{LC} = pressure drop in the liquid phase in the condenser region (lb_f-ft^{-2})

P_t = absolute pressure at transducer (lb_f-ft^{-2})

ΔP_V = pressure drop vapor phase (lb_f-ft^{-2})

Q = heat flow (Btu-hr^{-1})

r_c = capillary radius (ft)

r_m = meniscus radius (ft)

r_v = vapor channel radius (ft)

r_w = (inside diameter of pipe)/2 (ft)

$r(x)$ = radius of curvature at any point x (ft)

R = resistance coefficient for one- or two-layer screen wicks and V-groove wicks (ft^{-3})

R_e = Reynolds number, dimensionless

t_w = thickness of the wick (ft)

T = temperature (°R)

$\Delta T_{sat} = T_{wall} - T_{saturation}$ (°R)

V_o = average flow velocity (ft-sec^{-1})

x = distance in the plane and perpendicular to the flow direction (ft)

y = distance vertical to flow direction (ft)

z = distance in the liquid flow direction (ft)

Z = dy/dx

α = slope angle of gravity flow test apparatus

β = inclination of heat pipe with respect to gravity vector

γ = $1/2 \frac{g}{g_c} \frac{\rho}{\sigma}$ (ft^{-2})

ε = porosity

θ = contact angle

μ = viscosity

ν_L = kinematic viscosity of liquid (ft^2/hr)

ρ_L = density of liquid (lb_m/ft^3)

σ = surface tension $(lb_f\text{-}ft^{-1})$

DESCRIPTION OF TEST WICKS AND FLUIDS

Wicks

Many available materials may be used for capillary wicks. However, there are two prime properties of interest in wicks: a high pumping rate, and a low temperature drop normal to the plane of the wick. The first property dictates that the wick must have a high ratio of flow to pressure difference, and a large flow area. This means that the wick must have high porosity and a relatively thick cross-section. The second property may best be supplied by a thin wick of high thermal conductivity. Also of interest is the ability of a surface to pump liquid by its configuration rather than by a wick bonded to it.

Wick types. - Three basic types of wicks were selected. The first was a low-resistance wick (i. e. a wick with a high ratio of flow to pressure difference) to provide evaporative heat flux and permeability data. The second was a very thin wick (e. g. a single layer of 200 mesh screen). The third was a configuration pumping wick.

Five types of wick construction were used: multilayer screens, foams, and felts for low-resistance wicks; single-layer screens for thin wicks; and V-grooved material for configuration pumping wicks. In addition, composite wicks were fabricated to combine the desirable features of the different types into a single wick (e. g. foam nickel wick covered by screen).

For thin wicks, screens were selected that are readily available in a variety of pore sizes, open ratios (the ratio of open volume to total volume calculated from the product of thickness, length, and width), thicknesses, weaves, and materials. A stainless steel square mesh weave was chosen on the basis of favorable procurement time and because, although stainless steel does not provide the high thermal conductivity of copper, it is a necessary compromise between maximum conductivity and wick fabrication requirements.

Foams are available in porosities as high as 97%, with pore diameters up to 0. 020 in. and consequent low inverse permeabilities. Foams with large pore sizes and high porosities were selected because they represent nearly optimum-flow wicks. However, high porosity (low density) results in low thermal conductivity.

Metal felts are also available in porosities up to approximately 90%. Felts were selected because of high porosity and low inverse permeability, and because they represent an alternate to foams as a method of fabricating high-porosity wicks. Again, because of low density, thermal conductivity is low.

V-grooves were selected as an example of a surface with configuration pumping. They may be fabricated as an integral part of the wall of a heat pipe or vapor chamber. Composite wicks consisting of two layers of screen of different mesh size, foam covered by screen, and V-grooves covered by screen were selected to combine the desirable properties of two types of wicks.

Test wicks. - The wicks and their dimensional properties are outlined in table 1. Some of the wick properties such as thickness and porosity are listed as nominal values because they may be altered slightly during bonding of the wicks to test specimen holders. These properties of individual wicks are described in table 2.

Dimensional properties were selected to provide permeability and evaporative heat flux data on wicks for which such information has not previously been reported. Screens of 100 and 200 mesh sizes were selected on the basis of 0.010- and 0.005-in. thicknesses respectively. The 0.010- and 0.020-in. pore diameters selected for metal foams and felts are larger than those which have been reported, but they are feasible for use in heat pipes--particularly with water as a working fluid (ref. 15). The 0.100- and 0.050-in. thicknesses for foams and felts were based on making the wicks a minimum of 2 pore-diameters thick. Selection of 0.010-in. deep V-grooves was determined by the minimum size which could be manufactured accurately. Components of the composites were chosen from the above selection of wick materials.

Wick materials. - The choice of materials from which the wicks were constructed (stainless steel, nickel, and copper) was based on three criteria: fabricability, wettability, and thermal conductivity. All three materials are readily sintered into felts and foams and are sufficiently strong that they may be woven into screen. All three materials, with proper treatment, are wettable with the three test fluids chosen--water, methanol, and butanol. The thermal conductivity of copper is, of course, high. However, the values for nickel and stainless steel are quite low.

Wick properties. - The following properties are considered in selecting wicks for testing:

Compatibility: The wick materials (nickel, copper, and stainless steel) had good compatibility with the fluids (water, methanol, benzene, and butanol).

Thermal conductivity: Effective thermal conductivity of a saturated wick is an important parameter in selecting wicks for heat pipe design because the largest temperature drop in a heat pipe is associated with the heat conduction across a wick. Thermal conductivity data are scant for metal felts and foams but published data by Ipsen Industries (ref. 16) indicate that the thermal conductivities of metal foams are greater than for felts (ref. 17) of the same densities. Maximum and minimum values of effective thermal conductivity may be calculated by assuming parallel and series heat-flow paths, respectively. Equations for such calculations are given by Kunz (ref. 10).

TABLE 1

DESCRIPTION OF TEST WICKS

Type of wick	Designation	Material	Structure	Nominal thickness (in.)	Nominal porosity (%)	Nominal pore diameter (in.)	Measured pore diameter (in.)**	Supplier
Screen	50 x 50 mesh	304 SS	Square weave 0.009-in. wire diameter	0.025		0.011 pore width		All screens were supplied by Michigan Wire Cloth Company Inc.
Screen single layer	100 x 100 mesh	304 SS	Square weave 0.0045-in. wire diameter	0.0095	69*	0.0055 pore width		
Screen double layer	100 x 100 mesh	304 SS	Square weave 0.0045-in. wire diameter	0.016	64*	0.0055 pore width		
Screen single layer	200 x 200 mesh	304 SS	Square weave 0.0021-in. wire diameter	0.0049	73*	0.0029 pore width		
Screen double layer	200 x 200 mesh	304 SS	Square weave 0.0021-in. wire diameter	0.0094	72*	0.0029 pore width		
Foam	AmPorNik 210-5	Nickel	Open-celled foam	0.050 and 0.100	95	0.010	0.018 to 0.059	All foams were supplied by Astro Met Assoc. Inc.
Foam	AmPorNik 220-5	Nickel	Open-celled foam	0.050 and 0.100	95	0.020	0.010 to 0.025	
Foam	AmPorCop 210-5	Copper	Open-celled foam	0.050 and 0.100	95	0.010	0.008 to 0.039	
Foam	AmPorCop 220-5	Copper	Open-celled foam	0.050 and 0.100	95	0.020	0.012 to 0.040	
Felt		Nickel	Felted fiber	0.050 and 0.100	85	0.010	0.006 to 0.027	All felts were supplied by Astro Met Associates Inc.
Felt		Copper	Felted fiber	0.050 and 0.100	85	0.010	0.008 to 0.032	
V groove	60° V groove	304 SS	60° V-groove by 0.010 in. depth	0.010				Western Sintering Co., Inc.
Composite	single layer 50 mesh screen covered by one layer 200 mesh screen	304 SS	Square weave	0.025	73*	0.0029 pore width		
Composite	AmPorNik 220-5 covered by one layer 200 mesh screen	Nickel and 304 SS	Open-celled foam and square weave	0.042		0.0029 pore width		
Composite	60° V-groove covered by one layer 200 mesh screen	304 SS	V-groove and square weave	0.0149		0.0029 pore width		

* Open ratio (open volume to total volume).

** Pore dimensions were measured optically with a microscope and glass stage micrometer.

TABLE 2

DIMENSIONS OF TEST WICKS

(1) Capillary tests				
Wick	Effective pore diam (in.)	Test specimen dimensions Diam (in.)	Thickness (in.)	Porosity (%)
200 mesh screen	0.0043	3/4	0.035	73*
AmPorCop 210-5	0.018	3/4	0.108	95
AmPorCop 220-5	0.019	3/4	0.102	91
Copper felt	0.018	3/4	0.100	90
AmPorNik 210-5	0.018	3/4	0.102	94
AmPorNik 220-5	0.018	3/4	0.100	96
Nickel felt	0.013	3/4	0.101	89

(2) Forced-flow permeability					
Wick	Effective pore diam (in.)	Test specimen dimensions Thickness (in.)	Width (in.)	Length (in.)	Porosity (%)
AmPorCop 210-5	0.018	0.108	1.00	2.50	95
AmPorCop 220-5	0.019	0.102	1.00	2.50	91
Copper felt	0.018	0.100	1.00	2.50	90
AmPorNik 210-5	0.018	0.102	1.00	2.51	94
AmPorNik 220-5	0.018	0.100	1.00	2.50	96
Nickel felt	0.013	0.101	1.00	2.51	89

TABLE 2. - Continued

DIMENSIONS OF TEST WICKS

(3) Gravity flow test specimens					
Wick	Effective pore diam (in.)	Test specimen dimensions Thickness (in.)	Width (in.)	Length (in.)	Porosity (%)
100 mesh screen, single layer	----	0.0095	1.09	11.8	69*
100 mesh screen, double layer	----	0.016	1.11	11.8	64*
200 mesh screen, single layer	----	0.0049	1.01	11.8	73*
200 mesh screen double layer	----	0.025	1.01	11.8	73*
AmPorCop 210-5	0.018	0.048	0.99	11.7	92
AmPorCop 220-5	0.019	0.048	1.01	11.7	91
Copper felt	0.018	0.056	1.00	11.9	83
AmPorNik 210-5	0.018	0.058	1.00	11.9	94
AmPorNik 220-5	0.018	0.057	1.00	11.7	94
Nickel felt	0.013	0.062	0.99	11.7	84
200 mesh screen over AmPorNik 220-5	----	0.042	1.00	11.8	--
60° V groove	----	0.010 depth	1	6	--
200 mesh screen over 60° V groove	----	0.0149 depth	1	6	--

*Open ratio

TABLE 2. - Concluded

DIMENSIONS OF TEST WICKS

(4) Condenser flow test specimens

Wick	Effective pore diam (in.)	Test specimen dimensions Thickness (in.)	Width (in.)	Length (in.)	Porosity (%)
One layer 200 mesh screen	----	0.0049	1.0	30	73*
200 mesh screen over AmPorNik 220-5	----	0.042	1.0	30	--
AmPorNik 220-5	0.018	0.083	1.0	30	--

*Open ratio

(5) Evaporator heat flux tests

Wick	Effective pore diam (in.)	Test specimen dimensions Thickness (in.)	Width (in.)	Length (in.)	Porosity (%)
One layer 200 mesh screen	----	0.0049	1.0	4.0	73*
200 mesh screen over AmPorNik 220-5	----	0.061	1.0	4.0	93
AmPorNik 220-5	0.018	0.098	1.0	4.0	95
Nickel felt	----	0.049	1.0	4.0	--

Fabricability: The usefulness of any wick material for heat pipes or vapor chambers is determined by its ability to be fabricated in the required sizes and shapes. A second aspect of fabricability is the ability to secure a wick material in place by bonding or mechanical means.

In the same manner that wick material must be easily fabricable, it must also maintain dimensional stability if it is to retain its properties. Sintering was used as a fabrication technique with most of the wicks described in table 2 in bonding to test wick holders or in original manufacture. Some dimensional changes did occur during sintering with all wick materials, as may be seen in appendix B. The changes were slight decreases in overall dimensions. However, the changes were not sufficient to cause detectable changes in pore size. Reductions in length and width occurred in all cases, but in the case of single-layer screens, no change in thickness could be measured with a micrometer caliper. Tearing of the screens at points where they were spot-welded to wick holders indicates that shrinkage occurred during the sintering process before formation of the sintered bond between wick and holder. The reduction in dimensions also incurred a corresponding reduction in porosity.

Isotropy: Isotropy (i. e. having the same properties in all directions) is a desirable feature in heat pipe wicks. The most nearly isotropic wick tested was foam. The foam structure is virtually uniform in all directions. Felts are less isotropic in that the fibers tend to be oriented parallel to the plane of the wick. The fibers look like metal turnings and their surfaces are very rough. The size of the fibers' cross-section and the concentration of fibers throughout the felt vary greatly. As may be seen in figure 2, some locations in the felt are nearly devoid of fibers, giving the appearance of sizeable holes. In screens, the general orientation of the wires also is parallel to the plane of the wick. The most extreme deviation from isotropy is exhibited by the V-groove wick which is completely directional (fig. 3).

Fluids

Fluid selection criteria. - Fluid selection for the test program was based on the following criteria: (1) properties desirable for heat pipe use, (2) availability, and (3) ease of handling at room temperature. The first criterion dictates that test fluids must perform reasonably well as heat pipe fluids. Performance may be measured by the figures-of-merit (FOM) for zero- and 1-g operation defined in the section of this report entitled Design of Low-Temperature Heat Pipes. These FOM's are based on a theory which neglects the effect of nucleate boiling. For this reason, several fluids with good zero-g and 1-g FOM's were used in the evaporator tests. The second criterion reduces cost and procurement time; and the third eliminates the necessity for expensive, complicated, and possibly hazardous test equipment.

Fluids selected. - Based on the above criteria, four fluids were selected: water, methanol, benzene, and butanol.

68-1308

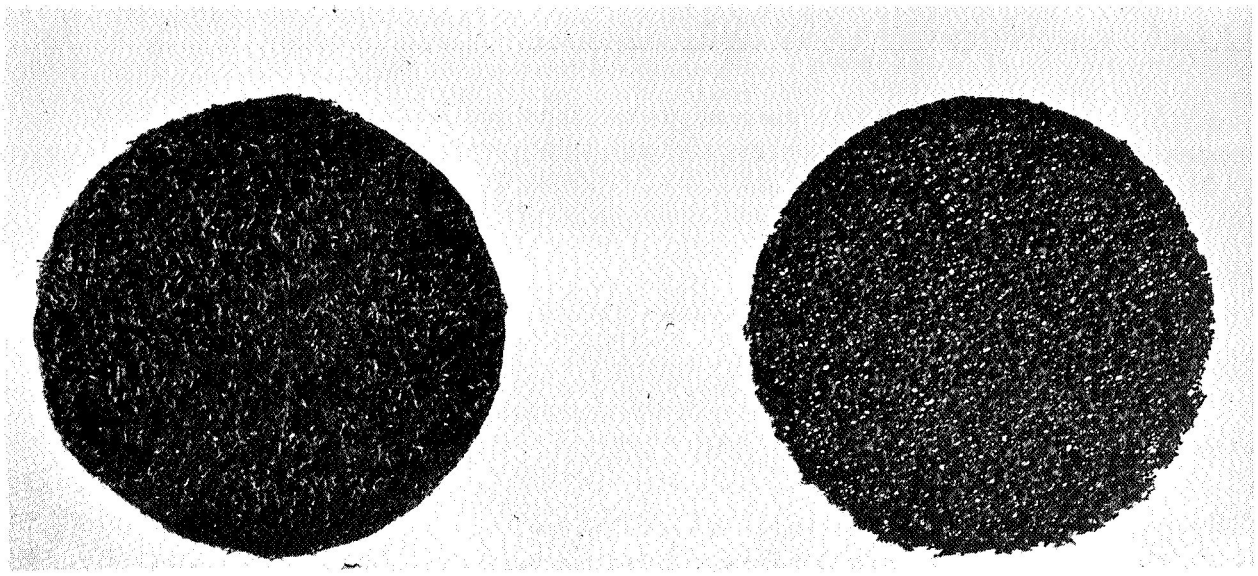

4X
COPPER FELT

4X
COPPER FOAM
(AMPORCOP-220-5)

Figure 2. Capillary Pressure Test Specimens Showing Wick Structure

68-934

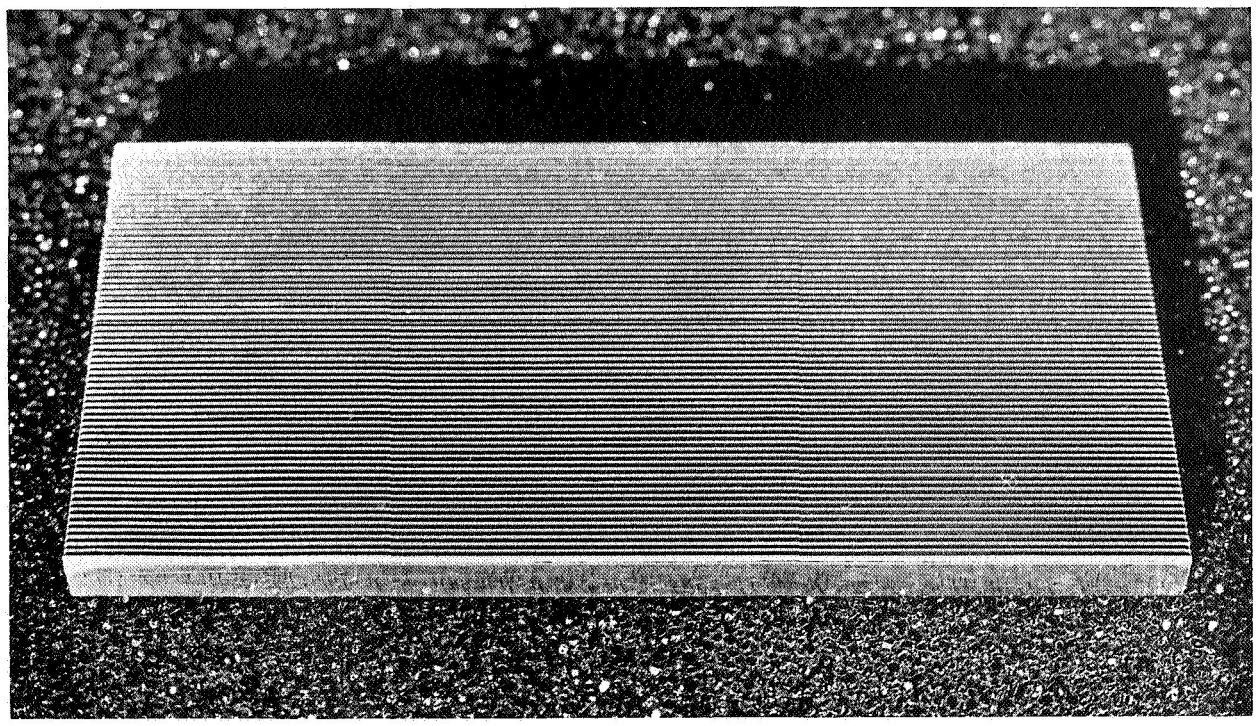

Figure 3. 60^{0} V–Groove Gravity Flow Test Specimen

In the temperature range from 50° to 200°F, at 1 g, fluids with the highest figure-of-merit are in descending order: water, ammonia, benzene, methylamine, acetone, and methanol. In the same temperature range for zero-g operation, the fluids rank: water, ammonia, methyl alcohol, and benzene. Ammonia was eliminated because of its high vapor pressure, and the final selections were water, methanol, and benzene because of their high FOM's. In addition to water and methanol, butanol was chosen for the evaporator tests to investigate the effect of fluid properties on nucleate boiling burnout. Since butanol is a member of the same homologous series as methanol, the burnout performance as compared with methanol should yield data which can be used to extrapolate to other members of the series, since fluid properties vary in a fairly systematic way for members of a homologous series.

Fluid treatment. - Removal of dissolved gases from the test fluids was necessary for all testing except gravity flow and capillary pressure tests in air. Deaerated distilled water was boiled before permeability tests and vacuum-distilled in a heat pipe before evaporator heat flux tests. Treatment of methanol varied with the grade of liquid. Spectrophotometric-grade methanol was distilled in a heat pipe before use in capillary and evaporator heat flux tests. Reagent-grade methanol was used without treatment for gravity flow tests. Butanol for evaporator heat flux tests was vacuum-distilled in a heat pipe. Untreated spectrophotometric-grade benzene was used for capillary pressure tests in air.

WICK CAPILLARY PRESSURE TEST

Maximum heat transfer capability in a heat pipe is directly related to the mass transfer capability of the system which, in turn, is closely related to the wick capillary pressure, ΔP_C. In order to establish the maximum heat transfer capability, therefore, the wick capillary pressure must be determined.

Wick capillary pressures for various screens, felt metals, and sintered powders have been measured by Kunz et al. (ref. 10). These data, however, are limited to wicking structures with porosities, ε, of less than 92%. In order to minimize flow resistance in the liquid return structure, wicks with high porosities are of interest. During this program, capillary pressure data were obtained for wicking structures including felt metal, foam and screen, with porosities as high as 96%.

Capillary pumping pressures may be measured by two methods: the first is the wicking rise height method, and the second is by measuring the pressure difference required to break the menisci in the evaporating surface of the wick. There would be no difference between these two methods if the wick were completely isotropic. However, this is usually not the case, and the second method must be used to provide the data necessary for heat pipe design.

Test Apparatus and Procedure

Maximum capillary pressures which could be sustained by test wicks were measured (1) under the vapor of the working fluid, and (2) in air. In the first case, the maximum height of the column of liquid which could be suspended from a wick whose surface was exposed only to the saturated vapor of the liquid was measured. In the second case, the pressure required to force an air bubble through the wetted wick was measured. Initially, the first technique was used since it represents the actual condition in a heat pipe. This method, however, is much more complicated and time consuming than measuring wick capillary pressure in air. Therefore, the second approach was used when it was ascertained that the two methods gave comparable results.

The test apparatus for measuring wick capillary pressure in working-fluid vapor consisted of a U-tube manometer with the legs connected at top and bottom by flexible tubing to form a closed system as shown in figure 4. The specimen was clamped in the specimen holder shown in figure 5 and held stationary. The opposite leg of the U was a length of Pyrex tubing fastened to a rack driven by a manually operated pinion. The vapor side of the system was valved to a vacuum station and liquid-filling system through a tee.

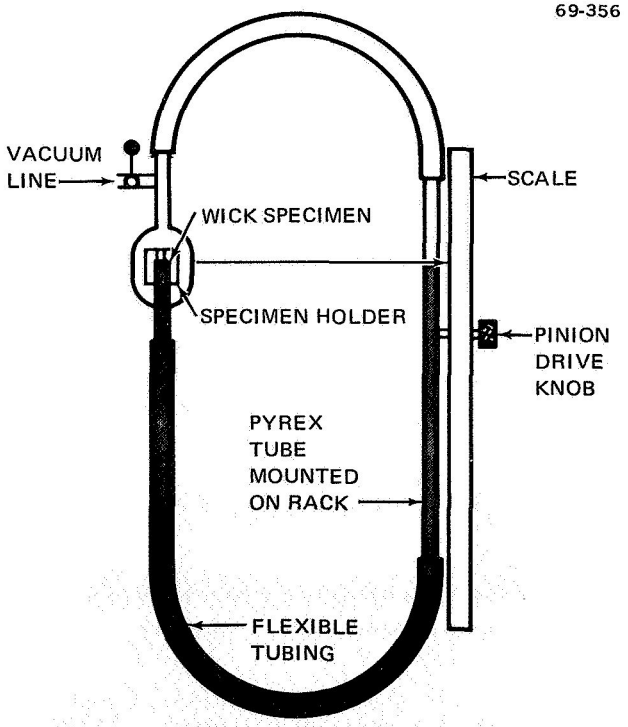

Figure 4. Assembly for Measuring Capillary Pressure in Vapor of Working Fluid

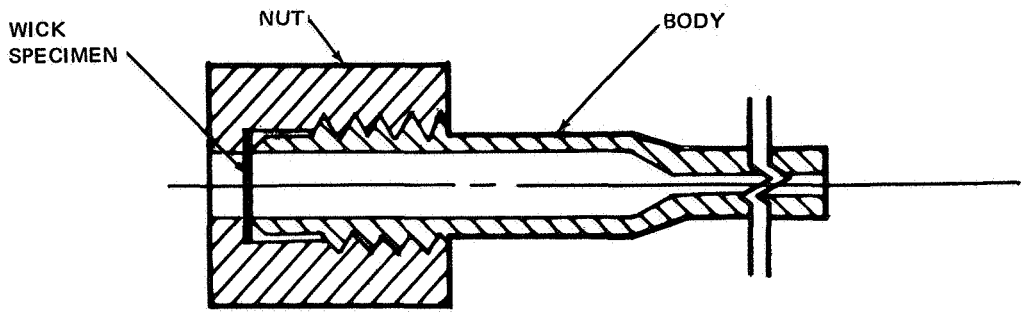

Figure 5. Capillary Test Wick Specimen Holder

The test apparatus for measuring wick capillary pressure in air used the same specimen holder inverted into a beaker of the test liquid and connected to a U-tube manometer as shown in figure 6. System pressure was controlled by a manually operated positive-displacement pump.

The wick capillary pressure under working-fluid vapor was measured in five steps:

(1) The system was evacuated.

(2) The lower part of the U was filled with liquid distilled in a heat pipe until the liquid level was close to the level of the wick.

(3) The Pyrex tube was raised until the wick surface was observed to wet. The meniscus level in the tube was recorded as the zero elevation.

(4) The Pyrex tube was slowly lowered with the rack and pinion until the wick could no longer support the column of liquid. This condition was evidenced by a sudden rise of the liquid level in the tube. The meniscus elevation at the time of sudden rise was recorded and subtracted from the zero elevation.

(5) The maximum capillary pressure was calculated from the measured difference in elevation.

Measurement of wick capillary pressure in air was performed in three steps:

(1) The wick was wetted by raising the liquid above the wick and then lowering it until the wick just touched the liquid. During this operation, both sides of the manometer were vented to air and the wick elevation was determined by a hook gage.

Figure 6. Assembly for Measuring Capillary Pressure in Air

(2) The vent was closed and pressure in the specimen holder was increased until an air bubble was forced through the wick.

(3) The maximum pressure differential indicated by the manometer was recorded.

The entire procedure was repeated five times for each wick, and maximum capillary pressure was calculated from the average maximum pressure differential.

Test Results

The results of these experiments are presented in table 3. Maximum capillary pressure was obtained from either the maximum head of liquid sustained or the height of the manometer when bubbles broke through the wick. Values of effective pore diameter, D_c, are calculated by using equation (6) with $\Delta P_C = \rho_L \left(\frac{g}{g_c}\right) h$ and $D_c = 2 r_c$:

$$D_c = \frac{4 \sigma}{\Delta P_C} = \frac{4 \sigma}{\rho_L \left(\frac{g}{g_c}\right) h} \qquad (6)$$

TABLE 3

WICK CAPILLARY PRESSURES

Wick	Liquid	Atmosphere	Measured maximum capillary press. (psi)	Calculated effective pore diam (in.)	Nominal pore diam (in.)	Measured open ratio (a) (%)	Measured thickness (in.)	Manufacturer or supplier
200 mesh stainless steel screen	Methanol	Vapor	0.12	0.0043	0.0035	73.3	0.0035	Michigan Wire Cloth Co.
200 mesh stainless steel screen	Methanol	Air	0.12	0.0044	0.0035	73.3	0.0035	
200 mesh bronze screen	Ethanol (b)	Air	0.12	0.0042	0.0029		----	----
200 mesh stainless steel screen	Benzene	Air	0.15	0.0045	0.0035	73.3	0.0035	Michigan Wire Cloth Co.
200 mesh stainless steel screen	Water	Air	0.36	0.0046	0.0035	73.3	0.0035	
200 mesh bronze screen	Water (b)	Air	0.35	0.0048	0.0029			
200 mesh nickel screen	Water (c)	Air	0.33	0.0049		67.6		
Copper foam (AmPorCop 210-5)	Methanol	Vapor	0.029	0.018	0.008	94.5	0.108	Astro Met Associates Inc.
	Benzene	Air	0.037	0.018	to	94.5	0.108	
	Water	Air	0.096	0.017	0.039	94.5	0.108	
Copper foam (AmPorCop 220-5)	Water	Air	0.088	0.019	0.012 to 0.040	91.2	0.102	Astro Met Associates Inc.
Copper felt	Methanol	Vapor	0.023	0.022	0.008	89.5	0.100	Astro Met Associates Inc.
	Benzene	Air	0.038	0.017	to	89.5	0.100	
	Water	Air	0.090	0.018	0.032	89.5	0.100	
Nickel foam (AmPorNik 220-5)	Methanol	Vapor	0.024	0.021	0.010	96.0	0.100	Astro Met Associates Inc.
	Benzene	Air	0.038	0.017	to	96.0	0.100	
	Water	Air	0.090	0.018	0.025	96.0	0.100	
Nickel foam (AmPorNik 210-5)	Water	Air	0.090	0.018	0.018 to 0.059	94.4	0.102	Astro Met Associates Inc.
Nickel felt	Water	Air	0.13	0.013	0.006 to 0.027	89.1	0.101	Astro Met Associates Inc.

a. Open volume to total volume
b. Katzoff (ref. 14)
c. Kunz et al. (ref. 10)

The nominal pore diameter is shown for reference and is the most probable size in the pore size distribution. This was obtained by inspection of the capillary material under a microscope. The nominal pore diameter is generally smaller than the effective pore diameter. Open ratios of the wicks ε, are listed in table 3 to more completely describe the wick. Porosity is obtained by careful measurements of the sample's weight and linear dimensions.

Because values of D_c for 200 mesh screen with methanol in vapor and in air are so similar, it was concluded that the test in air would yield data which would be sufficiently accurate for heat pipe design. Thus, most of the subsequent tests were performed in air.

It is instructive to compare the results for 200 mesh screen with those of Katzoff (ref. 14) and Kunz et al. (ref. 10). These data are also shown in table 3, and they agree remarkably well. At least for the 200 mesh screen wick, capillary pressure is the same for a meniscus receding either perpendicular or parallel to the long axis (evaporating surface) of the wick.

PERMEABILITY TESTS

The purpose of the permeability tests was to obtain values of K_p which can be used to determine the pressure drop in the liquid phase of a heat pipe.

The pressure drop for liquid flow in a wick, in the absence of evaporation or condensation, is given by:

$$\Delta P_L = \frac{\nu_L}{K_p} \frac{\ell_a}{A_w g_c} \frac{Q}{h_{fg}}$$

or, since $\frac{Q}{h_{fg}}$ = the mass flow, $\dot{m}$,

$$\Delta P_L = \frac{\nu_L}{K_p} \frac{\dot{m}\ell_a}{A_w g_c} \tag{7}$$

Thus, permeability may be measured by impressing a pressure gradient or gravity head on a wick and measuring the flow.

During this program, three test techniques were used to determine the permeabilities of wicks. They were:

1. Forced flow
2. Gravity flow
3. Condenser flow

Forced Flow Permeability Tests

This technique involved enclosing a long piece of test wick completely (except for the ends) by containing surfaces, forcing liquid through the wick and measuring the pressure distribution along the wick. This technique measures the flow resistance of the containing walls as well as the wick itself, and does not accurately simulate a situation in a heat pipe which has a free surface. For thick wicks, however, the wall effect will be very small and a forced flow technique is sufficient.

Description of apparatus. - Wick permeabilities were calculated from flows measured as a function of the liquid pressure drop over a given length in the apparatus shown in figure 7. The apparatus used water as a working fluid and consisted of three subsystems: liquid supply, test chamber, and pressure sensing equipment.

The liquid system was composed of a constant-level supply reservoir and a makeup reservoir. The makeup reservoir, capable of supplying liquid to the primary supply reservoir at a rate in excess of the flow to the wick, was used to maintain a constant level. Excess liquid flowed out through an overflow line into a beaker. The supply reservoir was connected to the test chamber by flexible plastic tubing.

The test chamber was fabricated from Plexiglas to allow observation of the test specimen as shown in figure 8. The 0.1- x 1.0- x 2.5-in. specimen was located in a channel sealed on two sides by thin rubber sheet to prevent any liquid flow around the specimen. At each end of the specimen, a chamber was located containing a pressure tap. Two additional pressure taps were inserted approximately 0.050 in. into the wick specimen, 1.5 in. apart, and 0.5 in. from each end of the specimen. These pressure taps were 1/16 in. OD, and connected to the pressure sensing system by flexible tubing. The pressure sensing system consisted of a differential pressure transducer, a selector valve, a reference pressure flask, power supplies for the selector valve and transducer, and a digital voltmeter. The transducer was a Statham Model PM5TC with a ±1/4 psi differential pressure range, and open to the atmosphere on one side of the diaphragm. The transducer was connected to each of the pressure taps and a reference pressure flask through a Scanni-valve switch. This system allowed use of a single transducer with a single calibration curve. Zero reference pressure for the transducer was provided by maintaining the level of water in a small flask at the same elevation as the transducer diaphragm.

A stopwatch with 1/5-second calibrations was used for timing flow samples, and a mercury thermometer was used for measuring water temperature.

Test procedure. - The test procedure consisted of establishing a pressure head on the inlet side of the wick, and measuring the pressure drop and flow through the wick. With this procedure, the pressure head could be limited only by the physical strength of the test device or the maximum pressure available. However, the maximum pressure difference a wick can sustain in

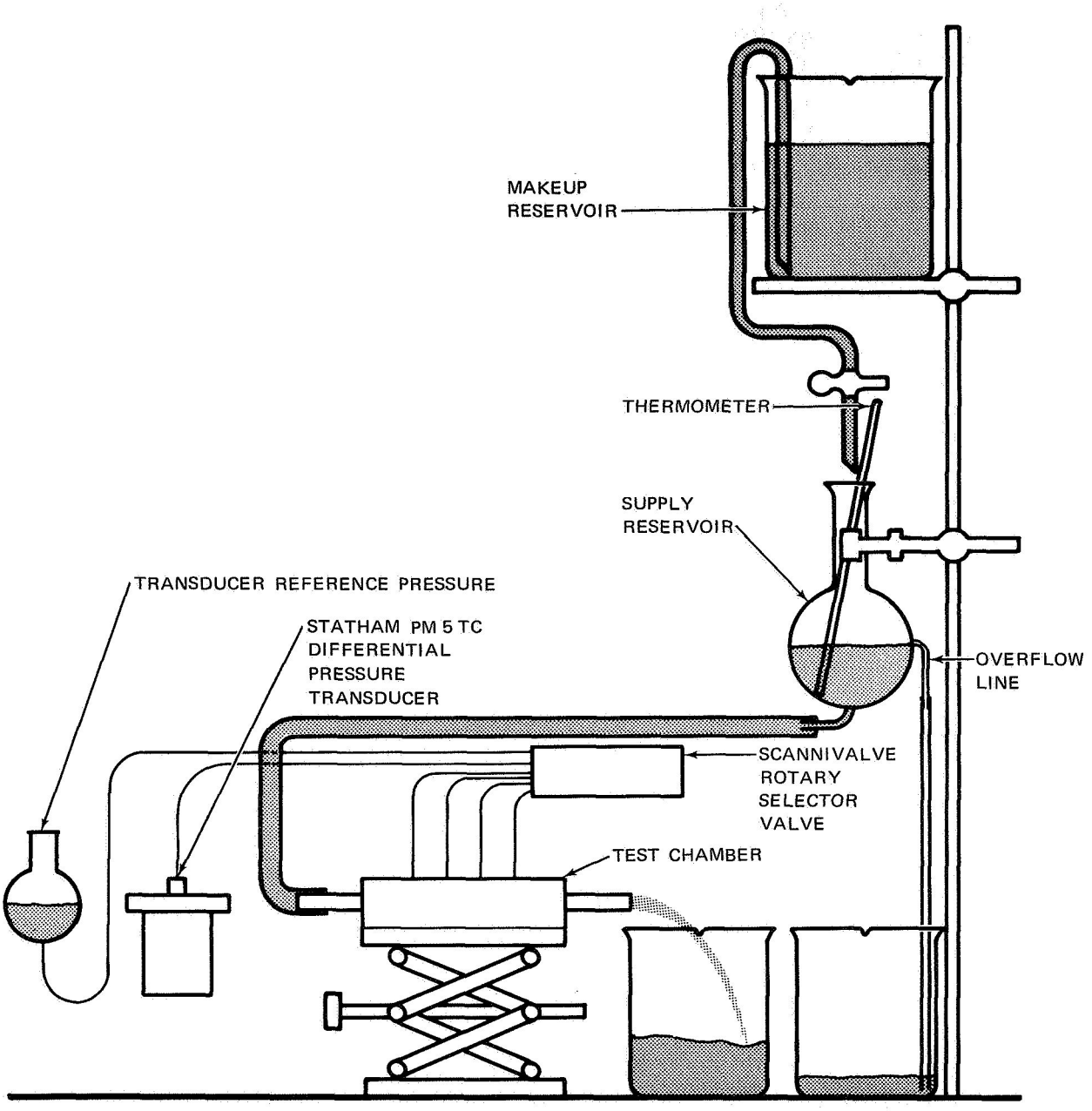

Figure 7. Forced Flow Permeability Test Apparatus

68-933

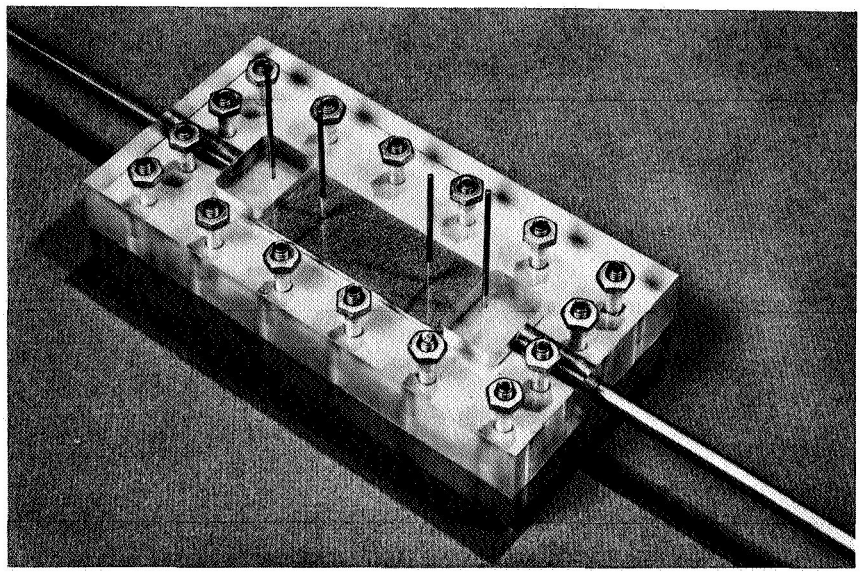

Figure 8. Forced Flow Permeability Test Chamber

a heat pipe or vapor chamber is the capillary pressure of the wick. Therefore, on the assumption that the maximum pressure gradient along a wick would hardly exceed that corresponding to application of maximum capillary suction over a 1-in. length of wick, for test purposes, measurements were restricted to pressure drop per unit length, $\Delta P/\ell$, equal to or less than the capillary pressure per inch of wick length.

The test was started by loading the system with boiled, deaerated distilled water and removing all bubbles from the wick, water supply lines, and pressure sensing lines. The water was placed in the makeup reservoir and syphoned into the supply reservoir. Flow was controlled by a pinch clamp on the flexible tubing between the reservoirs. Water flowed from the supply reservoir through the test chamber and wick. Bubbles were purged from the wick by drawing water rapidly through the test chamber with a pump. Bubbles were purged from all the pressure sensing lines, the Scannivalve transducer, and the reference pressure flask by flushing with water. The maximum pressure head was set by adjusting the elevation of the test specimen with a scissors jack to the desired distance below the level of water in the supply chamber.

Test measurements were made after the flow at maximum pressure head had become stable. Stable flow was achieved when the pressure profile through the wick was observed to be constant. Then, a specimen of water discharging from the test chamber was collected in a beaker for a measured period of time. During collection of the sample, the pressure profile was measured and recorded 10 times. The water specimen was weighed, and its temperature recorded. The same procedure was repeated for each of the pressure heads and for each of the wicks tested.

Test results. - Test results are plotted in figures 9 and 10. If Darcy's Law applied accurately to these wicks, the inverse permeability would be a constant. But inverse permeability is seen to vary with flow, and Darcy's Law does not provide an accurate description of the flow field for these wicks under these flow conditions.

It would be expected that higher-porosity wicks would have a higher permeability for a given value of D_c, and this is generally true; but the permeability of the copper foam wick with $\varepsilon = 95\%$ is less than that of the copper foam wick with $\varepsilon = 91\%$. This may be attributed to the smaller pore size of the higher-porosity wick. Thus, pore size is a very important parameter in the determination of permeability. This is also exemplified by the small value of K_p for the nickel felt wick, even though the porosity is not significantly less than some of the other wicks. The maximum Reynolds number ($Re = 1/\varepsilon \ \dot{m}/A \ D_c/\mu$) for any of these flows is about 100, so it is unlikely that turbulent velocity fluctuations will occur in the liquid. The expression for the Reynolds number is based on the assumption that flow occurs in parallel channels of size D_c. Scheidegger (ref. 18) points out that there will be three different flow regimes which describe flow in a porous medium as the flow is increased. For low flows, a Darcy's Law expression is valid because inertial effects will be small. But, as the Reynolds number increases, a flow regime will be reached in which the neglect of inertial effects is no longer valid and a different expression will be required to describe the flow. Many empirical expressions have been tried to describe this regime, but no universal correlation has been achieved. The third regime is turbulent flow, and a pressure drop vs mass flow expression which includes the effect of turbulent flow must be used for Reynolds numbers greater than approximately 2000.

Most of the data from the experiments appear to lie in the second flow regime. A plot of $1/K_p$ vs flow per unit area is very close to a straight line, with a positive slope for all but one of the wicks. There is a deviation from linearity at high flow rates, however, and so the flow can be characterized by a relationship between pressure gradient and mass flow which involves a quadratic correction term.

Gravity Flow Permeability Test

The gravity flow permeability test was used for testing thin wicks, including screen and V-groove wicks, because this method allows testing with a constant meniscus radius along the flow length, which is desirable since permeability is a function of meniscus radius. There is a free surface between the atmosphere and the liquid, which more closely approximates the situation in a heat pipe than a test which has restraining surfaces on all sides of the wick. With a free surface present, a constant capillary meniscus along the length of the wick may be achieved by inclining the wick at an angle to the horizontal, and regulating the flow of the liquid until the liquid pressure drop per unit length equals the change in pressure head per unit length.

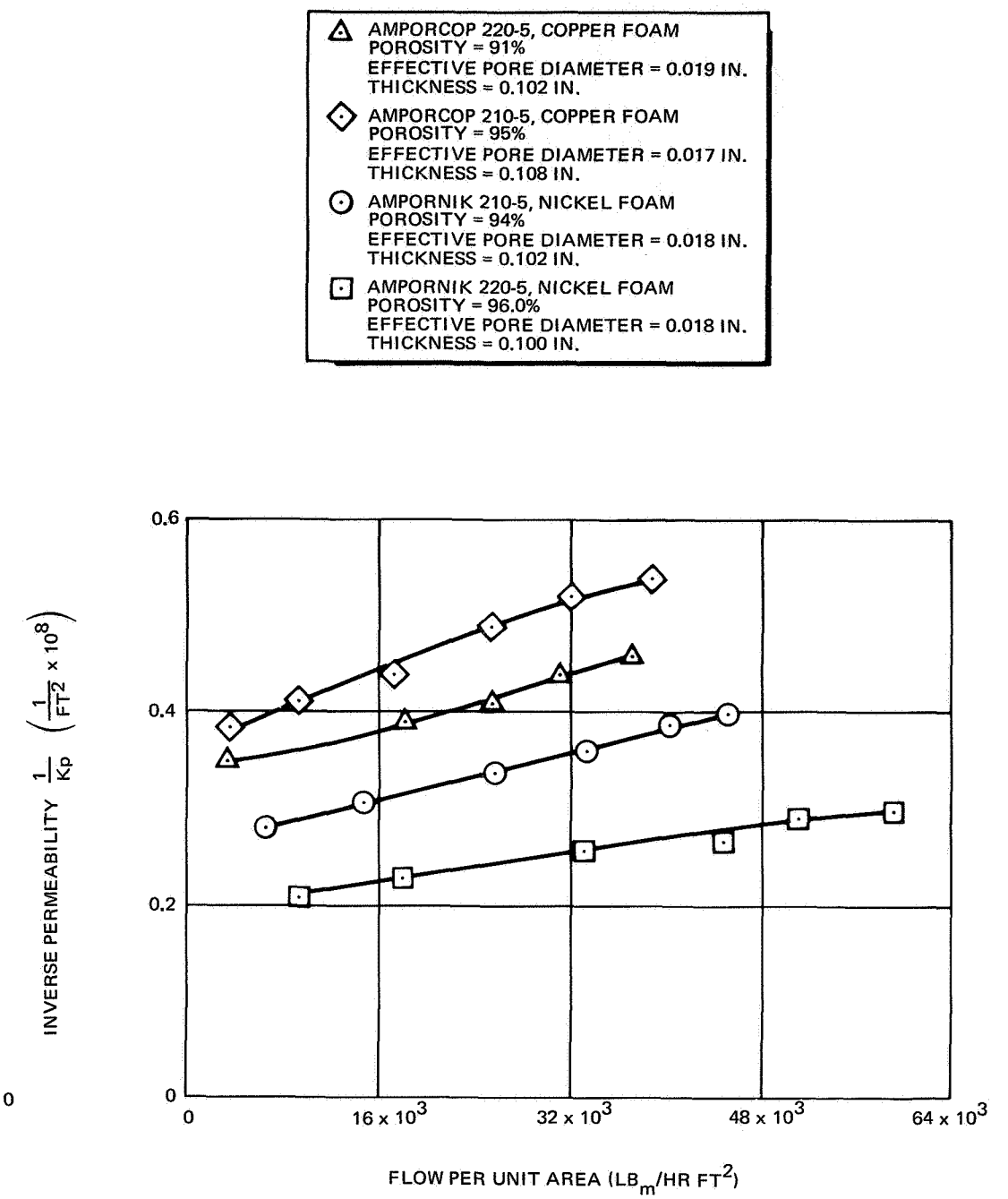

Figure 9. Inverse Permeability Data From Forced Flow Permeability Test with Deaerated Distilled Water

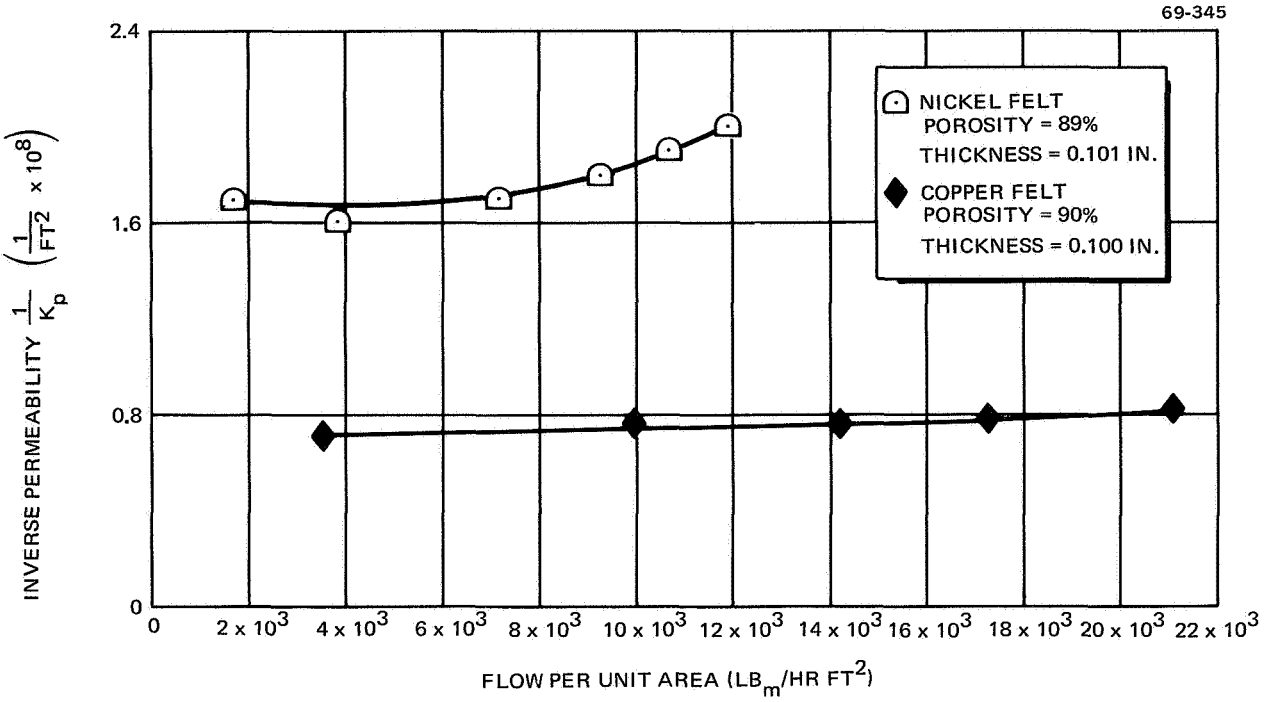

Figure 10. Inverse Permeability Data from Forced Flow Permeability Tests with Deaerated Distilled Water

In addition, the meniscus radius may be varied to investigate the effect of depth of meniscus on permeability. This is useful because in an operating heat pipe the meniscus radius will vary along the length in a definite way. If permeability is determined as a function of meniscus radius, it is possible to include this effect in determining the maximum heat transfer capability of heat pipes with thin wicks. The use of such data will be discussed more thoroughly in the Design of Low-Temperature Heat Pipes Section of this report.

Description of apparatus. - Permeabilities of wicks less than 0.050 in. thick were measured with the gravity flow device. The same basic apparatus was set up in two configurations. The first was used for permeability measurements with a flat (infinite radius) meniscus on the liquid-vapor interface, i.e. with a zero pressure differential across the meniscus. The second was used to measure permeability with the meniscus receding into the wick with a uniform small radius.

The apparatus consisted of a liquid supply system, the gravity flow test device, the test fixture, the pressure sensing system, and the methanol test fluid. A schematic of the test assembly is shown in figure 11. The liquid supply system was essentially the same as for the forced flow permeability tests, with a supply reservoir, makeup reservoir, and metering valves between the two reservoirs and between the supply reservoir and test device. Again, the supply reservoir maintained a constant liquid level by means of an overflow line.

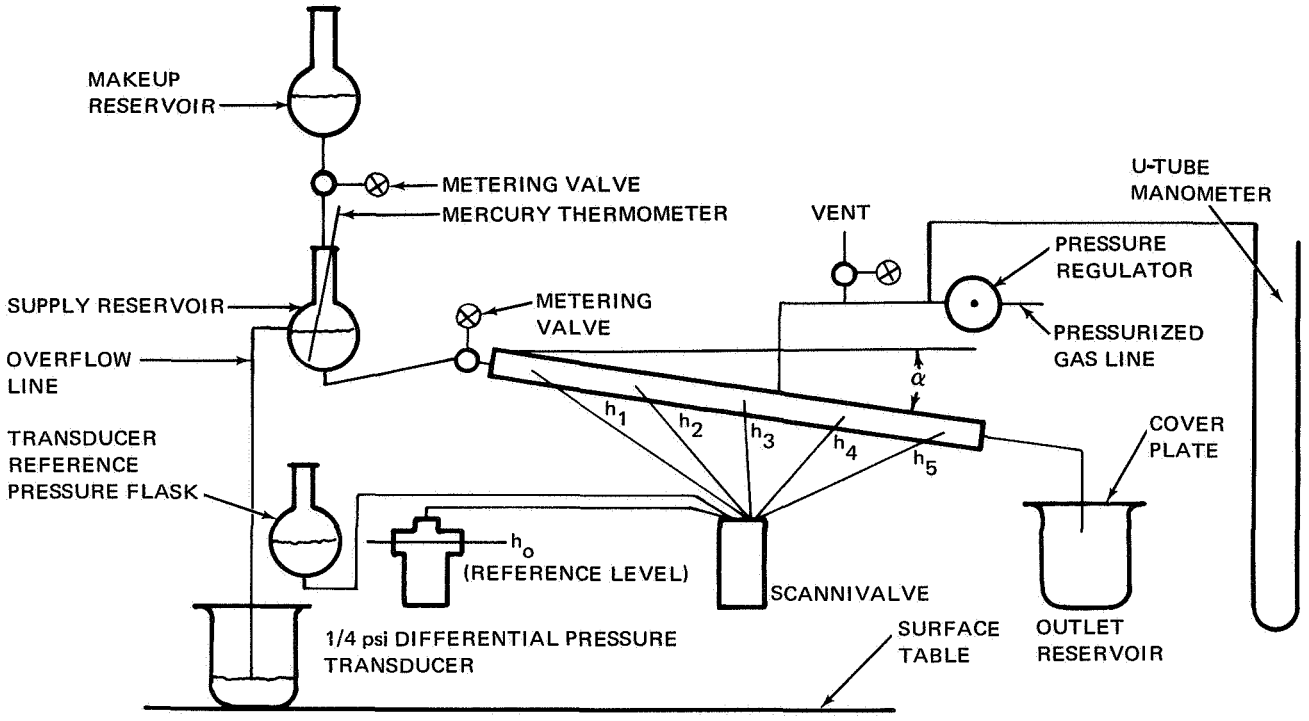

Figure 11. Gravity Flow Test Schematic

The gravity flow test device consisted of an enclosed chamber containing the wick specimen as shown in figure 12. The device was constructed of stainless steel with a transparent window to permit observation of the wick during test. The wick was diffusion-bonded to a wick holder (see appendix B) clamped to the bottom plate of the test device. Five pressure-tap slots passed through the holder and into the bottom plate. An elongated O-ring seal was placed around each slot between the wick holder and bottom plate. The slots on the upper side of the wick holder were covered by a thin layer of small-pore (< 0.001-in. pore diameter) nickel foam. The foam and wick holder were then covered by the wick specimen. The purpose of the foam layer over the pressure tap slot was to prevent entry of vapor into the pressure sensing system.

Pressure taps in the bottom plate consisted of 1/16-in. -diam tubing on one side of the device and 1/4-in. -diam tubing on the opposite side. The 1/16-in. taps were connected to the pressure sensing system, and the 1/4-in. tubes were either capped or used as liquid inlets or outlets. The 1/4-in. tube at the first pressure tap was used as the liquid inlet and a 1/4-in. line in the opposite end of the test device was used as the outlet. The path of liquid flow was through the inlet line, through the pressure tap slot and nickel foam, through the length of the wick, and out the outlet.

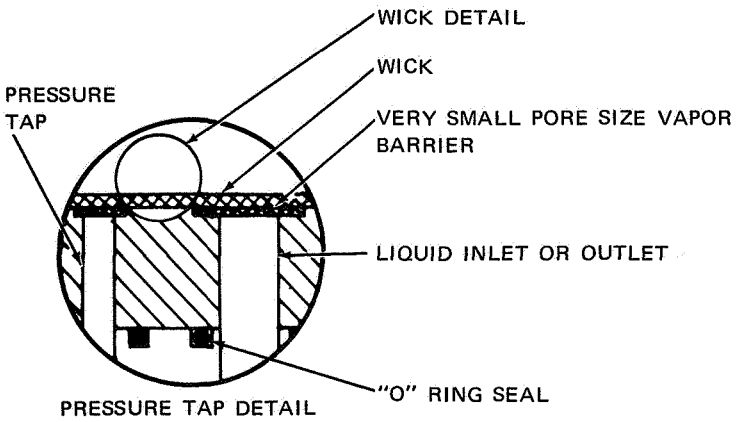

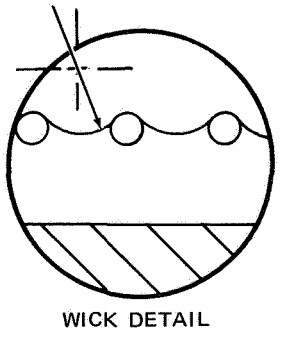

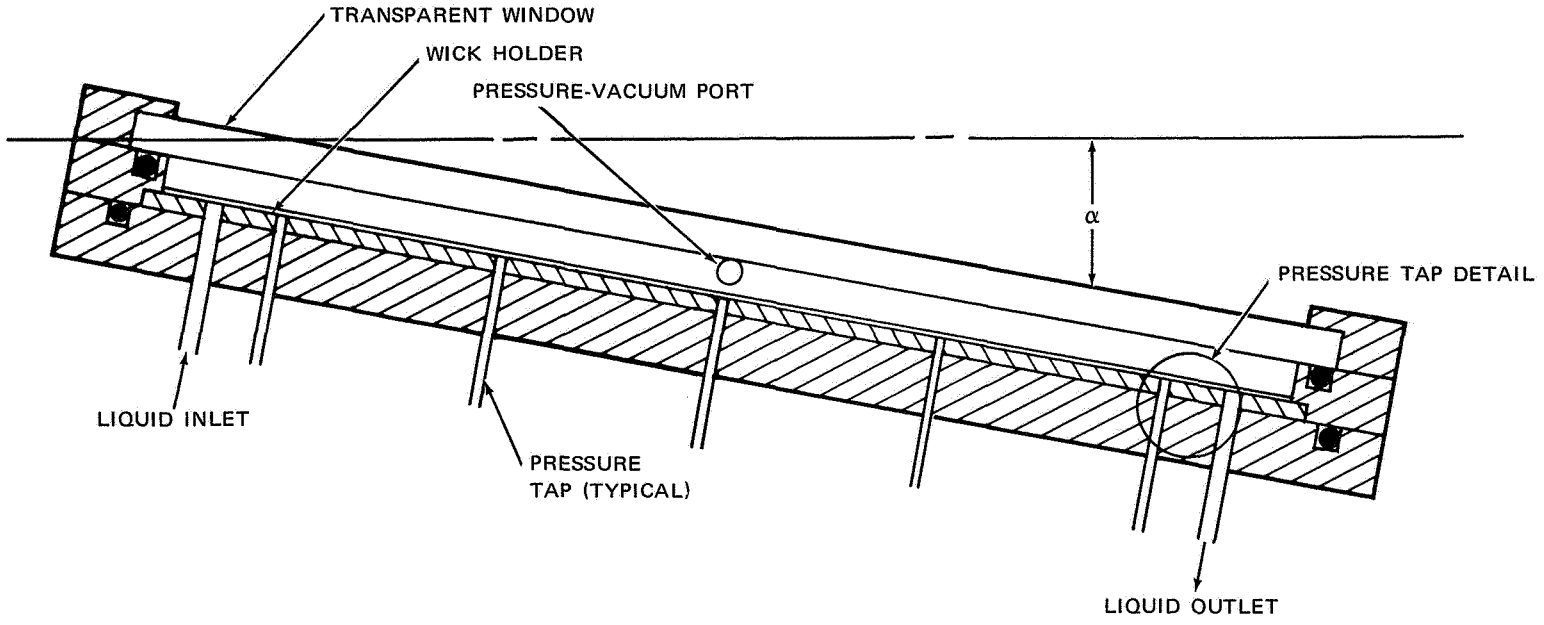

Figure 12. Gravity Flow Test Device

The wick specimen was 1 in. wide and 11.94 in. long (fig. 13). Flow baffles (fig. 14) were installed on the upper surface of the wick to break up flow over the top of the wick.

The test fixture which held the gravity flow test device consisted of a frame and an angle-setting mechanism. The frame was built of 1/2-in.-diam aluminum laboratory scaffolding and incorporated a pivot to which the liquid inlet end of the test device was attached. The mechanism for setting the angle of the test device with the horizontal was a cable wrapped around the shaft of a crank.

Test instrumentation consisted of a thermometer in the supply reservoir, a machinist's protractor for measuring angles, and the pressure sensing system. The pressure sensing system consisted of pressure transducers, a Scannivalve, a vacuum tube voltmeter, a reference pressure flask, and power supplies for the transducer and Scannivalve. The pressure transducer was a Statham Model PM5-TC with a ±1/4 psi differential pressure range; the vacuum tube voltmeter was a Fluke Model 801B.

To measure permeability as a function of meniscus radius, it was necessary to revise the test equipment. The liquid supply system was functionally identical to the forced flow test setup, but the test device was modified by addition of two more pressure taps to the wick and test device as shown in figure 15. The liquid outlet was sealed and the last pressure tap was used as the liquid outlet. The test apparatus was assembled on a level, granite-topped surface table. The apparatus was pivoted at the center, and a scissors jack was used to raise and lower the outlet end. The major change was the addition of a pressure regulation system by which air pressure inside the test device could be raised above atmospheric to establish a pressure differential across the wick's liquid/vapor interface. The regulation system consisted of a pump, vent valve, and U-tube manometer.

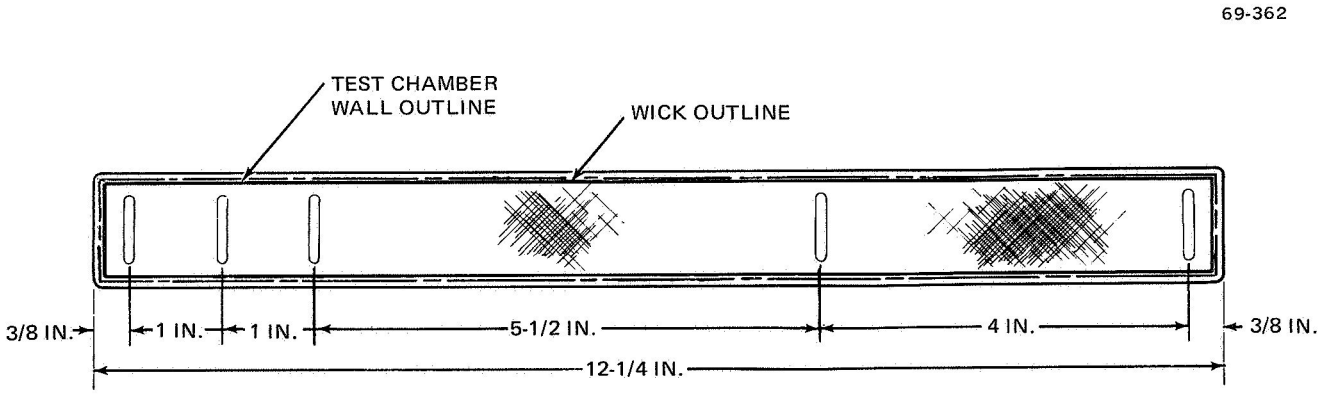

Figure 13. Gravity Flow Test Wick Holder Showing Pressure Tap Locations for Tests with Infinite Meniscus Radius

68-1716-A

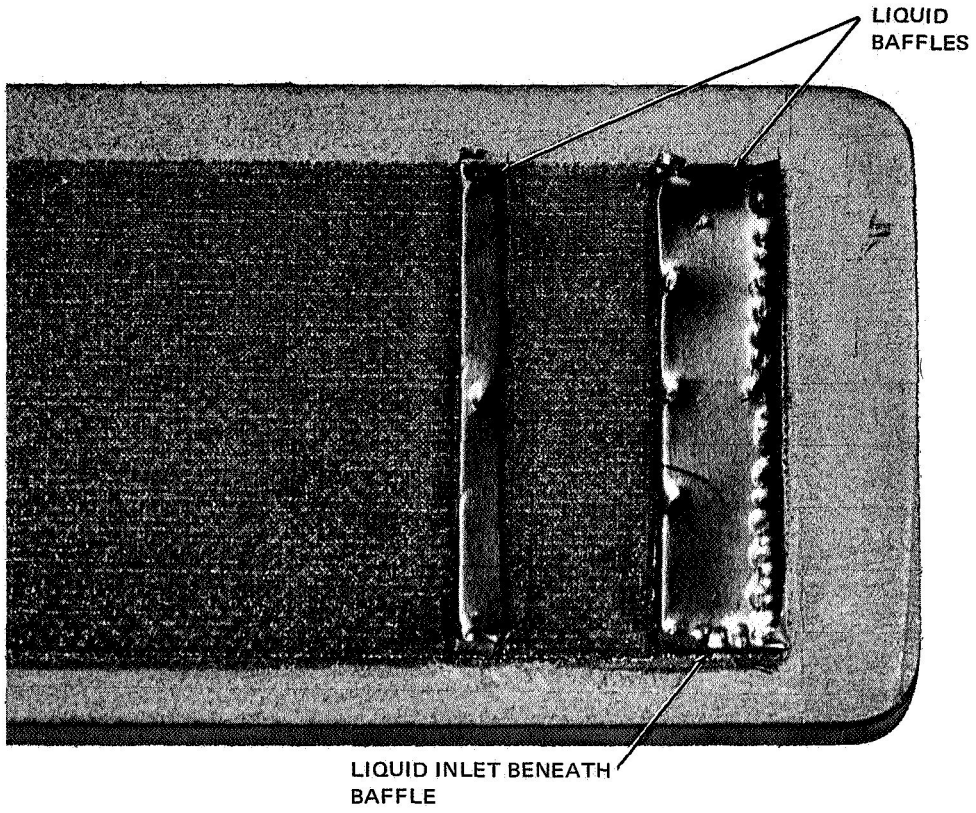

Figure 14. Gravity Flow Test Specimen (50 Mesh Screen Covered by 200 Mesh Screen) Showing Baffles at Liquid Inlet

69-363

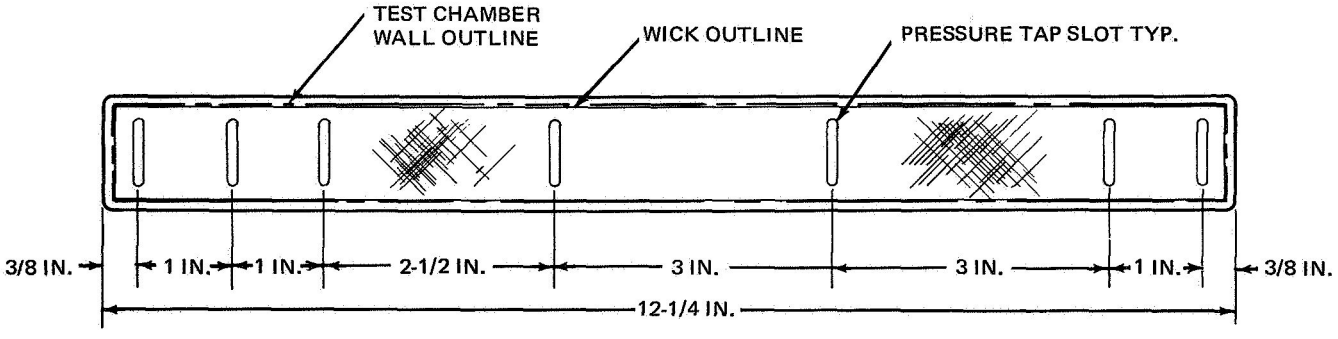

Figure 15. Gravity Flow Test Wick Holder Showing Pressure Tap Locations for Tests with Small Meniscus Radius

Test instrumentation included a pressure sensing system, mercury thermometer in the supply reservoir, and vernier gage for measuring elevations. The system was the same as described above except that the Scanni-valve was replaced by a valve and manifold. A constant-voltage power supply was used for all electrical equipment. A 2-ft vernier height gage was used in conjunction with the granite surface table to measure elevations of pressure taps, the transducer diaphragm, and the liquid level in the reference pressure flask.

Test procedure. - To measure the permeability of a wick with a constant flow area, i.e. a constant radius of menisci curvature of the liquid vapor interface, the internal liquid pressure must be constant throughout the wick. This condition can exist in an inclined wick along which liquid is flowing when the pressure gradient caused by viscous drag is exactly balanced by the pressure gradient due to gravity

$$\Delta P_L/\ell_a = \rho_L(g/g_c)\sin\alpha \tag{8}$$

With a given pressure difference across the liquid/vapor interface, and a given angle α, there is only one flow value which can maintain a constant liquid pressure along the wick. This follows from equation (7) where it is apparent that for a given $\Delta P_L/\ell_a$, and given values of K_p and A_w, $\dot{m}$ will be fixed. In practice, the test wick is set at an angle, α, with the horizontal, and liquid flow is varied with the metering valve until the pressures measured at the different pressure taps are equal. The friction pressure differential per unit length is given by $\Delta P_L/\ell_a = \rho_L\, g/g_c \sin\alpha$. Substituting this value of $\Delta P_L/\ell_a$ in equation (7), the following expression for $1/K_p$ would result:

$$\frac{1}{K_p} = \frac{\rho_L\, g \sin\alpha\, A_w}{\nu_L \dot{m}} \tag{9}$$

However, the actual flow area is a function of the meniscus radius of the liquid/vapor interface. In addition, the flow pattern will change as the meniscus recedes into the wick. Both of these effects may be lumped together in the permeability, if flow is based on the actual cross-sectional area of the wick as measured with a micrometer. The radius of curvature of the meniscus may be calculated from the following pressure balance equation:

$$P_G - \left(P_t - \rho_\ell \frac{g}{g_c} \Delta h\right) = \frac{2\sigma}{r} \tag{10}$$

where

P_t = absolute pressure of transducer.

Δh = elevation of pressure measurement point in wick above transducer diaphragm.

P_G = pressure in the vapor space above the wick.

σ = surface tension.

r = radius of liquid-vapor meniscus.

These items may be measured experimentally and inverse permeability may be measured as a function of the liquid/vapor meniscus radius. In a heat pipe, the radius may vary from the wick pore radius to infinity. The radius of the meniscus in the test wick may be varied by changing P_G. In practice, this is done by varying the gas pressure in the chamber with the pressure regulation system.

In actual tests, this test system proved to be difficult. Adjusting the flow to get a uniform pressure throughout the wick is very tedious. Initial pressure response to a change in flow is rapid, but the system requires a long time to reach equilibrium. Thinner wicks are particularly sensitive to changes in flow; any tendency of the liquid to form a meniscus between the wick and the side walls of the test device induces an error due to excess liquid flow under that meniscus. This effect is discussed more fully later in this section and in appendix A.

The detailed test procedure is outlined below. It consisted of preparing the equipment for test, establishing flow, setting the angle, α, adjusting flow, and measuring flow and pressures.

Preparing the test equipment included charging the device with liquid, purging the pressure sensing and liquid lines, and zeroing the pressure transducer reading. Reagent-grade methanol was placed in the makeup reservoir and allowed to flow into the supply reservoir until the latter overflowed. The test device was leveled and filled with methanol from the supply reservoir. The pressure sensing lines, transducer, and Scannivalve were purged with methanol. The wick was flooded and pressures in the stagnant liquid were measured. Any deviation in pressure reading indicated presence of bubbles in the pressure sensing lines, and lines with deviant readings were repurged until uniform readings were obtained. The pressure transducer reading was zeroed by adjusting the level of liquid in the reference pressure flask to that of the transducer diaphragm and then shifting the voltmeter reading to zero. With no flow through the test specimen and the transducer zeroed, the equipment was ready.

Testing was initiated by setting the angle of inclination at 10°, establishing maximum flow, adjusting the flow to the constant liquid pressure condition, measuring the pressure, and measuring the flow. Maximum flow was achieved by opening the metering valve to its limit. The 10° inclination angle was set using a machinist's protractor. Flow was adjusted to the constant liquid pressure condition by slowly closing the metering valve and observing the pressure profile. Note that the pressure transducer reads the pressure in the wick plus the pressure head due to the difference in elevation between the pressure tap and transducer diaphragm. The test operator was provided a

chart listing the difference in pressure heads between adjacent pressure taps for all angles of inclination. Flow was decreased until the charted pressure difference readings were achieved. Establishing equilibrium flows at 10° with a constant liquid pressure in the wick was difficult--sometimes impossible. This was particularly troublesome with the thinnest wicks. When equilibrium flow and constant pressure were established, flow was measured and pressure readings recorded. Five pressure readings were made while the flow sample was being taken and the average readings were recorded.

The same procedure was followed at inclination angles of 20°, 30°, 40°, 50°, 60°, and 70°.

The procedure was altered to measure permeabilities for wicks with small, constant radii in the liquid/vapor interface. A constant meniscus may be imposed on the liquid/vapor interface by creating a pressure differential across the meniscus. This is done by increasing the pressure above the wick by an amount ΔP_G above atmospheric pressure while maintaining the liquid at atmospheric pressure. The liquid outlet was at atmospheric pressure and, therefore, the liquid in the wick was at atmospheric pressure when the liquid pressure was constant. The liquid outlet line was a tube, but because the flow was too small to fill the tube, the outlet line was functionally an open channel.

Adjusting of flow to reach a constant pressure in the liquid was the same as described above.

The specific procedure for measuring permeability was to first measure the permeability with infinite radius and then measure it with a small radius. The same procedure discussed previously in this section was used to measure permeability with infinite radius except that the angle of inclination was set using a 2-ft vernier height gage to measure elevations. When the angle was correctly set, the vernier was used to measure the elevations of each pressure tap at the wick level and level of the transducer diaphragm; and to set the height of the liquid in the pressure reference flask to the elevation of the diaphragm. Permeability was then measured for an infinite radius as outlined above.

Without changing the angle of inclination, a positive pressure, ΔP_G was imposed on the surface of the wick in order to provide menisci of finite radius. For a desired radius, r, the required ΔP_G is given by $\Delta P_G = \frac{2\sigma}{r}$. For convenience, a U-tube manometer was used to set ΔP_G, but for the sake of accuracy ΔP_G and r were calculated from the pressure transducer readings. The permeability was measured using the same procedure as before by adjusting the flow until the liquid pressure was constant.

This procedure was followed for inclination angles of 10°, 30°, 50°, and 70° for single- and double-layer 200 mesh screen wicks. Tests were performed with ΔP_G's of zero, 30, 80, and 120 mm of methanol. It was not possible to obtain data at the 10° inclination angle for the single-layer wick and difficult to obtain data for the double-layer wick.

Gravity flow test results. - Results of the gravity flow permeability tests are plotted in figures 16 through 20. These figures show the results of tests with zero pressure difference across the liquid/vapor interface. Figure 19 also shows the results of tests with a nonzero chamber pressure (a meniscus radius of less than infinity). Results for the 200-mesh screen are tabulated in table 4. Results for thick wicks are presented in terms of $1/K_p$ defined by equation (11), and for thin wicks, in terms of R defined by equation (12).

$$1/K_p = \frac{\Delta P}{\ell} \frac{A_w g_c}{\nu_L \dot{m}} \tag{11}$$

$$R = \frac{\Delta P}{\ell} \frac{A_w g_c}{\nu_L \dot{m} t_w} \tag{12}$$

The reason the results for thin wicks are presented in terms of R (which is based on the flow width of the wick--not the flow area) is that $1/K_p$ for a wick consisting of a few layers of screen can be a function of the number of layers. Thus, it would not be correct to assume that ΔP_L for a screen-type wick could be calculated by using $1/K_p$ in equation (11) and by using the area of the wick, regardless of whether one or many layers of screen were used in making up the area. To avoid this error, data are presented in terms of R; they may only be used for calculating ΔP_L for one or two layers of screen.

Foam wicks: According to the manufacturer's specification, AmPorNik and AmPorCop 210-5 and 220-5 have nominal pore diameters of 0.010 and 0.020 in., respectively. Thus it would be expected that, for a given porosity, the 210-5 wicks would have a smaller value of K_p than the 220-5 wicks. However, reference to figure 17 indicates this is not true. In addition, our results on effective pore diameter, D_c, (table 5) indicate little difference between 210-5 and 220-5 wicks. Inspection under a microscope indicated there was no appreciable difference in the size and range of sizes of pores for the 210-5 and 220-5 wicks. This is contrary to the manufacturer's specification and may have been the reason why the foam metal wicks did not follow the expected relationship between permeability and pore size. In addition, the tortuosity of the wick and the percentage of noninterconnected pores may also influence the results if these parameters are not constant from wick to wick.

Felt wicks: Data for the metal felt wicks (fig. 17) appear to be consistent with the concept that wicks with larger pores have a larger value of permeability, since the copper felt had a nominal pore size larger than the nickel felt. However, there is a large variation in $1/K_p$ for the nickel felt, indicating a change in flow regime or operation in an inertial flow regime. This would not be expected because the flow per unit area is relatively small. The $1/K_p$ values for copper felt are relatively constant over a large range of flows, indicating operation in a laminar, noninertial flow regime.

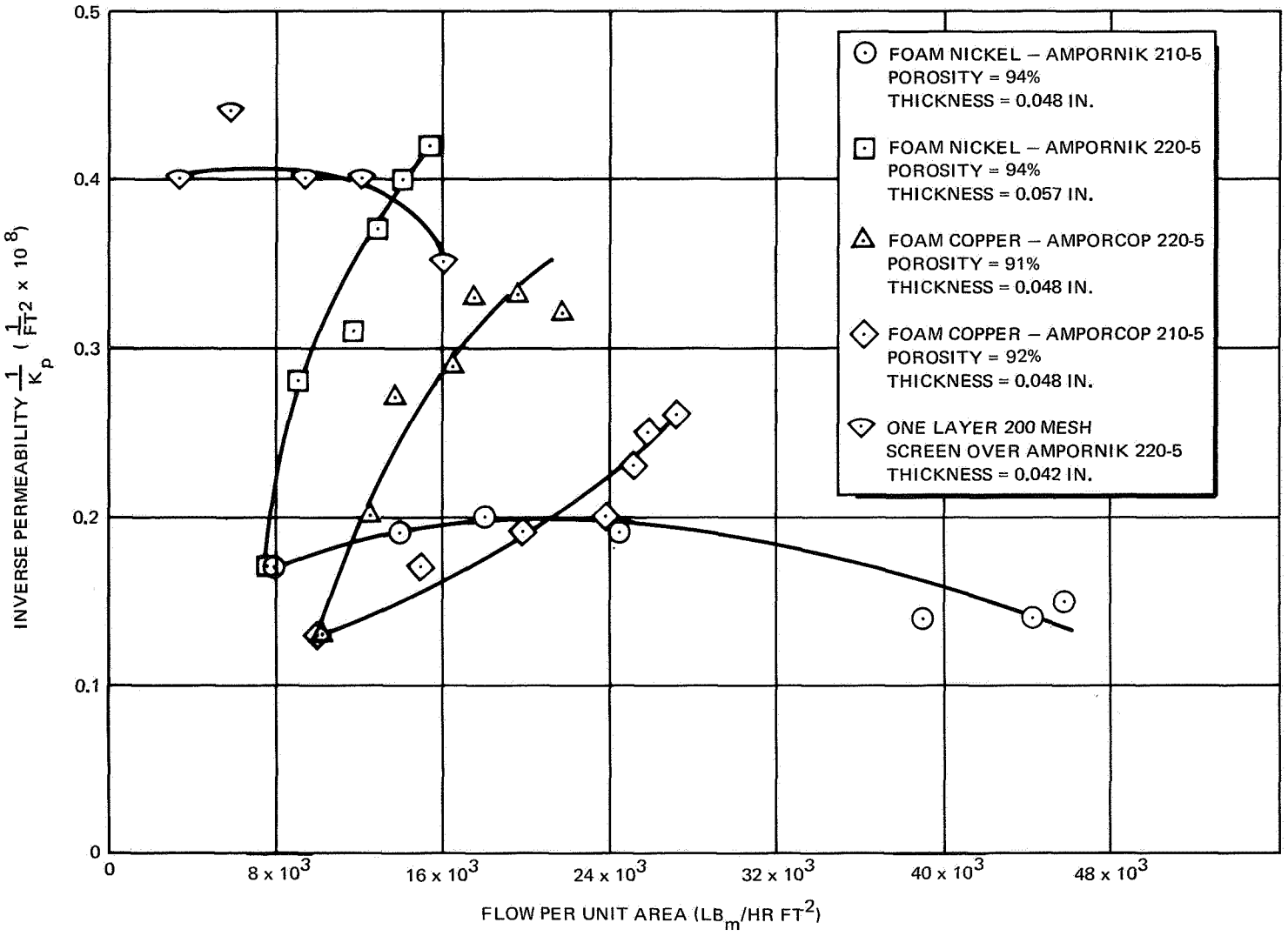

Figure 16. Inverse Permeability Data from Gravity Flow Tests with Methanol and Zero Pressure Difference Across the Liquid-Vapor Interface (i.e., Infinite Meniscus Radius)

TABLE 4

WICK RESISTANCES AS A FUNCTION OF MENISCUS RADIUS

Single layer 200-mesh screen
Thickness = 0.0049 in.
Porosity = 73.3 %

Slope angle (deg)	Chamber pressure (mm methanol)	Resistance $R\left(\frac{1}{ft^3}\right)$	Flow/ width (lb_m/ hr-ft)	Calculated meniscus radius (in.)	Recession depth / wick thickness $\frac{d_r}{t_w}$
30	0	3.7×10^{12}	0.20	∞	0
	30	5.6×10^{12}	0.13	0.0096	0.133
50	0	4.4×10^{12}	0.25	∞	0
	30	6.6×10^{12}	0.17	0.0085	0.139
	80	14×10^{12}	0.079	0.0025	0.282
70	0	4.9×10^{12}	0.29	∞	0
	30	5.6×10^{12}	0.25	0.0178	0.106
	120	17×10^{12}	0.081	0.0020	0.337

Double layer 200-mesh screen
Thickness = 0.0094 in.
Porosity = 72.2 %

Slope angle (deg)	Chamber pressure (mm methanol)	Resistance $R\left(\frac{1}{ft^3}\right)$	Flow/ width (lb_m/ hr-ft)	Calculated meniscus radius (in.)	Recession depth / wick thickness $\frac{d_r}{t_w}$
10					
	30	2.6×10^{12}	0.053	0.0086	0.072
30	0	1.9×10^{12}	0.20	∞	0
	30	3.7×10^{12}	0.10	0.0091	0.071
50	0	2.0×10^{12}	0.30	∞	0
	30	3.1×10^{12}	0.19	0.0093	0.070
70	0	2.3×10^{12}	0.32	∞	0
	30	3.2×10^{12}	0.22	0.0100	0.068

TABLE 5
COMPARISON OF INVERSE PERMEABILITIES MEASURED BY GRAVITY FLOW AND FORCED FLOW TESTS

Wick	Range of $1/K_p$ ($1/ft^2$)		Flow at which $1/K_p$ is compared ($\frac{lbm}{hr.\ ft^2}$)	$\frac{\text{Forced flow}(1/K)}{\text{gravity flow}(1/K_p)}$
	Forced flow permeability test	Gravity flow permeability test		
AmPorCop 210-5	$0.38-.54\times10^8$	$0.13-0.26\times10^8$	20×10^3	2.50
AmPorCop 220-5	$0.35-.46\times10^8$	$0.13-0.32\times10^8$	15×10^3	1.33
AmPorNik 210-5	$0.28-.40\times10^8$	$0.17-0.20\times10^8$	25×10^3	1.82
AmPorNik 220-5	$0.21-.30\times10^8$	$0.17-0.42\times10^8$	14×10^3	1.25
Copper felt	$0.69-.82\times10^8$	$0.37-0.68\times10^8$	10×10^3	1.50
Nickel felt	$1.65-.1.99\times10^8$	$1.08-1.89\times10^8$	3×10^3	1.05

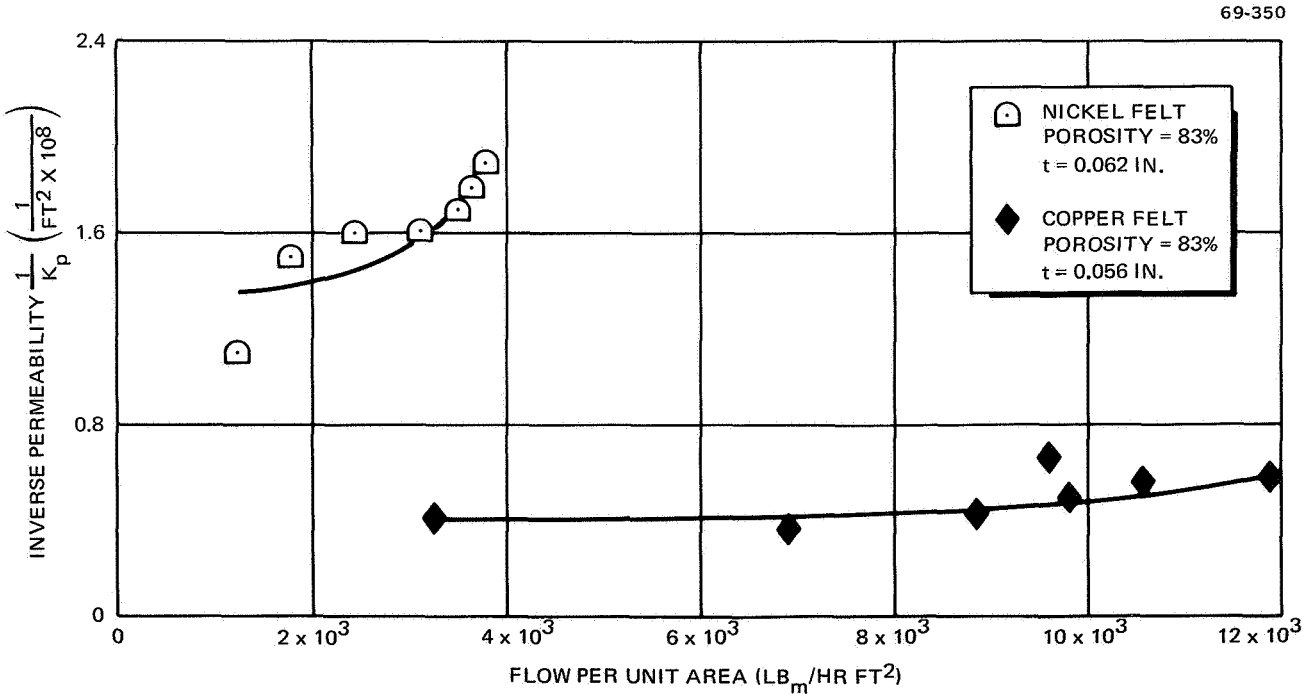

Figure 17. Inverse Permeability Data from Gravity Flow Tests with Methanol and Zero Pressure Difference across Liquid-Vapor Interface (i.e., Infinite Meniscus Radius)

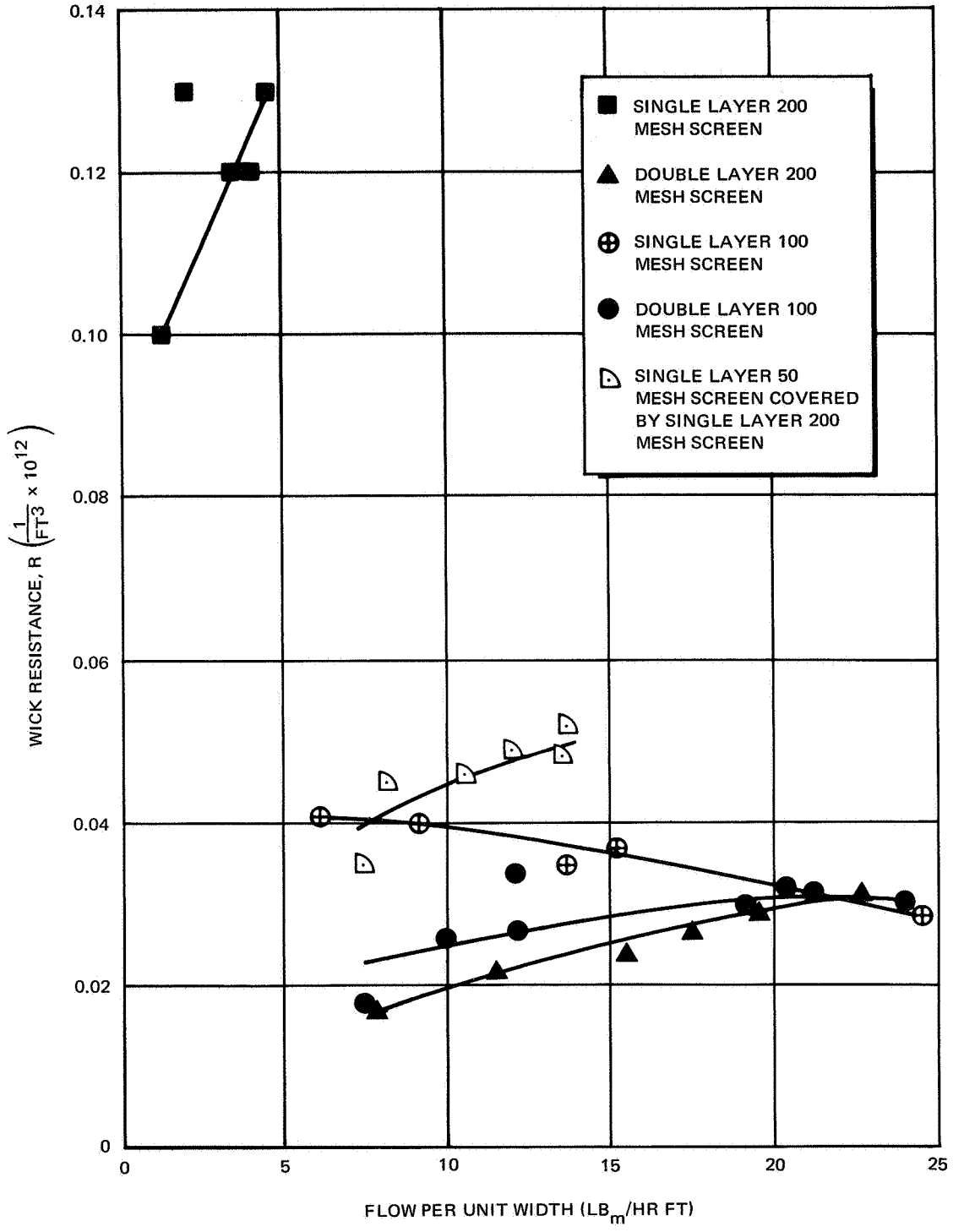

Figure 18. Resistance Data from Gravity Flow Tests with Visible Corner Flow with Methanol and Zero Pressure Difference across Liquid-Vapor Interface, (i.e., Infinite Meniscus Radius)

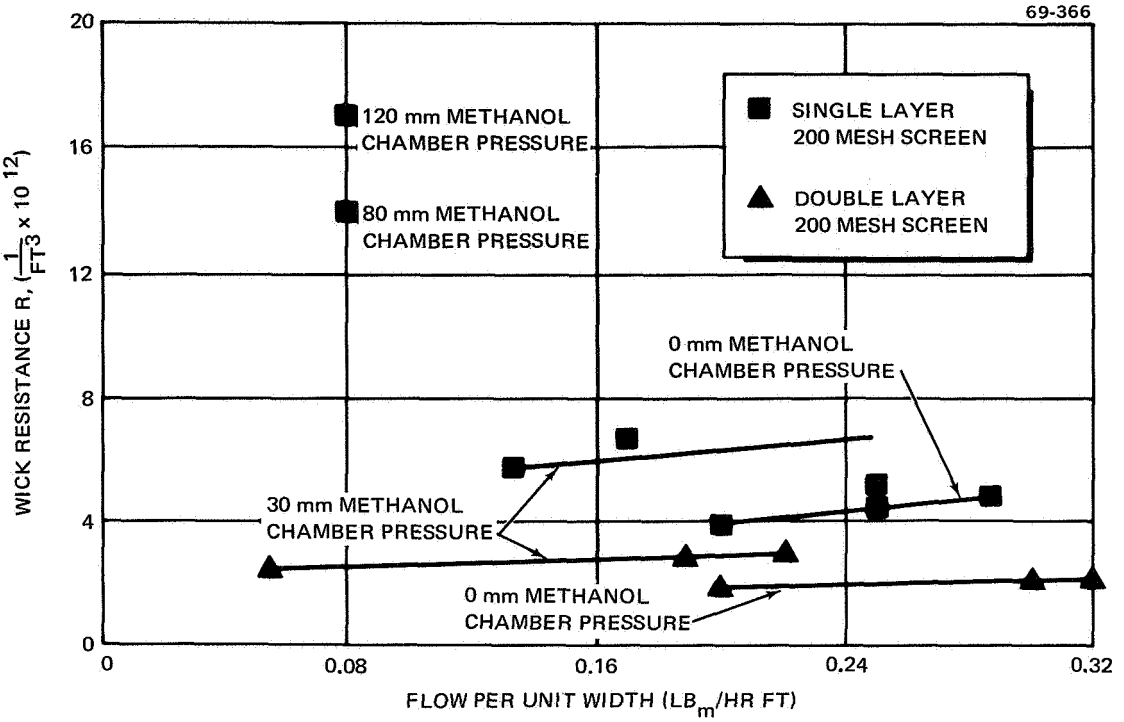

Figure 19. Wick Resistance Data from Gravity Flow Test with Methanol as Functions of Meniscus Radius Due to Pressure Difference Across Liquid-Vapor Interface Caused by Positive Test Chamber Pressure (See table 5)

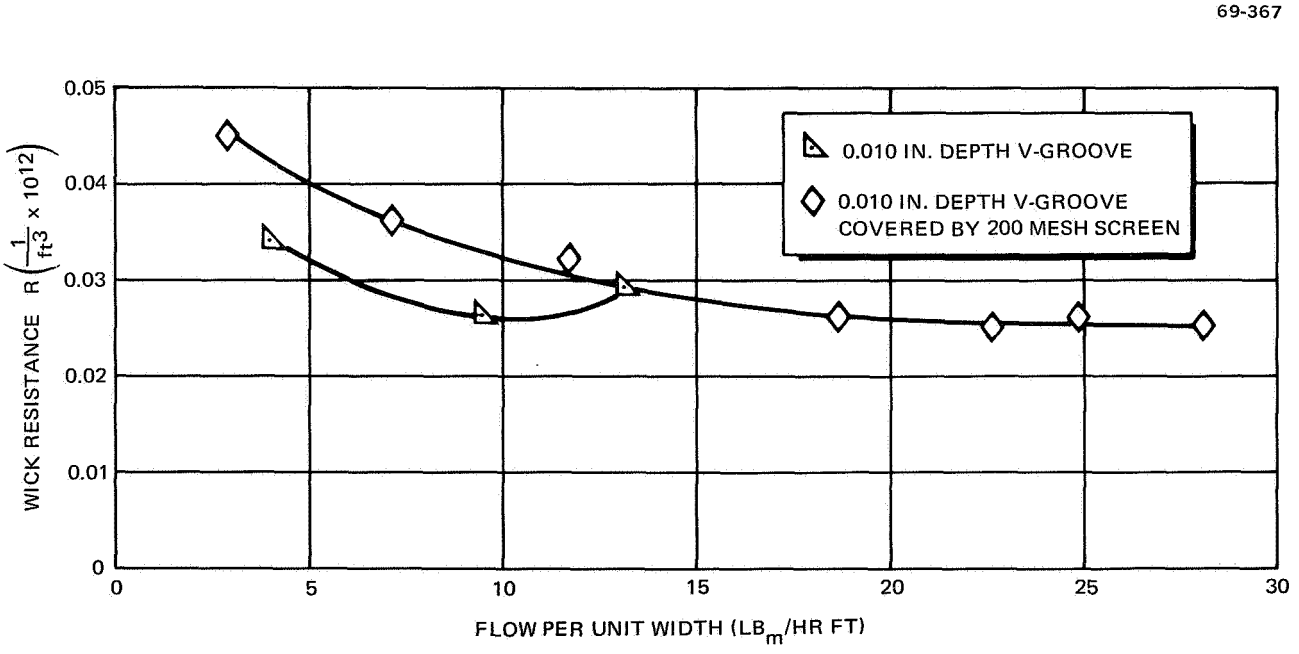

Figure 20. Resistance Data from Gravity Flow Tests with Methanol and Zero Pressure Difference across the Liquid-Vapor Interface (i.e., Infinite Meniscus Radius)

V-groove wicks: Data for V-groove capillary structures (fig. 20) are quite consistent with the correlation between pore size and permeability. The V-groove plate has a larger effective pore size than any of the other wicks. Addition of screen to the top of the V-groove plate results in greater resistance to fluid flow than is found with a free surface.

Meniscus recession test: Test results for screen wicks with gas pressure greater than atmospheric above the wick are shown in figure 19. The permeability of one and two layers of 200 mesh screen is seen to be a very strong function of the meniscus radius. The value of meniscus radius is obtained by measuring the difference in pressure between the liquid and the vapor.

Comparison of $1/K_p$ for forced flow and gravity flow tests: A comparison of inverse permeability $(1/K_p)$ for porous metal wicks which were tested using forced flow and gravity flow test techniques is given in table 5. The disagreement is possibly due to the fact that the comparison is between wicks of different thicknesses and, presumably, corresponding small differences in internal structure. The small differences in porosity between corresponding samples would cause differences opposite to those observed. The fact that the two sets of tests were made with different liquids would not be expected to appreciably influence the comparison, since the only obvious implication--a difference of about 30% in Reynolds number--should not be significant in the range where Darcy's Law is approximately obeyed. Results obtained by the two methods were generally not in agreement.

The differences between the two methods could be accounted for by flow in the fillets as previously mentioned. For forced flow tests, the wicks are completely enclosed and the measured permeability should measure flow only through the porous structure. In the gravity flow tests, a fillet of the type shown in figure A-3, appendix A can cause a bypass and therefore increase the effective permeability of the wick. A detailed discussion of this phenomenon and its effect on the data obtained on both thin screen and thick foam wicks is presented in appendix A. In some of the gravity flow experiments with wetted walls, it was visually observed that fillets of approximately 1/8 in. did exist in the corners. It is shown in appendix A that a fluid rise of 1/8 in. up the wetted wall is not unreasonable.

Because of the above-mentioned discrepancy, the gravity flow permeability apparatus was modified by coating the sidewalls with a commercially available nonwetting Teflon compound called Tefix, manufactured by Wantz Consumer Products, Rockford, Illinois. The substance was applied to the surface with a brush and baked at 350°F. The screen wicks were retested and the permeability was found to be significantly lower. The wick resistance for the wetted wall gravity flow tests are shown in figure 18 and the wick resistance for the nonwetted wall tests are shown in figure 19. The values for zero over-pressure in figure 19 are equivalent to those depicted in figure 18 except that the data presented in figure 19 was obtained using the test apparatus with the Tefix-coated walls. The differences between these two methods can be explained by a corner flow described in appendix A.

Thus, the values of $1/K_p$ in figure 18 are not directly applicable to heat pipe design; only the results in figure 19 should be used. Results of the gravity flow tests with wetted walls are somewhat questionable for reasons discussed previously; preference should be given to the forced flow permeability data. The cross-sectional area of thick wicks is much larger than for thin wicks, and the effect of corner flow is less important--but not insignificant.

Condenser Flow Permeability Test

The permeability of a wick in an operating heat pipe may be determined by measuring the pressure drop in the condenser. The inverse permeability is thus given by equation (13) where $\dot{m}$ is replaced by $Q/2h_{fg}$.

$$1/K_p = \frac{\Delta P_L}{\ell_c} \frac{A_w (2) h_{fg} g_c}{\nu_L Q} \tag{13}$$

where ℓ_c is the length of condenser and Q is the total heat transferred by the heat pipe.

Description of apparatus. - The approach to measuring wick permeability in the condenser of an operating heat pipe was to measure liquid pressure distribution in the wick. Pressure taps were located beneath the wick in the condenser of an experimental heat pipe. Four test assemblies were made with two heat pipes; all were unsuccessful. In each case, a common problem was encountered of accurately sensing the pressure in the wick. A description of the test equipment follows.

The initial heat pipe tested was fabricated of stainless steel with a square cross-section. To facilitate changing of wicks, the pipe was made in two pieces that could be sealed with a gasket as shown in figure 21. The top part of the pipe was a long rectangular box with six thermocouple wells, a valved fill line, and a valved vacuum line. The top section was sealed to the lower section with a flat neoprene gasket. The lower part of the pipe consisted of a tray to which the wick was bonded and to which an evaporator heater was soldered at one end.

Three trays were fabricated; each had one of the following wicks bonded to it: (1) a single-layer 200 mesh stainless steel wick, (2) a nickel foam wick (AmPorNik 220-5) 0.050 in. thick, covered with one layer of 200 mesh screen, and (3) a foam nickel (AmPorNik 220-5) wick 0.100 in. thick. Five 1/16-in. OD stainless steel pressure taps were welded to each tray at the wick-tray interface. The evaporator heat block was a rectangular piece of copper with a 500-W cartridge heater imbedded in it. Dimensions of the contact surface between the block and tray were 1 by 4 in.

The heat pipe was mounted in a test fixture which allowed adjustment of the elevation of one end of the heat pipe above or below horizontal. A burette

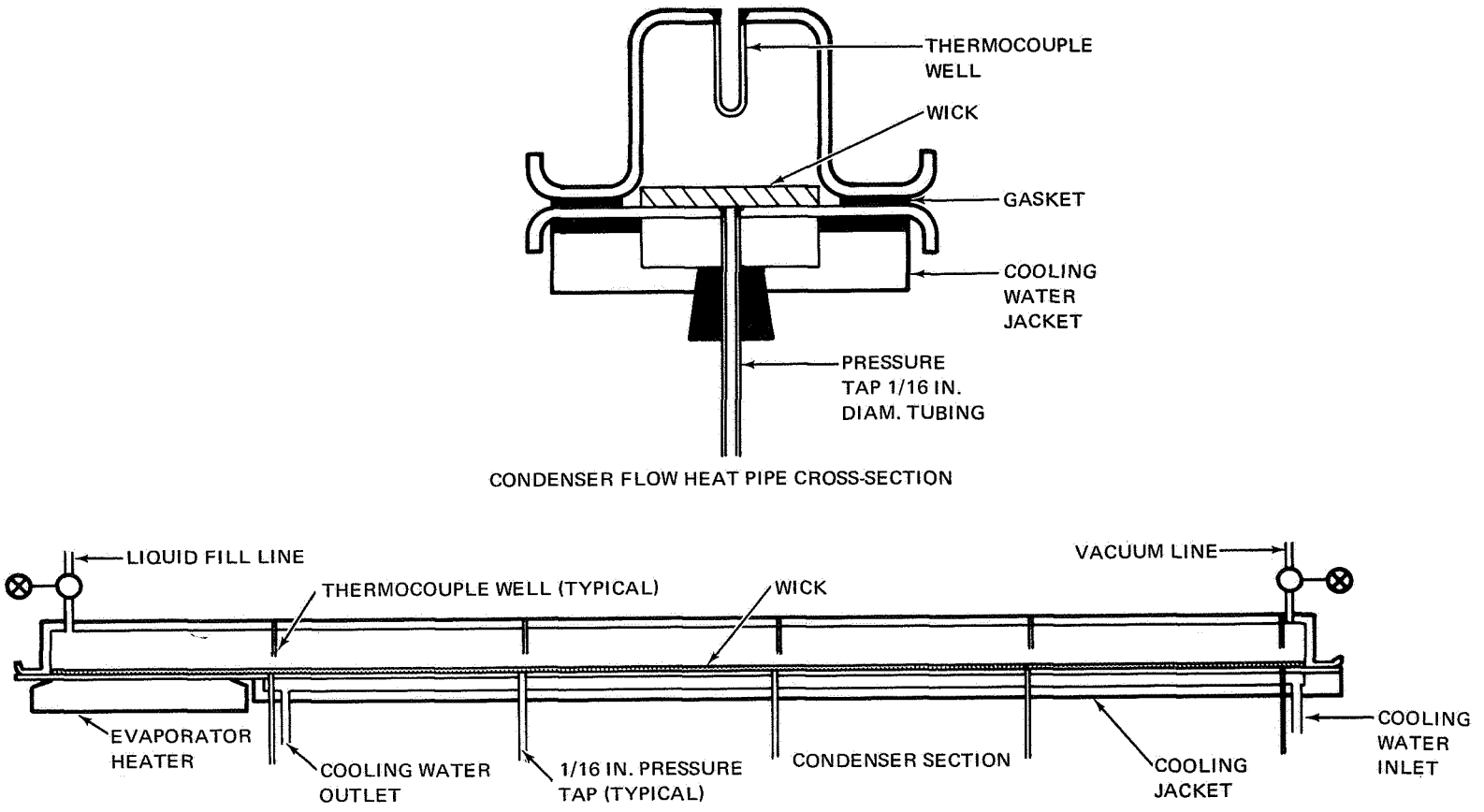

Figure 21. Condenser Flow Heat Pipe

was attached to the fixture and valved to the heat pipe for charging the heat pipe with liquid. A vacuum manifold was fixed to the heat pipe condenser end of the fixture for evacuating the heat pipe or removing accumulated non-condensible gases.

Temperatures were recorded on a Minneapolis Honeywell Series 15 recorder with 24 channels. Copper-constantan thermocouples were used.

The difference in tests was the pressure measuring system. In the first two tests, methanol was the working fluid and pressures were measured with a Statham Model PM 131 transducer with a 0- to 2.5-psi differential pressure range (fig. 22). This transducer could withstand a 25 psi pressure differential which made it practical for use with a heat pipe. In the third test, a five-tube manometer was used for measuring pressures (fig. 23).

Pressures in the initial test were measured with the Statham PM 131 transducer through a valved manifold system. Difficulty was encountered with bubbles in the 1/16-in. -diam tubing connecting the pressure taps in the heat pipe with the transducer manifold. The pressures recorded appeared to drift continually but slowly. Measurement time, using the manifold, was too long to permit measurement of a pressure distribution while the pressures were drifting.

To decrease measurement time, the Scannivalve was substituted for the manifold. Again, the pressures were not stable and bubbles were visible in the pressure lines.

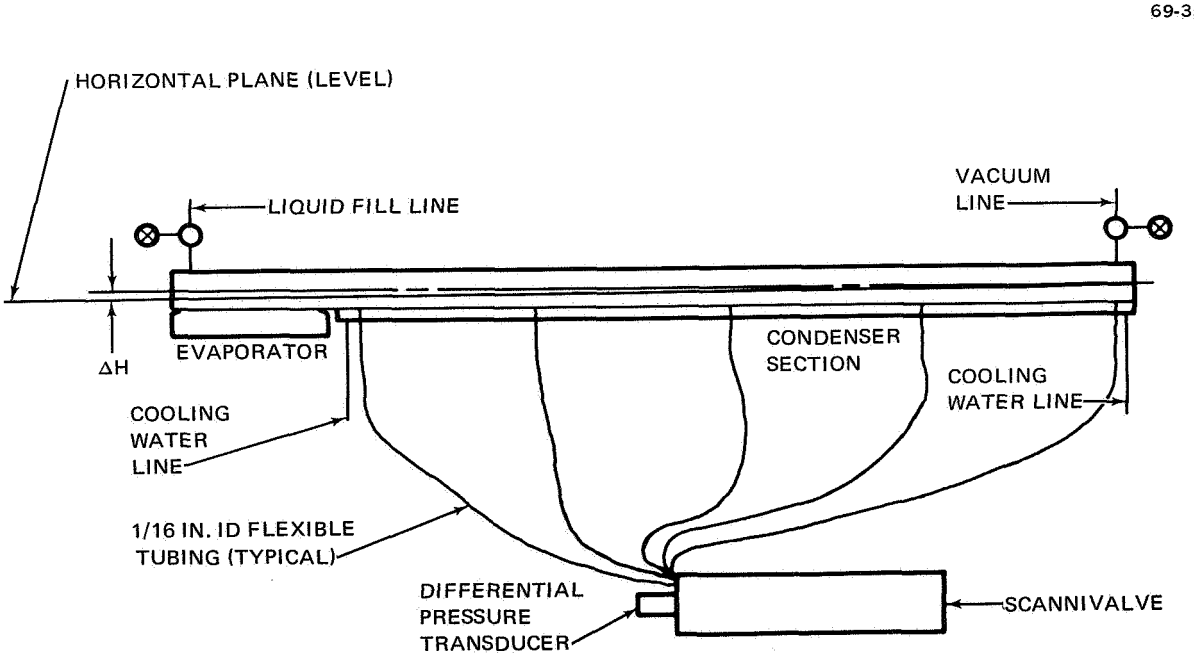

Figure 22. Condenser Flow Test Schematic using Pressure Transducer

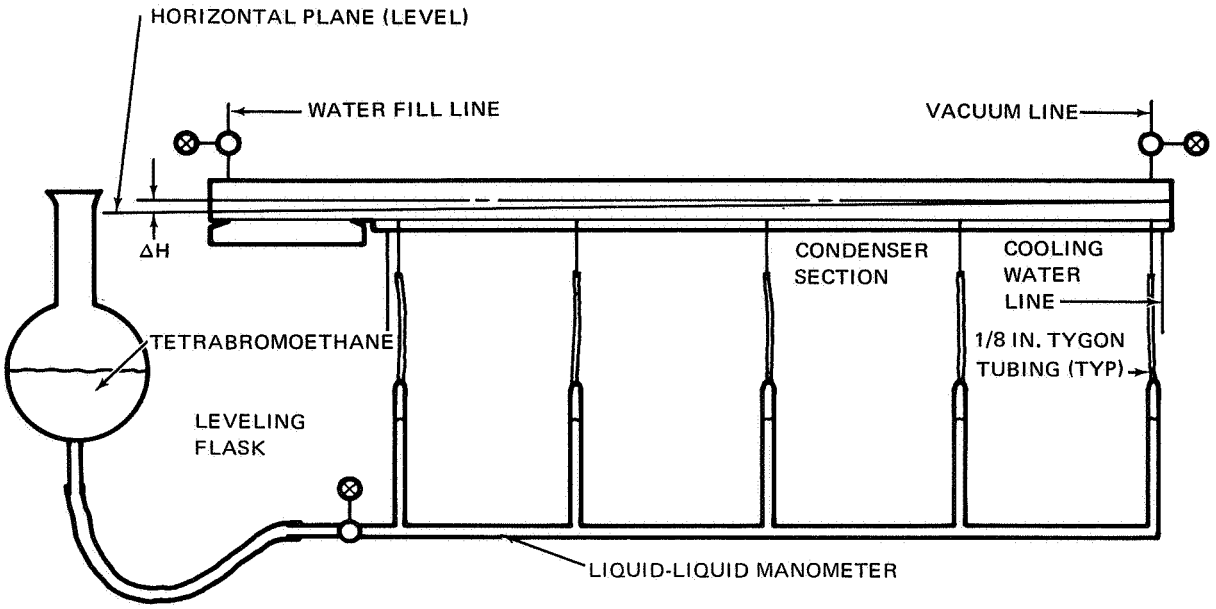

Figure 23. Condenser Flow Test Schematic using Liquid-Liquid Manometer

A liquid-liquid manometer was substituted for the Scannivalve-transducer system and water was used as the working fluid. The tubing between the pressure taps on the heat pipe and the manometer was changed from 1/16-in. to 1/8-in. ID. Tetrabromoethane, with a density of 2.96 g/cc, was used as the manometer fluid and formed a clearly visible meniscus with the water. Once again, bubbles were observed in the system and tubing, though the number was reduced.

A glass heat pipe was constructed to permit observation of the pipe in operation. The casing of the pipe was 18-mm Pyrex tubing with five 1/8-in. ID pressure taps and 2 layers of 100 mesh stainless steel screen for a wick. The pipe was connected to the differential manometer in the same manner used for the metal equipment. In operation, this equipment proved more dependable because anomolous results could be explained visually by a bubble in the connecting tubing or entrapped at the interface between the wicking and the pressure orifice. Bubbles in the tubing could usually be removed by raising the tetrabromoethane level, and those trapped at the orifice disappeared after quick evacuation of the heat pipe.

Test procedures. - The test procedure for the metallic heat pipe consisted of the following steps: (1) cleaning and assembly of the heat pipe, (2) mounting and leveling the heat pipe, (3) assembly of the pressure sensing system, and (4) measurement of pressures, temperatures, and heat input to the operating pipe.

The first step consisted of cleaning the wick and interior of the pipe, and assembling the cleaned components. The cleaning procedure was identical for all tests. Wicks were rinsed in benzene to remove the diffusion pump oil residue of the sintering process. Next, they were cleaned in an ultrasonic cleaner using Freon 113. The wicks were then cleaned with Pasa Jell 105-M (for stainless steel) or Pasa Jell 107-M (for nickel). If a wick was to be used with methanol, the Pasa Jell was rinsed out using hot, boiled, distilled water, and the wick was dried. If it was to be tested with water, the Pasa Jell was rinsed out with hot distilled water, but the wick was kept wet. The interior of the pipe was cleaned with Pasa Jell 105-M, rinsed with distilled water, and dried.

Assembly of the pipe was accomplished by bolting the halves together and mounting the pipe in the test fixture. The pipe was then leveled. The vacuum line, filling burette, and thermocouples were attached, and the pipe was ready for connection to the pressure measuring system.

In the initial test, the pressure tap lines were connected to the pressure transducer through a valved manifold. After these connections were made, pressure tap lines were shut off with pinch clamps, and the heat pipe and vacuum system were leak-checked. When the pipe was leak-tight, vacuum-distilled methanol was injected into the pipe through the burette. In the final step before starting the data run, the pipe was wrapped in foil-backed fiber-glass insulation.

The test was initiated by heating the pipe with hot water in the cooling jacket and depressing the end of the condenser 0.25 in. below the end of the evaporator. Using the evaporator heater, the heat pipe was then heated up to temperatures of 150°F. At each increase in power input, noncondensible gases were removed when necessary, and temperatures and liquid pressures were recorded.

The same procedure was followed for the second test except that the Scannivalve was used for monitoring pressures. The third test was the same as the first and second except that the five-legged manometer was used as the pressure sensor, and vacuum-distilled water was the working fluid.

The test procedure for the glass pipe was similar to that for the metal pipe. When the pipe was level, boiled distilled water was added to the manometer section with no manometer fluid present. Each leg of the manometer was fitted with a pinch clamp on the tygon tubing and a small side-connection for excess fluid outlet. With all pinch clamps closed, manometer fluid was admitted to the manometer one leg at a time by opening the appropriate fluid outlet and releasing excess distilled water. All legs were adjusted to have the meniscus at a known position relative to a reference level indication bar which had been leveled with a surveyor's transit. Once the manometer had been filled, the pinch clamps were left closed. The pipe was evacuated and an appropriate quantity of distilled water added, using a burette connected to the water inlet. Pipe operation was started at low power. Ten thermocouples arranged along the length of the pipe indicated the length of the pipe in operation. As dissolved gases were released from the distilled water, they were concentrated at the condenser end of the pipe

where the vacuum connection was located. When accumulation of gas was indicated by a temperature drop in that end of the condenser, gas was removed as required by opening the vacuum connection, briefly bringing the entire pipe to isothermal operation. At this point, the evaporator section was raised to 0.25 in. above the condenser section, the pinch clamps were removed, and the equipment was in operation. Data were taken by recording the operating temperature of the pipe, the power input, and the heights of the liquid in the five manometer legs relative to the reference bar. After each change in power or operating condition, at least 15 minutes were allowed for equilibrium operation before data were recorded.

Test results. - The test results were erratic and reproducibility for identical runs was poor. Pressures at the five locations in the condenser and the temperature at thermocouple locations indicated in figure 21 were recorded as a function of heat input. A typical pressure distribution is shown in figure 24. The pressure increases in the direction of flow for values of heat input greater than 20 W. The pressure drop decreases as heat input increases. During some tests, the pressure would decrease in the direction of flow for the same test conditions shown in figure 25. The temperature as a function of heat input for various parts of the test apparatus is shown in figure 25. Temperatures increase about as expected. Note that for Q = 0 W, the condenser section is actually acting as an evaporator and supplying heat from the circulating water to the heat pipe. It is a small amount, however, and certainly not enough to account for the large pressure drop at Q = 0 W. In any event, the pressure drop should be in the other direction if the condenser is acting as an evaporator.

Both of these effects are anomalous and incapable of explanation by any presently accepted theories of heat pipe operation. It is suspected that the pressure measuring technique was the source of the error that prevented useful data from being obtained. The nonreproducibility of results for a given set of test conditions lends credence to this supposition.

Bubbles were observed in the pressure tap lines and other parts of the system. Vapor bubbles in the pressure-sensing taps and lines change the pressure head because of the decreased density of the column and, consequently, the indicated pressure. These bubbles could have easily agglomerated in a position between the wick and the pressure tap opening. In such a condition, the liquid pressure characteristic at that position along the wick could not be transferred to the pressure line leading to the transducer. Thus, pressures measured at some taps could be erroneous while pressures measured at others might be accurate. The net effect could be pressure distributions similar to those shown in figure 25.

Comparison of $1/K_p$ and R with Data of Other Experimenters

A summary of DWDL data for $1/K_p$ and R for various wicks is contained in tables 6 and 7 along with values for $1/K_p$ obtained by Kunz, et al. for several wicks. Table 7 also contains values of $1/K_p$ based on equation 11 for comparison with values in table 6. In all cases, data included in the table

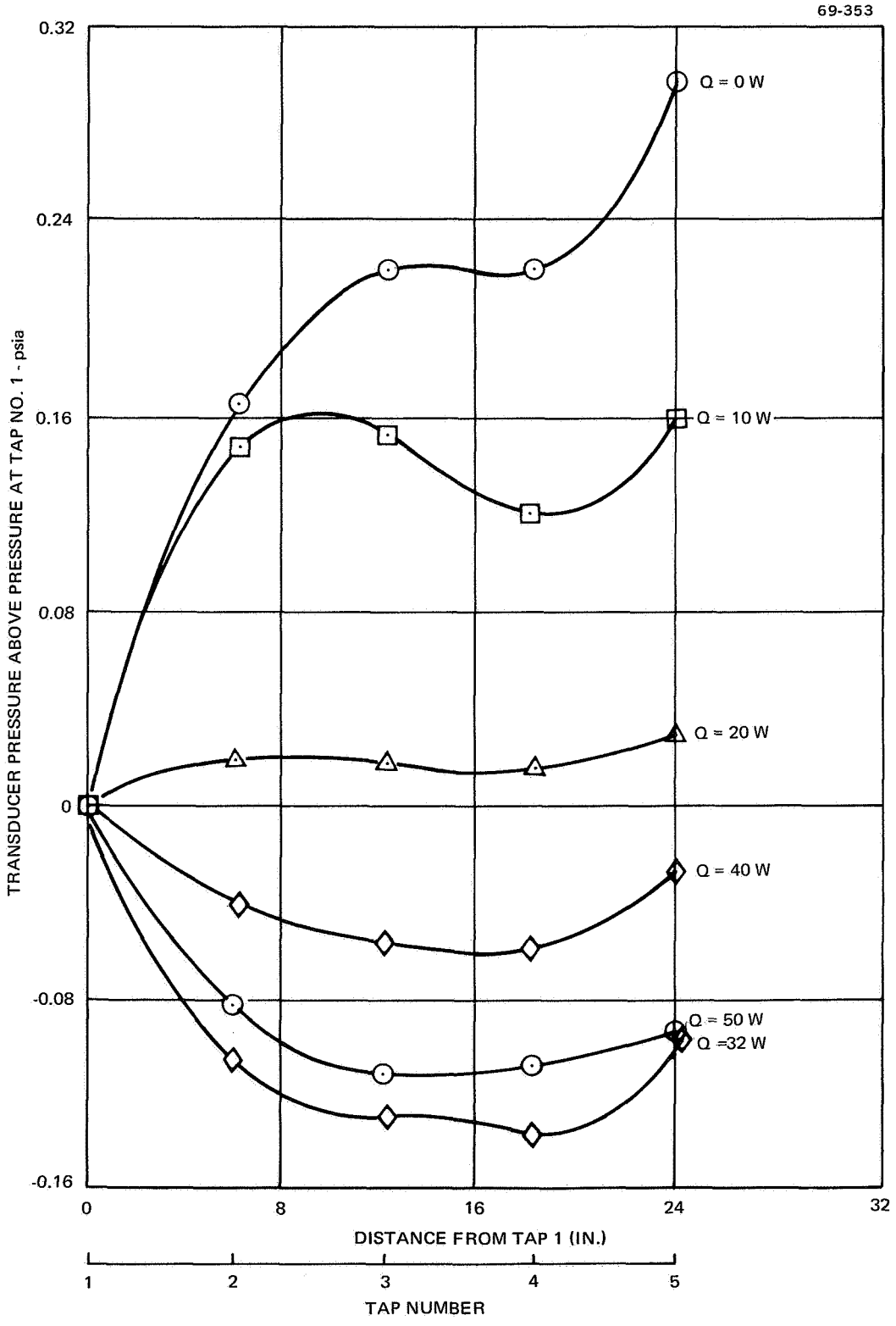

Figure 24. Typical Pressure Profile for AmPorNik 220-5 Covered by One Layer of 200 Mesh Screen with Methanol (Condenser Permeability Test) (Pressure Tap 1 is Closest to the Evaporator and Tap 5 is Farthest from Evaporator)

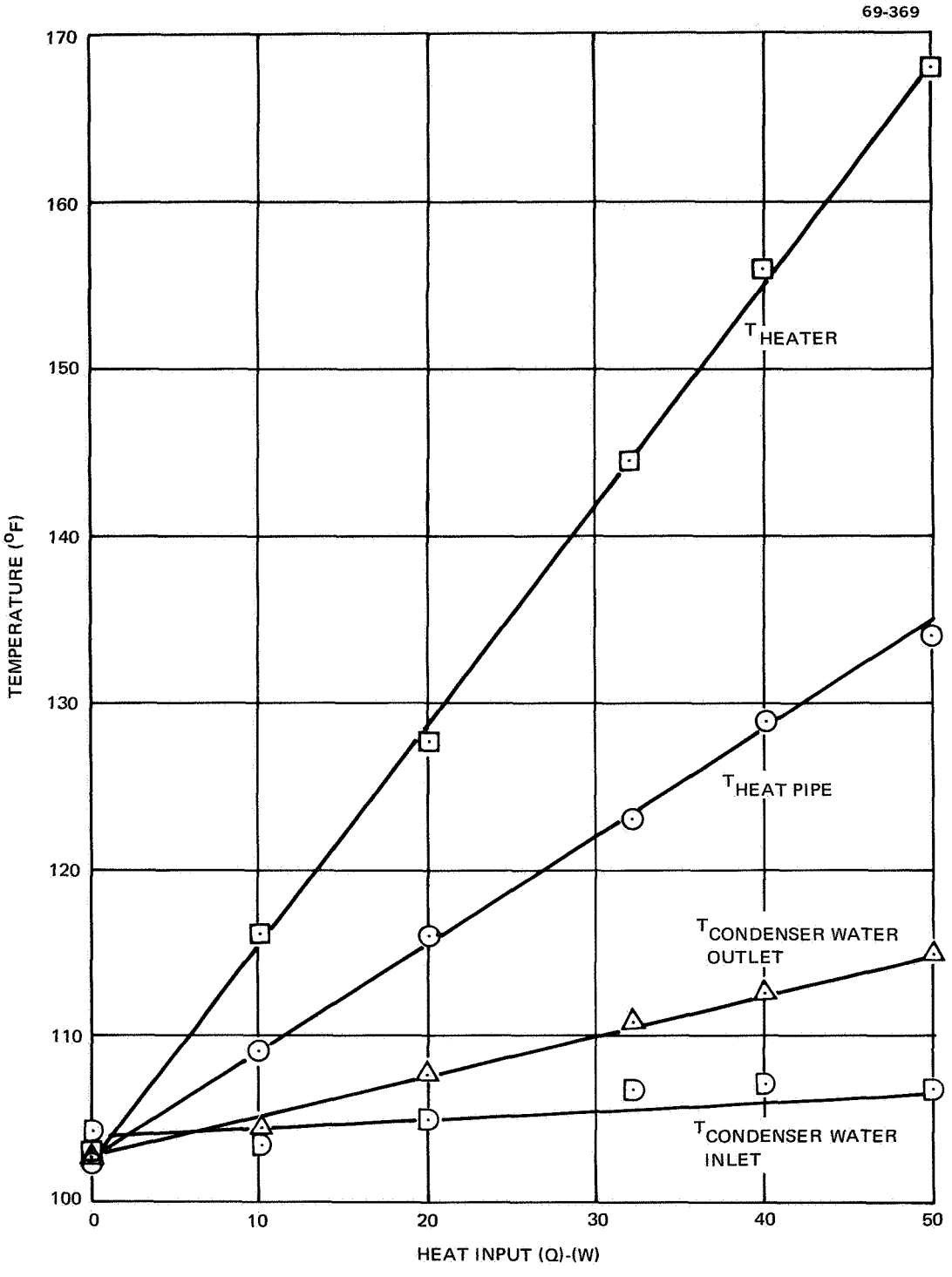

Figure 25. Temperature vs Heat Input for Condenser Permeability Test

TABLE 6

INVERSE PERMEABILITY FOR WICK MATERIALS
FROM FORCED FLOW TESTS
(Defined in equation 11)

No.	Wick	Experimenter	Porosity (ε)	Inverse permeability Midrange value ($1/K_p$ - $1/ft^2$)
1	AmPorCop 210-5 (foam)	DWDL	0.945	0.46×10^8
2	AmPorCop 220-5 (foam)	DWDL	0.912	0.40×10^8
3	AmPorNik 210-5 (foam)	DWDL	0.944	0.34×10^8
4	AmPorNik 220-5 (foam)	DWDL	0.960	0.25×10^8
5	Copper felt	DWDL	0.895	0.75×10^8
6	Nickel felt	DWDL	0.891	1.8×10^8
7	Nickel felt (H1)	Kunz et al. (ref. 10)	0.836	21.2×10^8
8	Nickel felt (H3)	Kunz et al.	0.689	61.3×10^8
9	Nickel sintered powder (M2)	Kunz et al.	0.645	3.4×10^8
10	Nickel sintered 200 mesh screen	Kunz et al.	0.651	12.0×10^8

TABLE 7

WICK RESISTANCE FROM GRAVITY FLOW TESTS FOR SCREEN AND V-GROOVE WICKS AS DEFINED IN EQUATION 12

(Tests with methanol)

No.	Wick	Experimenter	Resistance Midrange value ($R\text{-}1/ft^3$)	Comments
7	One 200 mesh SS screen	DWDL	4.3×10^{12} ($1/K_p = 17 \times 10^8$)	0 chamber pressure (gage) $d_r/t_w = 0$ methanol
8	Two 200 mesh SS screen	DWDL	2.1×10^{12} ($1/K_p = 16 \times 10^8$)	0 chamber pressure (gage) $d_r/t_w = 0$ methanol
9	One 200 mesh SS screen	DWDL	6.0×10^{12} ($1/K_p = 25 \times 10^8$)	30-mm methanol chamber pressure (gage) $d_r/t_w = 0.13$ methanol
10	Two 200 mesh SS screen	DWDL	2.8×10^{12} ($1/K_p = 22 \times 10^8$)	30-mm methanol chamber pressure (gage) $d_r/t_w = 0.07$ methanol
11	One 200 mesh SS screen	DWDL	14.0×10^{12} ($1/K_p = 59 \times 10^8$)	80-mm methanol chamber pressure (gage) $d_r/t_w = 0.28$ methanol
12	One 200 mesh SS screen	DWDL	17.0×10^{12} ($1/K_p = 70 \times 10^8$)	120-mm methanol chamber pressure (gage) $d_r/t_w = 0.34$ methanol
13	0.010-in.-deep V-groove	DWDL	0.028×10^{12}	Methanol
14	0.010-deep V-groove with 200 mesh screen	DWDL	0.030×10^{12}	Methanol

from the present program is that for which the test is thought to be most valid. Thus, values for foam and felt are from the forced flow permeability test and data from the screens are from the gravity flow test with nonwetted sidewalls. Data from the V-groove wicks are included in the table even though these data were obtained from the wetted-wall gravity flow test; they should be used with caution. All $1/K_p$ and R values are about midway between the extremes of the range of values. For detail design, actual values for a given flow should be used as depicted in figures 9, 10, 19, and 20.

It is of interest to compare the values of permeability obtained for infinite meniscus radius with the permeability as calculated by Schmidt's equation (ref. 12):

$$\frac{dp}{dz} = - \frac{\rho V_o^2}{D_P} \frac{1-\varepsilon}{\varepsilon^3} \left(\frac{275}{Re} + \frac{6.25}{2} \right) \tag{14}$$

where

$\frac{dp}{dz}$ = pressure gradient = $\frac{\Delta P}{\ell}$

D_P = 1.5 times the screen wire diameter

V_o = liquid flow velocity averaged over wick

$$Re = \frac{D_P V_o \rho_L}{\mu} \left(\frac{1}{1 - \varepsilon} \right)$$

The other parameters are defined in the nomenclature list. Using Schmidt's equation, calculated values of K_p are about twice as large as the measured values presented in figure 19 for zero gage pressure in the chamber above the wick. This is not surprising because Schmidt's equation is based on data for several layers of screen enclosed in an apparatus with no free surface. Schmidt's equation does correlate the 50- and 200-mesh multiple-layer screen tests of Kunz, et al. (ref. 10), but it predicts a value approximately 100% too large for the 100-mesh screen test.

Another interesting comparison may be made between the 200 mesh screen values of Kunz and those of the present work. The value of $1/K_p$ for many layers of sintered 200 mesh screen (table 6) is less than the values for either one or two layers of 200 mesh screen (table 7) obtained during the present program. Thus, an extrapolation, based on assumed constancy of $1/K_p$ as the number of layers is increased, is not valid, and the reasoning for presenting wick resistance in terms of R rather than $1/K_p$ is justified.

Summary and Conclusions

The permeabilities of various metal foam, metal felt, and screen wicks were measured by three techniques: (1) forced flow testing, (2) gravity flow testing, and (3) measurement of condenser pressure drop at a known heat input for an operating heat pipe.

Forced flow permeability tests. - The forced flow permeability test proved to be a relatively easy method of obtaining reproducible permeability results. A wick was put in a closed container with all but the end surfaces of the wick in contact with containing walls; and water was flowed through the wick. The flow and the pressure drop along the flow length were measured. As flow increased, inverse permeabilities calculated from the measured properties were observed to increase, indicating that a Darcy's Law correlation is not entirely valid for these wicks throughout the range of flows tested. Values of $1/K_p$ ranged from 0.25×10^8 to 0.46×10^8 for the foams and 0.75×10^8 to 1.8×10^8 for the felts.

Gravity flow permeability tests. - A device for testing a wick with a free surface was constructed and tested. The flow was induced by tilting the apparatus. Results were erratic until it was discovered that a flow fillet was forming in the corner of the sidewall enclosing the wick; this resulted in a fluid bypass of the wick, and resultant calculated inverse permeabilities were too low. The device was modified by coating the sidewalls with a nonwetting substance that prevented flow fillets from forming. The modified apparatus was used for testing one and two layers of 200 mesh screen. These wicks were found to have a higher resistance to fluid flow than multiple layers of sintered screen tested by Kunz et al. (ref. 10).

The gravity flow device was also used for testing the effect of meniscus depth on wick resistance. For example, the resistance of one layer of 100 mesh screen as defined by equation (12) was observed to increase from 4.3×10^{12} to 17.0×10^{12} as the ratio of meniscus recession depth to wick thickness increased from 0 to 0.34.

Condenser flow permeability tests. - The determination of wick permeability by the measurement of pressures and heat inputs in an operating heat pipe was beset by difficulties because of problems associated with the pressure measuring system. Generation of bubbles and their subsequent agglomeration in the region of pressure taps caused anomalous results.

EVAPORATOR HEAT FLUX TESTS

The purpose of these tests was to determine heat transfer rates in wicks supplied with fluids via a tube artery and to better understand the heat transfer process.

A tube artery has not been used in previous fundamental wick heat transfer studies; its use is unique to the DWDL tests. A tube artery provides a low-resistance path for returning the working fluid from the condenser section of a heat pipe to the evaporator section. Theoretically, use of an artery provides a means for increasing the fluid flow and evaporator heat flux for a given wick capillary pressure head. Practically, however, flow in the artery can be easily reduced or stopped if bubbles accumulate. Consequently, the maximum heat flux that can be attained in a given wick can be reduced by improper use of an artery. These tests demonstrate that with the type of

artery used, vapor accumulation is a problem that contributes to reduction of the maximum heat flux a wick can sustain. Therefore, the use of barriers to prevent vapor accumulation was studied during these tests.

The DWDL program also differs from previous wick heat transfer studies in that the tests were conducted at low saturation vapor pressures (e. g. 1 psia for water). The maximum heat flux a wick can sustain under nucleate boiling conditions may be a function of the environment pressure. In pool boiling without a wick, the bubble departure diameter significantly increases with reduced environment pressure. Consequently, if heat transfer characteristics of the surface beneath the wick are unaffected by the presence of the wick, large bubbles may spread through the wick at low pressures and significantly affect the maximum heat flux. This effect was studied during the tests.

Test Description

Description of equipment. - The test device consisted of the following components assembled in a 4-in. Pyrex tee as shown in figures 26 and 27: (1) electrical-resistance heater block, (2) wick, (3) artery, (4) liquid reservoir, (5) liquid-leveling flask, (6) condenser, and (7) instrumentation. Three fluids were used: water, methanol, and butanol.

A copper heater block, 1 in.^{2} x 4 in. long, was swaged over a 3/4-in. -diam, 5-kW electrical resistance heater with a 4-in. heated length. The wick was diffusion-bonded to a 0. 025-in. -thick stainless steel plate and soft-soldered to the heater. The sides of the wick were sealed with epoxy resin to prevent horizontal vapor flow from the wick. Two strips of 0. 013-in. -thick nickel foam with a pore diameter of less than 0. 001 in. were located on the top of the wick to act as vapor barriers between the wick and the artery. Two foam strips were used to provide enough thickness of foam to yield in compression and form seals with the artery and the wick. As long as both the foam and wick are wetted, the foam acts as a barrier to vapor from the wick. This is because the pore size of the foam (0. 001 in. maximum diameter) is much smaller than that for any of the wicks tested (i. e. 0. 0028 in. pore diameter for 200 mesh screen), and the vapor follows the path of least resistance (through the wick, bypassing the foam). The flow resistance of these nickel foam strips is negligible except in the case of some tests with butanol. It is possible that the maximum heat flux limitation of some of the tests with butanol was caused by the flow resistance of the nickel foam strips.

The artery was a composite structure consisting of a 0. 252-in. - OD tube clamped to the wick and joined to a second tube by a flexible coupling. The second tube was connected to a liquid reservoir. Liquid flowed from the artery to the wick through a 0. 020- x 4-in. slit in contact with the vapor barriers on the wick. A 1/16-in. -diam stainless steel tube was connected to the sealed end of the slitted artery, passed through a seal in the flange, and was connected to a vacuum system to act as a pump-out tube during charging of the artery with liquid.

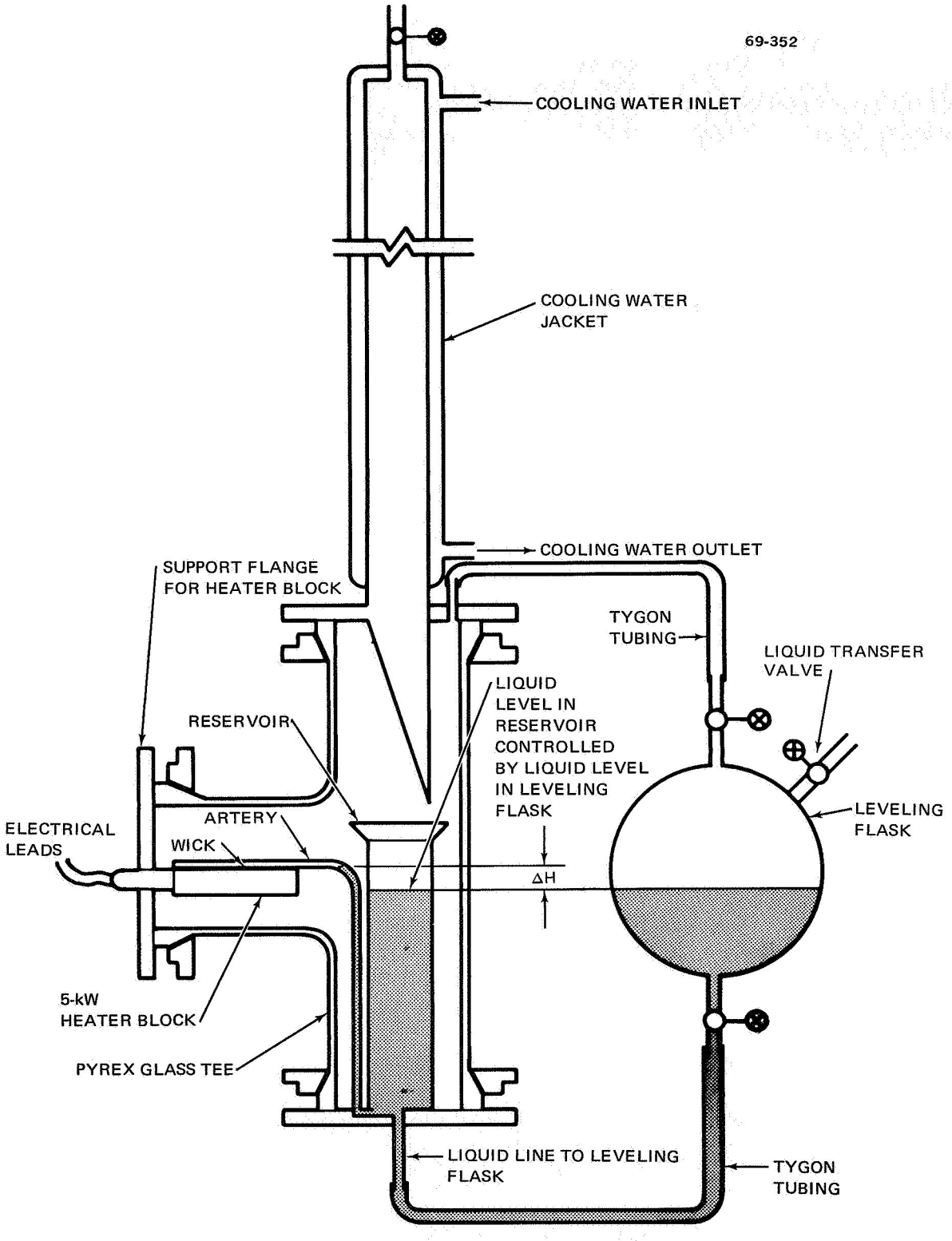

Figure 26. Evaporator Heat Flux Test Device

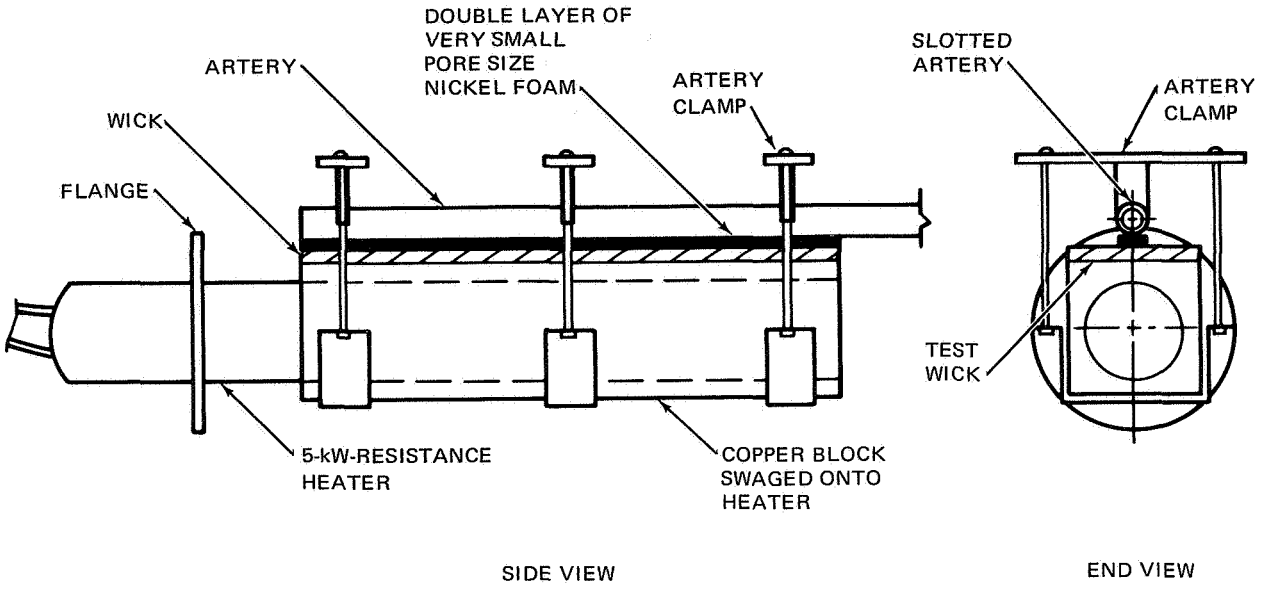

Figure 27. Evaporator Heat Flux Test Device Heater Block, Wick, and Artery Assembly

Two systems were used to connect the artery to the liquid reservoir. The first consisted of a copper tube, an O-ring sealed flange, and a metal bellows flexible joint. This was replaced by a glass tube using Latex surgical tubing as the flexible joint to the liquid reservoir.

The liquid reservoir consisted of a flared-lip tube situated under the condenser to receive the condensate. The level in the reservoir was controlled by an external leveling flask connected on the liquid side to the reservoir, and on the vapor side to the vapor volume of the test device.

The vertically mounted condenser was water-cooled and wickless to enable gravity return of the condensate. A vacuum valve was situated at the top of the condenser so that noncondensible gases could be removed.

Thermocouples were attached to the heater block, wick surface, artery, and inner face of the flange holding the heater block; one was exposed only to the vapor in the chamber.

The test chamber was a 4-in. Pyrex pipe tee. One leg of the tee was oriented horizontally, and contained the heater and wick assembly in a horizontal position. The cross of the tee was vertical, with the condenser in the upper leg and the liquid reservoir in the lower. The surface of the tee was wound with electrical-resistance heater tape to allow temperature control of the test chamber. Thermocouples were attached to the outer surface.

External test equipment included electrical power supplies, a temperature recorder, a vacuum distillation heat pipe, and a vacuum system. Two electrical power sources were used; a 150-W Electronic Measurements Regotran dc power supply and a 10-kW Harrison Model 6483A dc power supply. A Minneapolis-Honeywell Series 15 24-channel temperature recorder and copper-constantan thermocouples were used to record temperatures. The vacuum distillation heat pipe consisted of a 1000-ml flask with a 4-ft-long neck closed by a stopcock. The vacuum system was a 15 ft^3/min mechanical vacuum pump in conjunction with two liquid-nitrogen cold traps.

Test procedure. - Preparation of the wick and test device was as follows: (1) wick installation, (2) wick cleaning, (3) evacuation of the test device, (4) vacuum distillation of the test fluid, and (5) filling the device with test fluid. The wick was bonded to a 0.025-in.-thick stainless steel plate as described in appendix C; then, the plate was soft-soldered to the heater block. After installation, the edges of the wick were sealed with epoxy resin to prevent vapor escape from the wick except through the thickness of the wick as in a heat pipe. When the epoxy resin had set, the wick was cleaned by treating with the following liquids: (1) for stainless steel, Pasa Jell 105-M, (2) for nickel, Pasa Jell 107-M, and (3) for stainless steel and nickel, Pasa Jell 107-M. For tests run with water, the wick was left wetted after rinsing with distilled water.

When butanol or methanol was used as the working fluid, the wick was rinsed in distilled water, then in isopropyl alcohol, and dried. After cleaning, six thermocouples were spotwelded to the upper surface of a screen wick or imbedded in the upper surface of a foam or felt wick. The wick, heater, and flange assembly was installed in the horizontal leg of the Pyrex tee. The artery was connected to the liquid reservoir, after which final seals were made.

Prior to charging with test fluid, the device was evacuated through a liquid nitrogen cold trap to the limit of the vacuum pump. When pressure was at a minimum, the leveling flask was separated from the test device by valves and then connected to the outlet of the vacuum distillation heat pipe.

The vacuum distillation heat pipe was used to remove dissolved noncondensable gases from the test fluid. The fluid was placed in the heat pipe with the flask at the bottom and the condenser vertical. The pipe was heated and noncondensable gases were withdrawn by a vacuum pump through a liquid nitrogen cold trap. When the heat pipe operated with no cold zone at the top of the condenser (indicating that all noncondensable gases were removed), the heat pipe was connected to the leveling flask and the interconnecting line was evacuated to prevent contamination of the fluid during filling of the leveling flask.

The leveling flask was filled using either of two procedures. One was to open the interconnecting valves between the heat pipe and flask, and distill the fluid into the flask. The second was to open the interconnecting valves and raise the heat pipe, allowing the liquid to flow under gravity. After all liquid was transferred, the flask was valved-off from the heat pipe and

the vent line was opened to the test device. When the test device and leveling flask reached equilibrium pressure, the liquid was allowed to flow from the leveling flask into the liquid reservoir.

The artery was charged by raising the leveling flask until the artery was filled and the wick saturated. The leveling flask was then lowered until the liquid level was at the same elevation as the upper surface of the wick. The artery pump-out tube was briefly opened to vacuum, drawing out any trapped vapor bubbles. The evaporator heat flux test device was then ready for testing.

Tests were conducted at two vapor temperatures and three pressure heads against which the wick pumped. Test temperatures were 100° and 150°F as determined by a thermocouple located in the vapor space above the wick. At each temperature, tests were performed with the liquid level at the surface of the wick, and at 1/2 in. and 1 in. below the surface of the wick.

Under each set of test conditions, all components of the device with the exception of the condenser and leveling flask were heated to the test temperature. The test pressure head was set by moving the leveling flask to the proper elevation. Power was applied to the wick heater in small, uniform increments. After each incremental increase, the system was allowed to come to thermal equilibrium. Power was increased in this manner until burnout occurred. Burnout manifested itself by complete wick drying, a sudden excursion in heater block temperature, or vapor blockage of the artery with the vapor proceeding from the wick. In tests with an all metal artery, burnout was inferred from heater block temperatures and appearance of the wick. With the use of a glass artery, the occurrence and origin of bubbles in the artery could be observed.

Heat fluxes were determined by subtracting the heat losses from the power input to the heater. From the measured temperature of the heater block, vapor, flanges and container of the test device, the heat losses by conduction, convection, and radiation were calculated.

During the tests, the temperature of the test device and vapor was controlled by varying the heat input to the flanges and tee, and by controlling the water flow around the condenser. During some tests, bubble formation was observed in the artery away from the wick. These bubbles were removed with the vacuum system through the artery pump-out tube.

Discussion of Results

Results of the evaporator heat flux tests are shown in figures 28 through 44. Each figure gives the heat flux vs ΔT_{sat} for a particular wick and fluid at various liquid heads and a narrow range of saturation pressures. The results for experiments 1 through 8 and 123 through 128, which were for a wick consisting of one layer of 200 mesh stainless steel screen, are not shown because an accurate ΔT_{sat} could not be measured. However, the maximum heat flux attained is shown in table 8.

Liquid head.-The liquid head given in the figures refers to the vertical distance (in inches) between the top of the wick and the liquid level in the reservoir. For instance, a liquid head of -1 in. means that the liquid level in the reservoir is 1 in. below the top of the wick; and that the liquid must be pumped up through the artery (by the wick capillary pressure) to 1 in. above the liquid level in the reservoir. For a given maximum wick capillary pressure, the liquid flow to the wick (burnout flow) should decrease as the liquid head becomes more negative.

Careful examination of the data reveals that for these tests, under the conditions imposed, there is no clear dependence of Q/A on the liquid head. Only the data given in figure 34 show an apparent dependence on liquid head. However, considering that no other tests show this dependence, the variation shown in figure 34 may actually be due to surface conditioning which is discussed later. In these tests, the expected effect must be masked by more dominant mechanisms (e. g. bubble blockage of the wick). It is worth noting that Costello and Redecker (ref. 7) observed no change in Q/A with liquid head until the head decreased below -3. 75 in. ; they boiled ethanol in wicks.

Maximum heat flux.- The maximum heat flux given in the figure legends corresponds to the value at which burnout occurred. Equilibrium was never reached at these values. The last equilibrium heat flux obtained in each experiment is the highest data point plotted, and the actual maximum heat flux lies between this value and the maximum value given in the legend. In many cases, the difference is very small since small increases in heat flux were used.

69-371

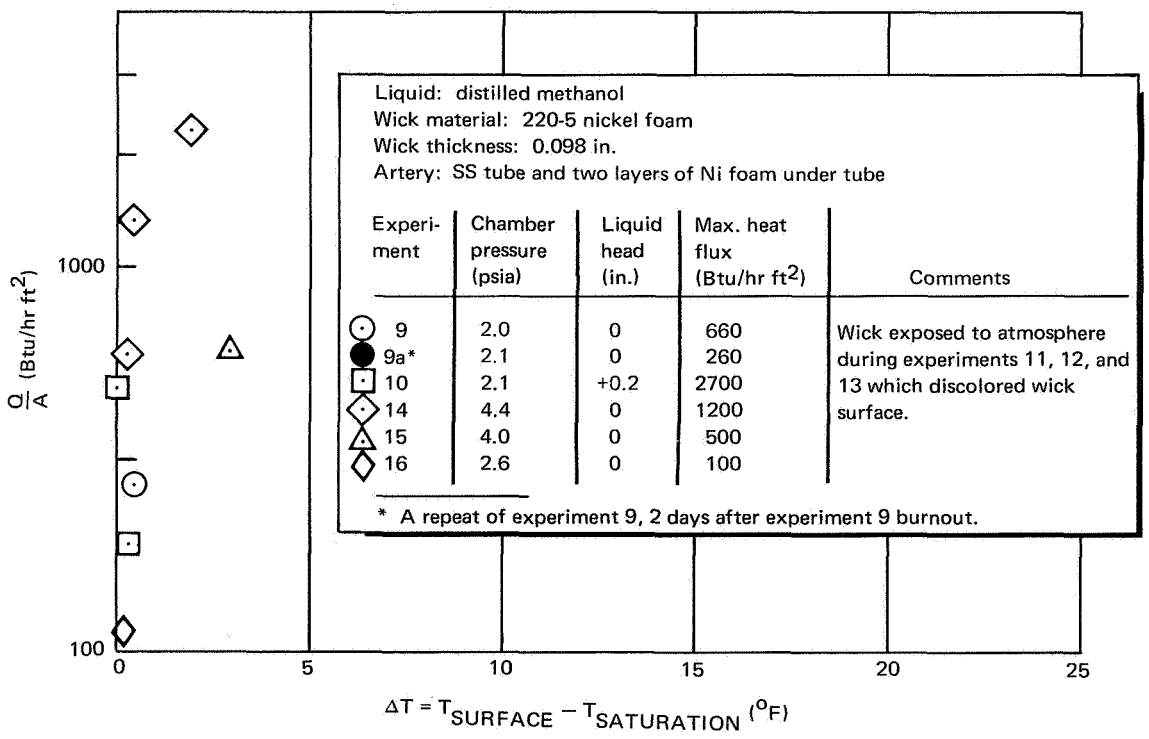

Figure 28. Experimental Results for Distilled Methanol and 0.098-In. Nickel Foam

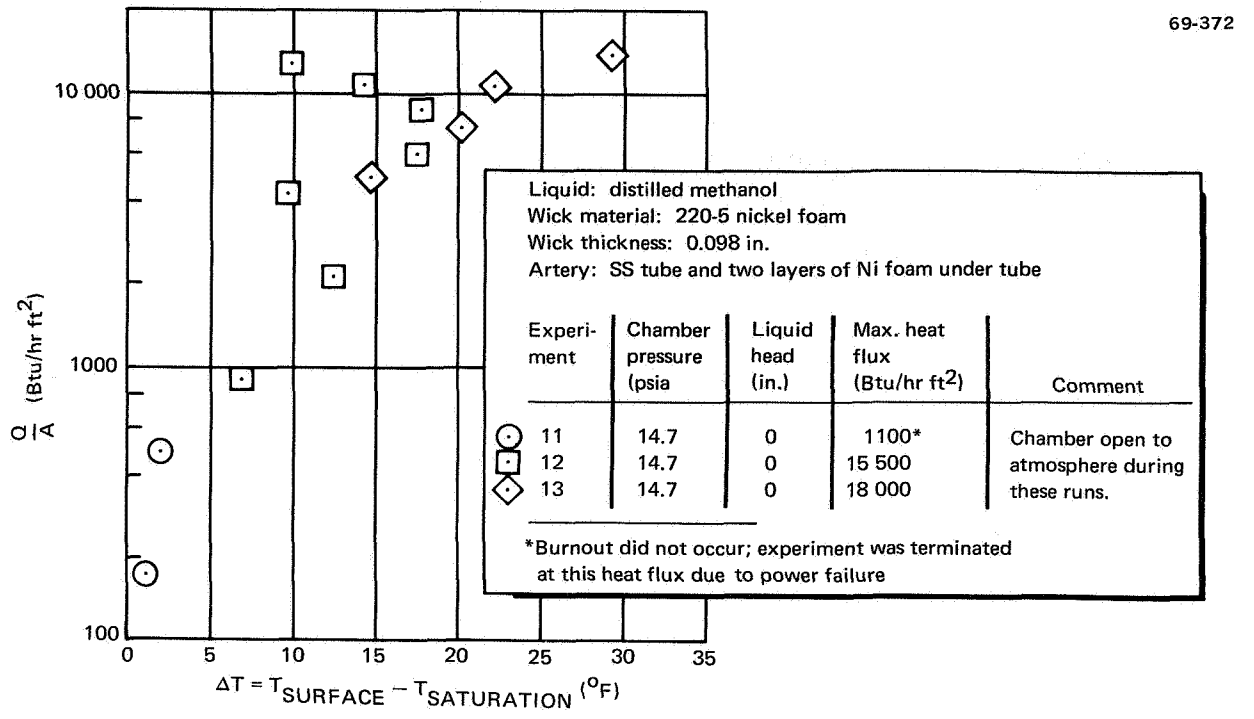

Figure 29. Experimental Results for Distilled Methanol and 0.098-In. Nickel Foam; Tests Open to Atmosphere

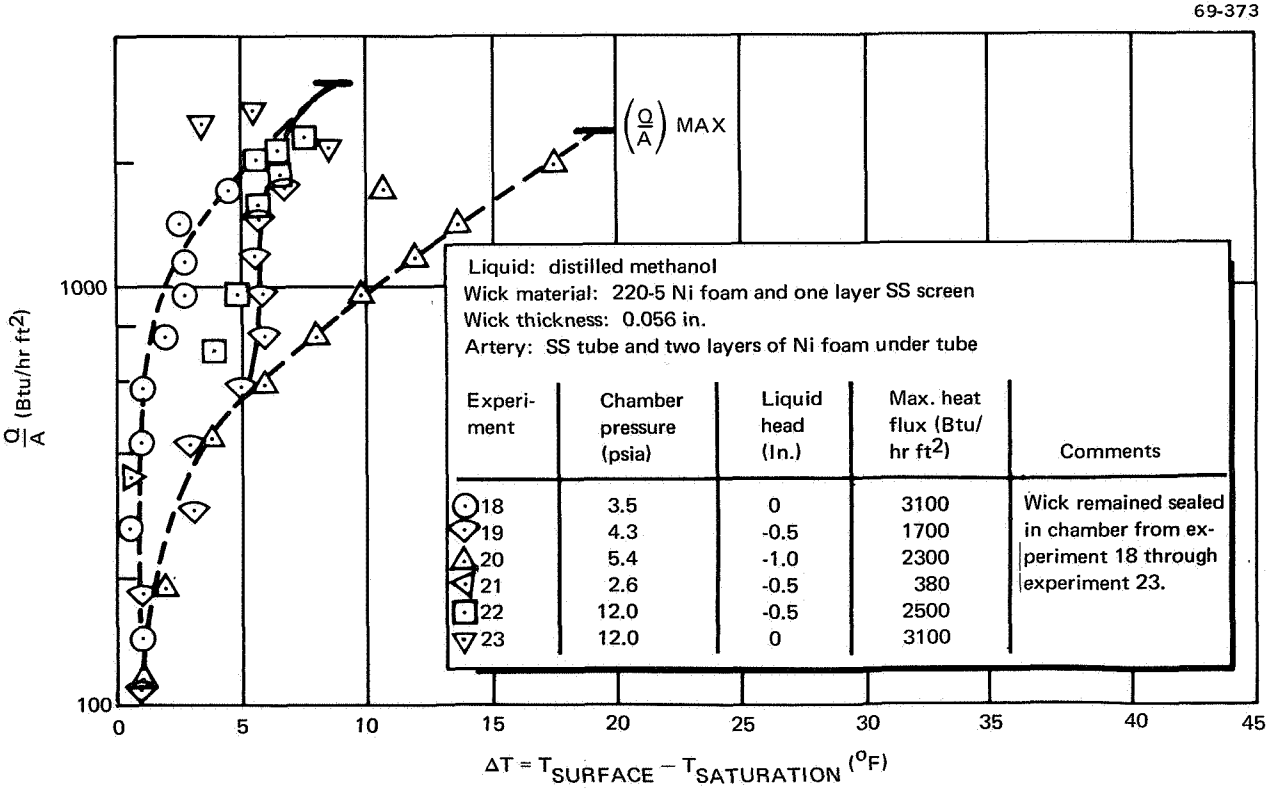

Figure 30. Experimental Results for Distilled Methanol and Nickel Foam

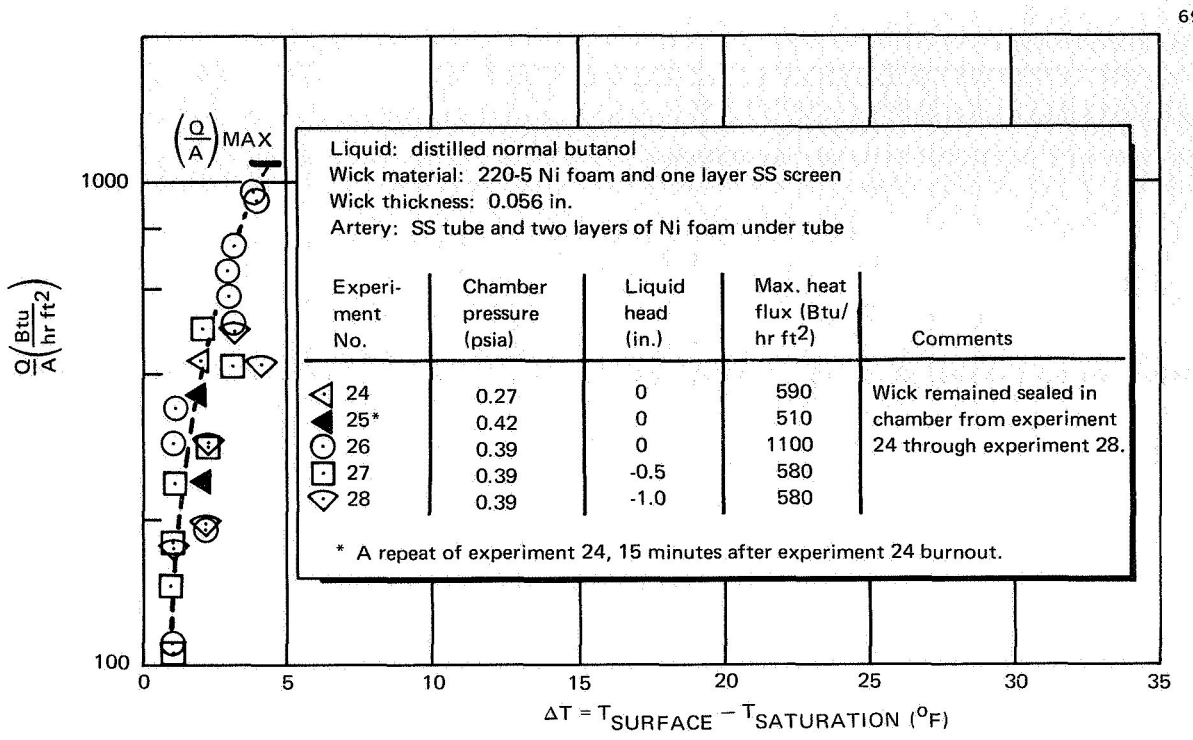

Figure 31. Experimental Results for Distilled Normal Butanol and Nickel Foam

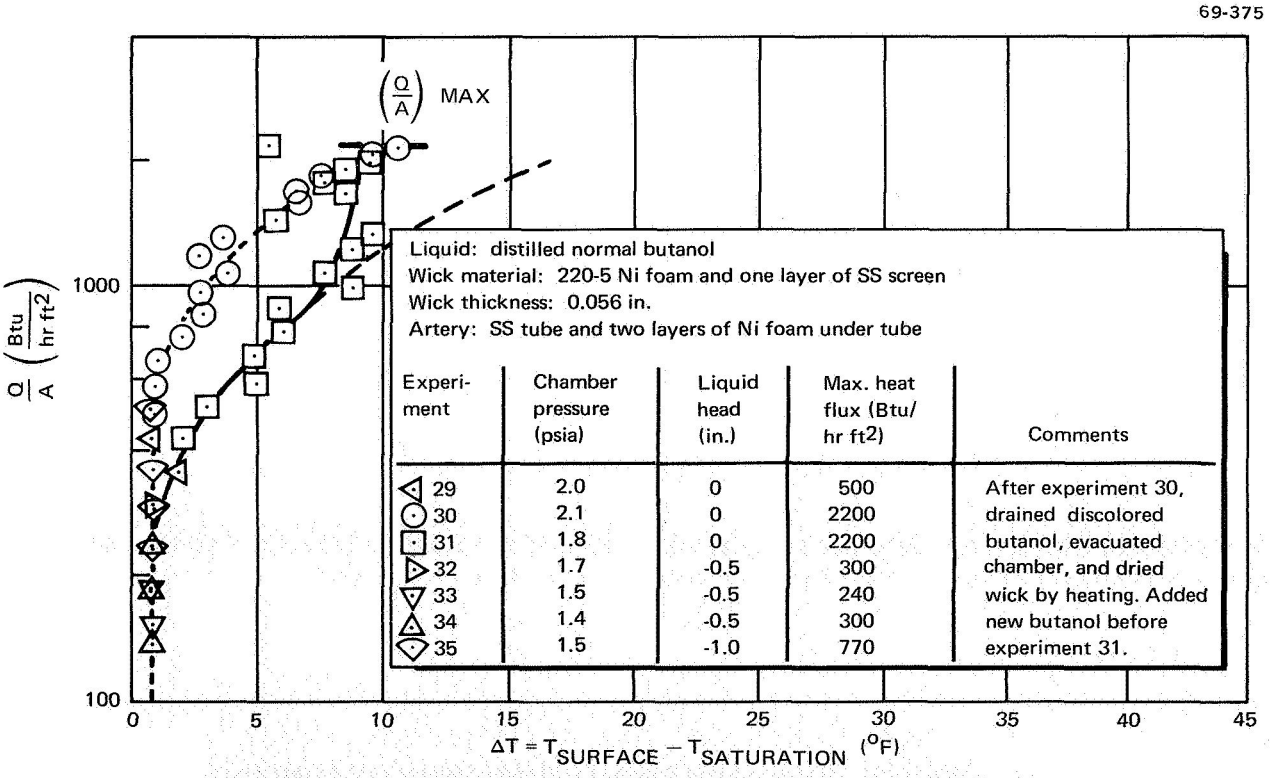

Figure 32. Experimental Results for Distilled Normal Butanol and Nickel Foam

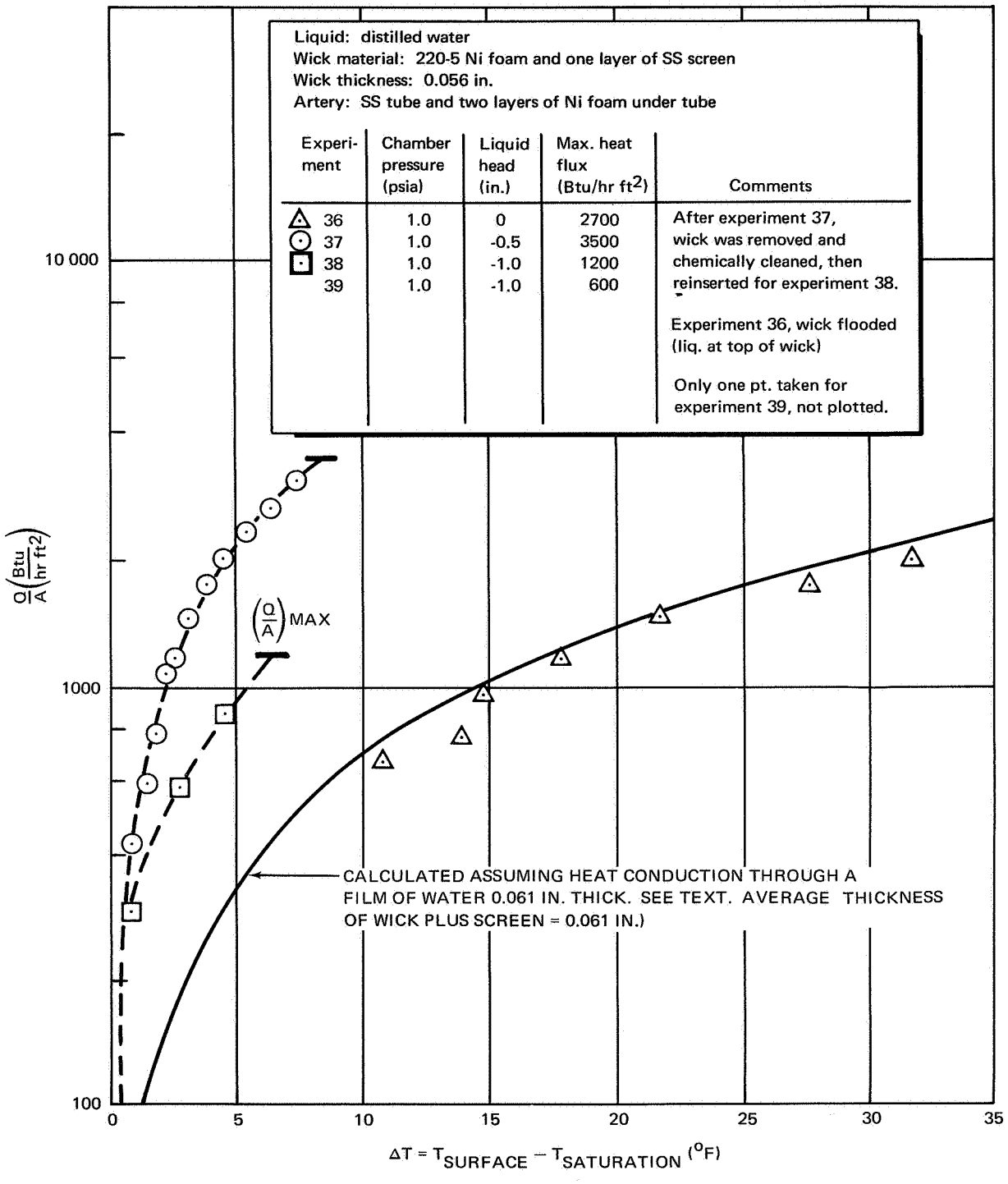

Figure 33. Experimental Results for Distilled Water and Nickel Foam

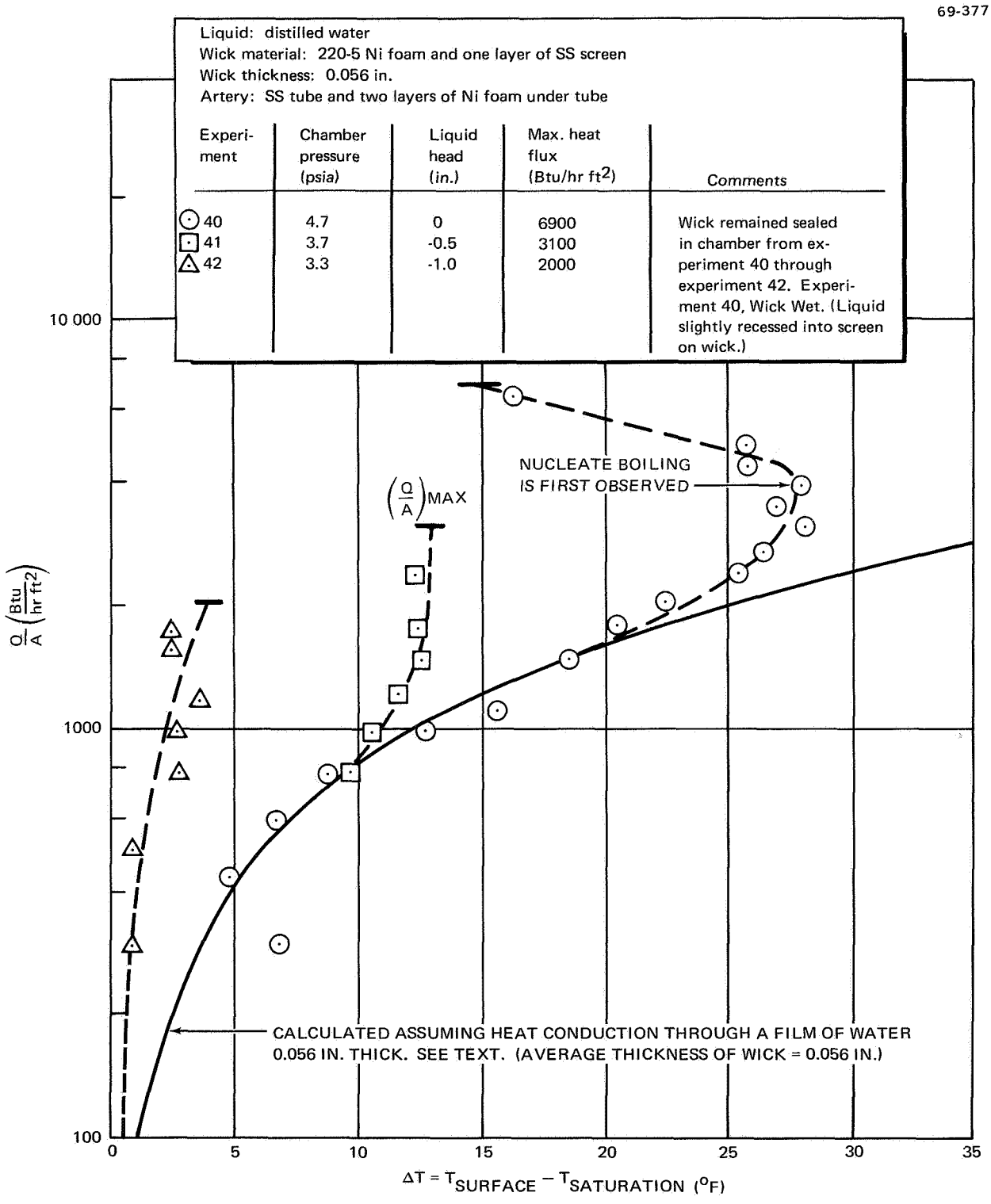

Figure 34. Experimental Results for Distilled Water and Nickel Foam

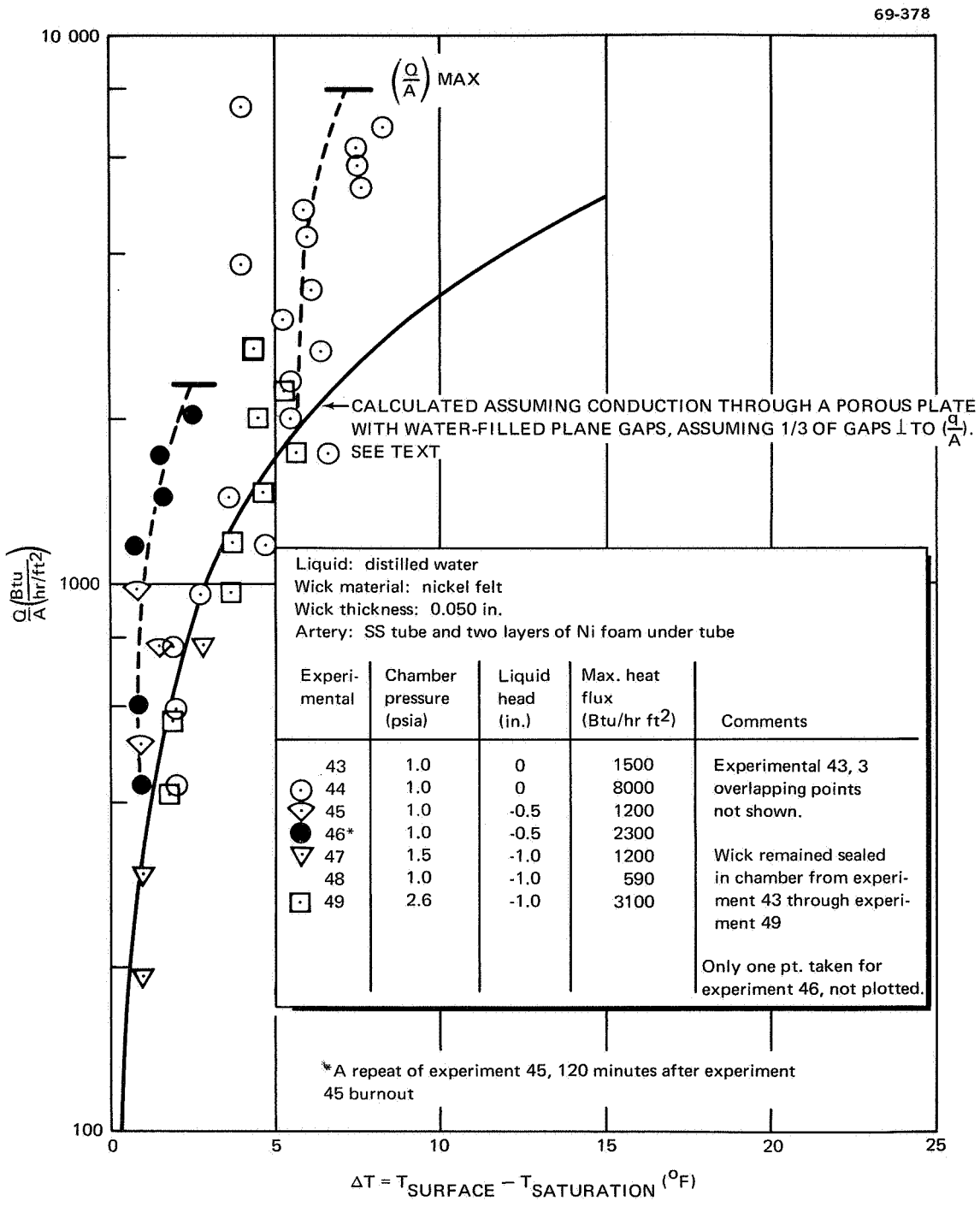

Figure 35. Experimental Results for Distilled Water and Nickel Felt

Liquid: distilled water
Wick material: nickel felt
Wich thickness: 0.050 in.
Artery: SS tube and two layers of Ni foam under tube

Experiment	Chamber pressure (psia)	Liquid head (in.)	Max. heat flux (Btu/hr ft^2)	Comments
⊙ 50	10.8	0	15 000	Wick remained sealed in chamber from experiment 50 through experiment 52.
⊡ 51	12.2	0	18 000	
△ 52	14.1	0	21 000	

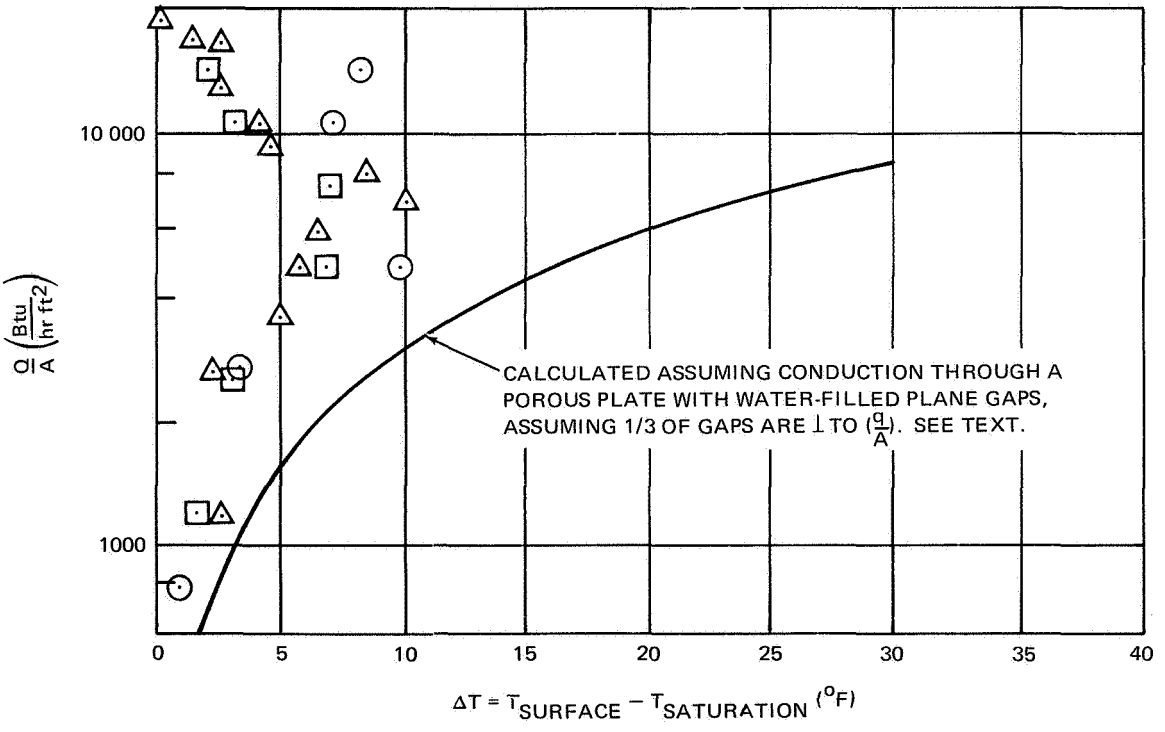

Figure 36. Experimental Results for Distilled Water and Nickel Felt

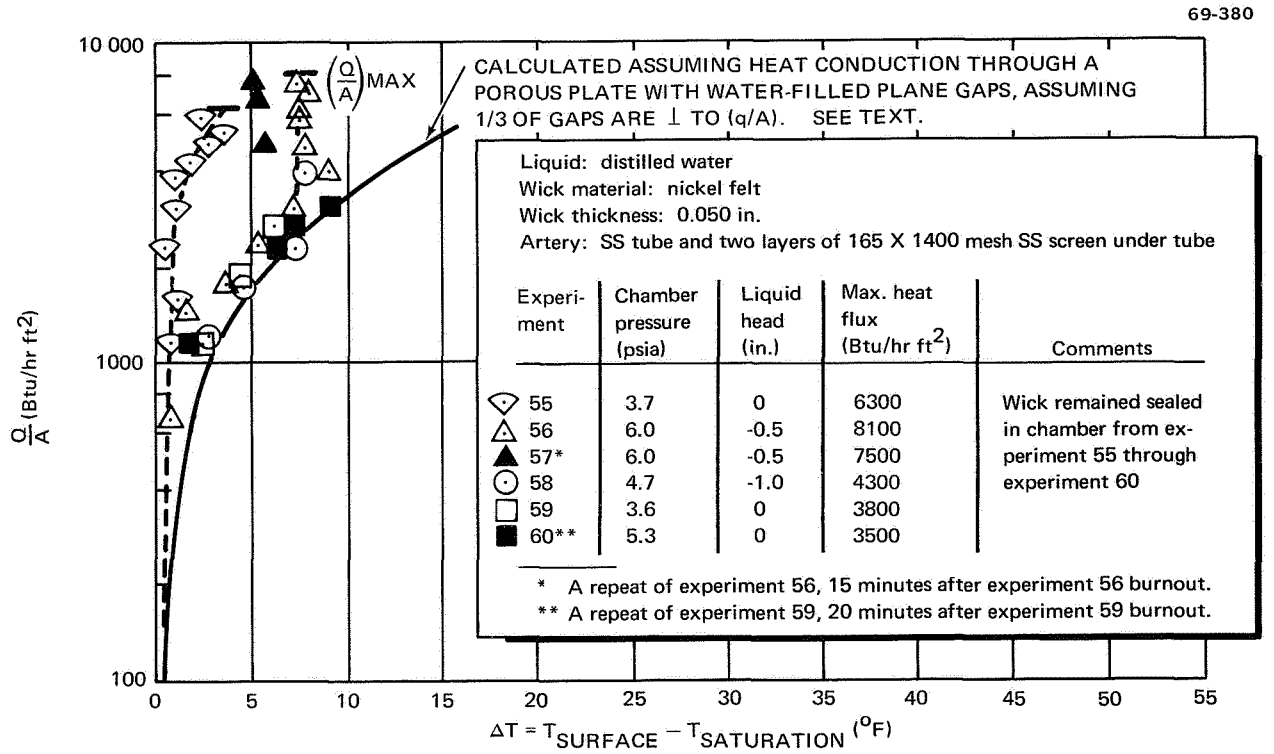

Figure 37. Experimental Results for Distilled Water and Nickel Felt; SS Screen Vapor Barrier under Artery

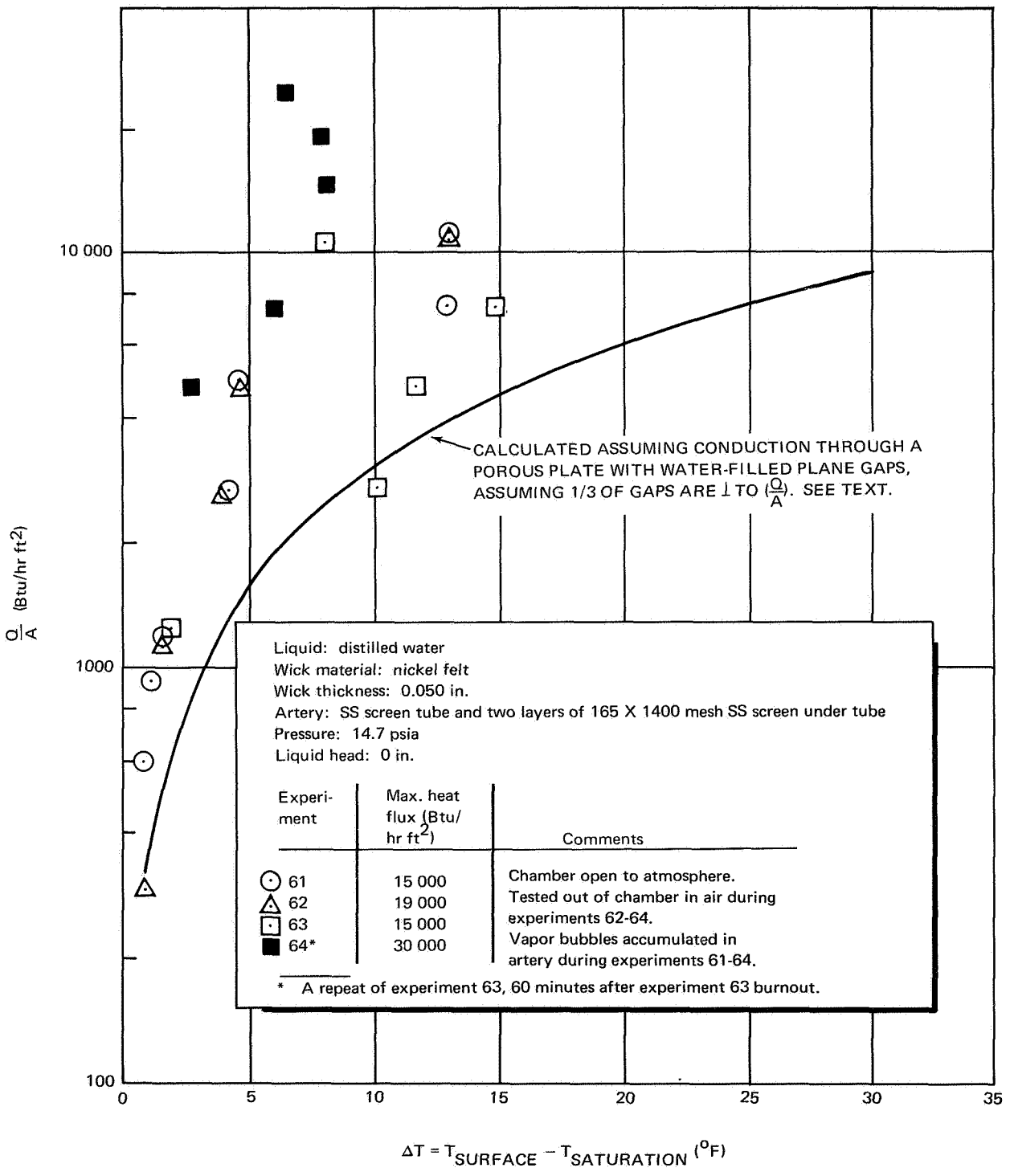

Figure 38. Experimental Results for Distilled Water and Nickel Felt (Stainless Steel Screen Artery; Atmospheric Tests: Outside Chamber)

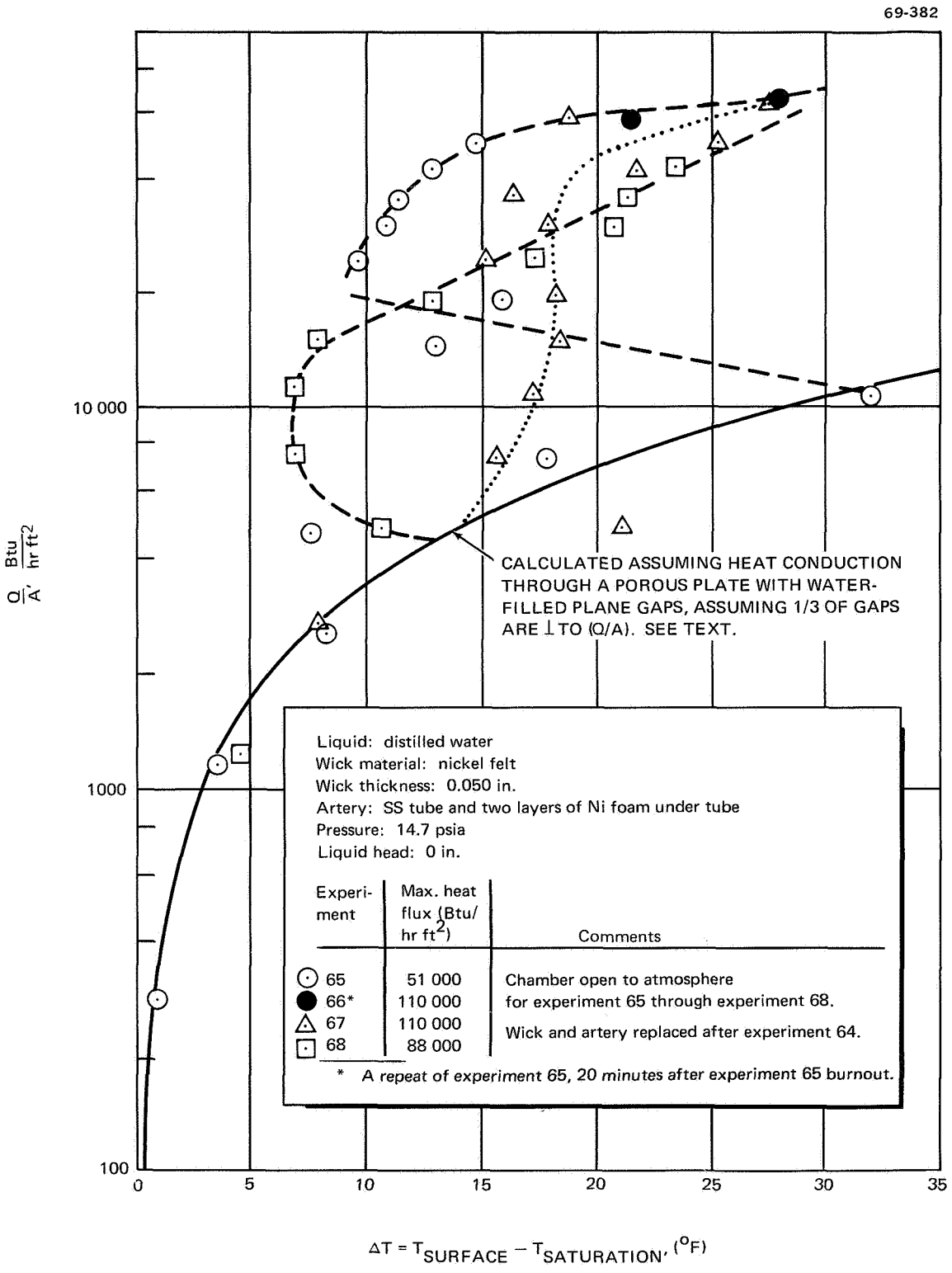

Figure 39. Experimental Results for Distilled Water and 0.050-In. Nickel Felt (Tests Open to Atmosphere)

Liquid: distilled methanol
Wick material: nickel felt
Wick thickness: 0.050 in.
Artery: SS tube and two layers of Ni foam under tube

Experiment	Chamber pressure, (psia)	Liquid head, (in.)	Max. heat flux (Btu/hr ft^2)	Comments
△ 71	17.0	0	7700	Replaced foam strips under artery and chemically cleaned wick after experiment 76.
⊙ 72	16.0	-0.5	6000	
■ 73	10.4	-1.0	3600	
⊡ 74*	20.4	-1.0	3200	
▼ 75	22.6	0	4900	Experienced difficulty in maintaining liquid in artery during experiments 71, 72, and 82.
▽ 76**	19.7	0	4900	
⊙ 77	24.6	0	4700	
◇ 82	19.2	0	810	
◁ 95	16.0	0	7400	

* A repeat of experiment 73, 5 hr. after experiment 73 burnout.
** A repeat of experiment 75, 2 hr. after experiment 75 burnout.

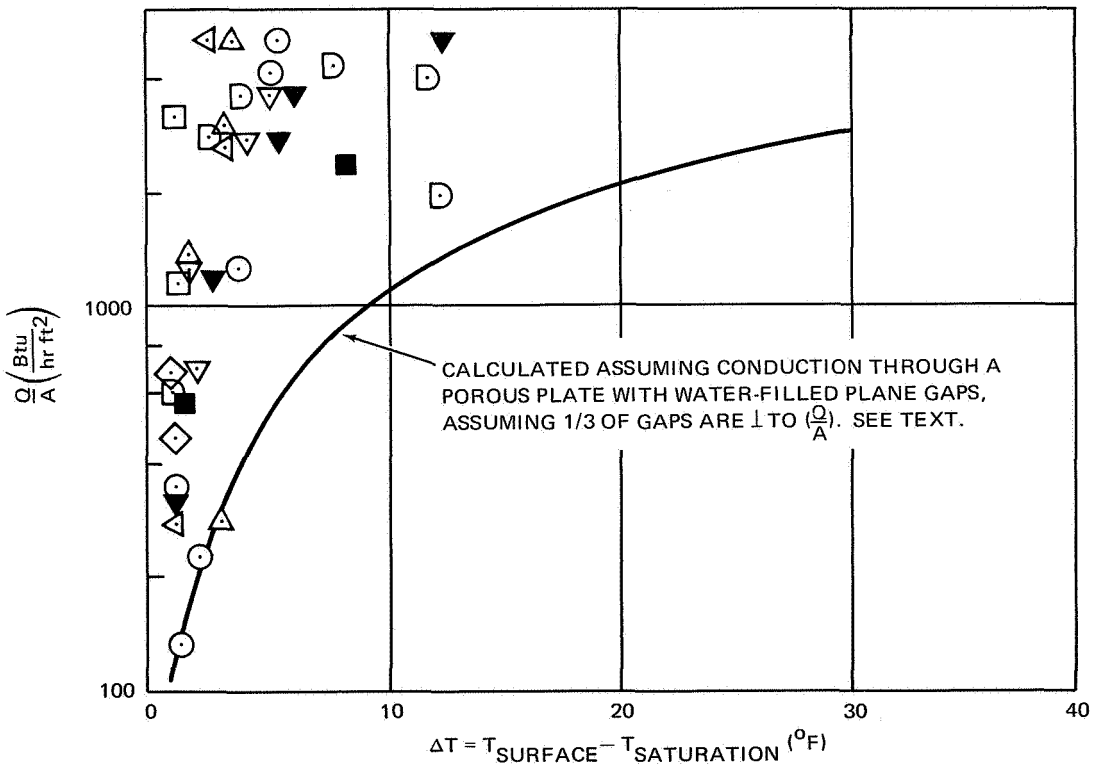

Figure 40. Experimental Results for Distilled Methanol and 0.05-In. Nickel Felt

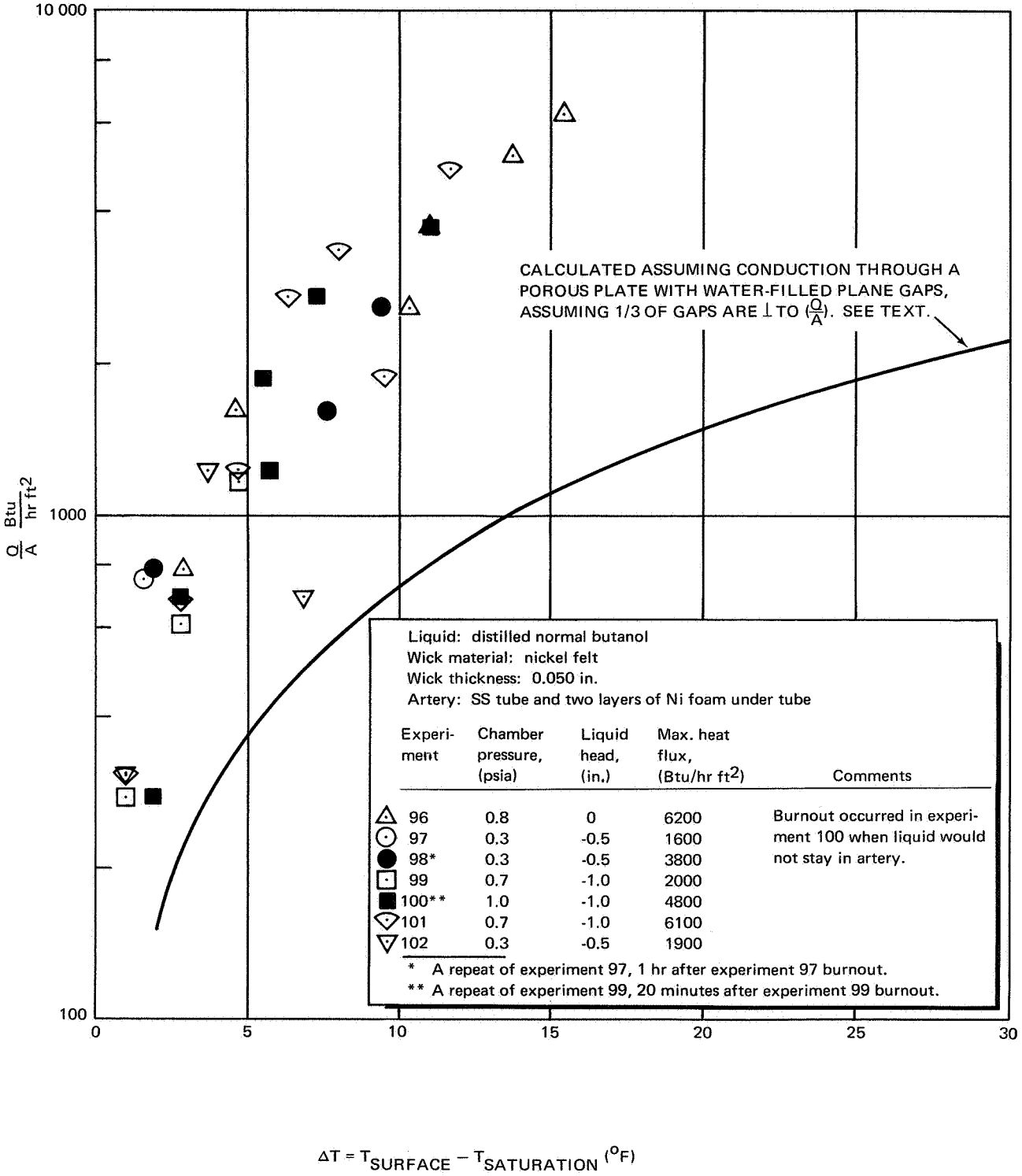

Figure 41. Experimental Results for Distilled Normal Butanol and 0.050-In. Nickel Felt

69-385

Liquid: distilled normal butanol
Wick material: nickel felt
Wick thickness: 0.050 in.
Artery: SS tube and two layers Ni foam under tube

Experiment	Chamber pressure, (psia)	Liquid head, (in.)	Max. heat flux (Btu/hr ft^2)	Comments
103	1.4	0	6000	Wick remained sealed in chamber from experiment 103 through experiment 109.
104	1.5	-0.5	4800	
105	1.5	-1.0	3700	
106	1.6	0	10 000	
107*	2.9	0	11 000	
108	1.5	-0.5	6000	
109	1.5	-1.0	7600	

* A repeat of experiment 106, 30 minutes after experiment 106 burnout.

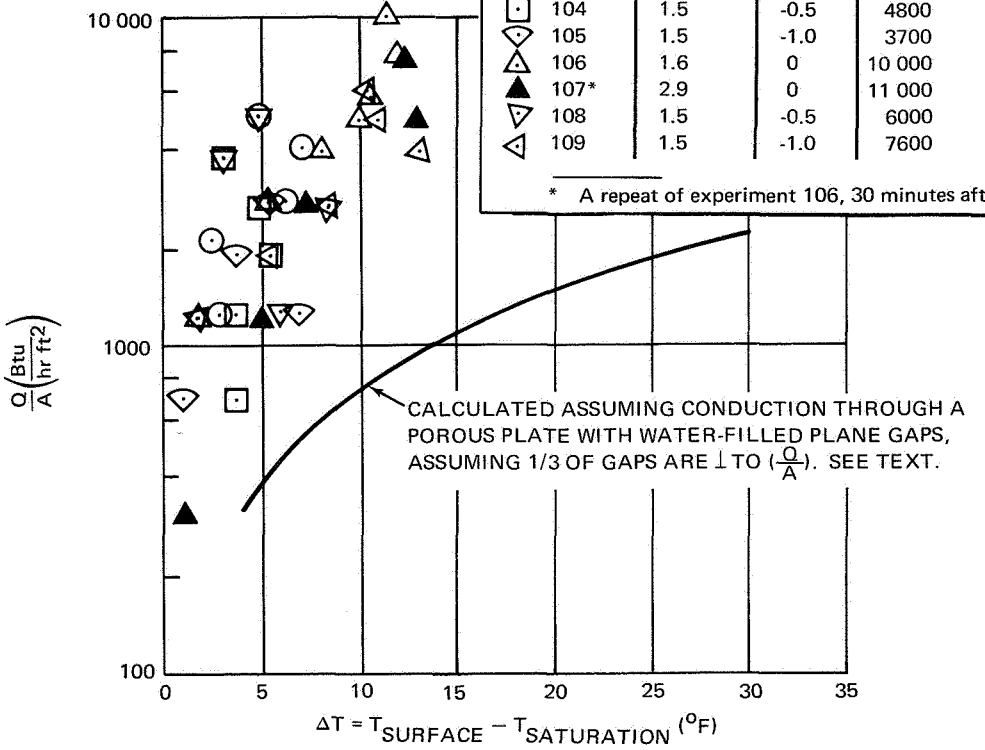

Figure 42. Experimental Results for Distilled Normal Butanol and 0.050-In. Nickel Felt

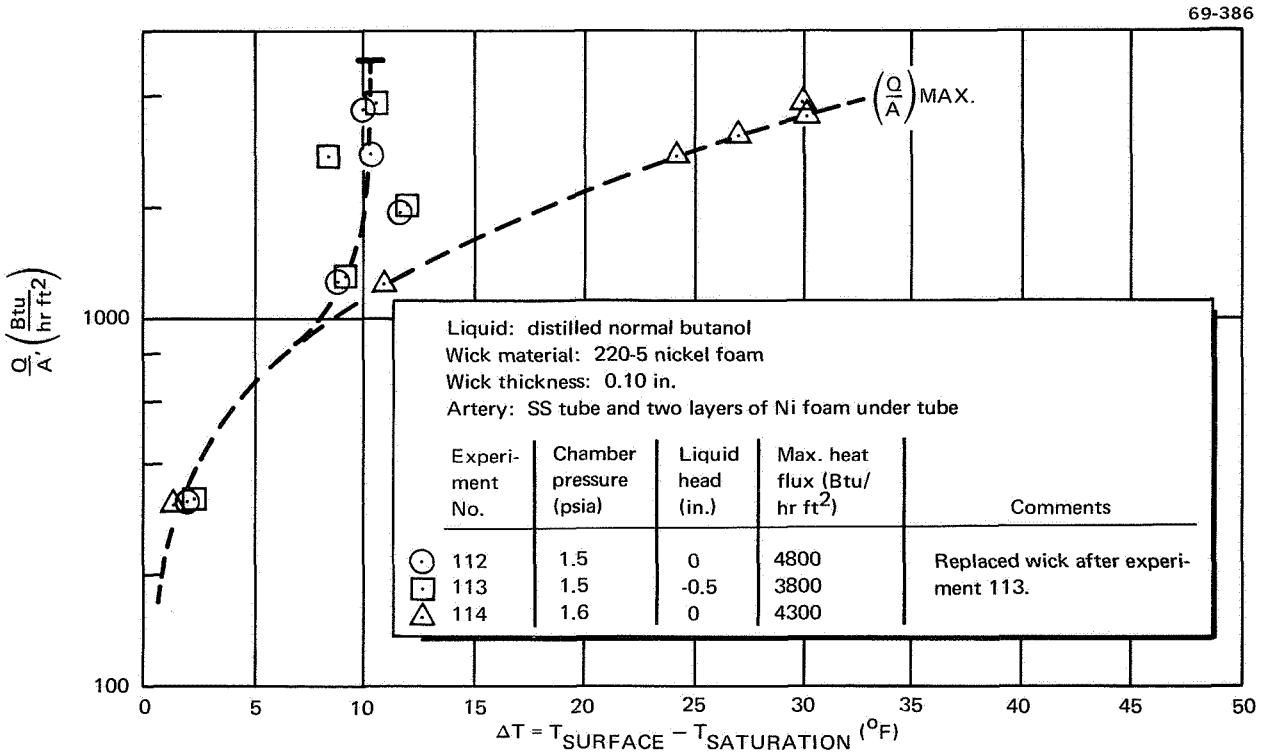

Figure 43. Experimental Results for Distilled Normal Butanol and 0.098-In. Nickel Foam

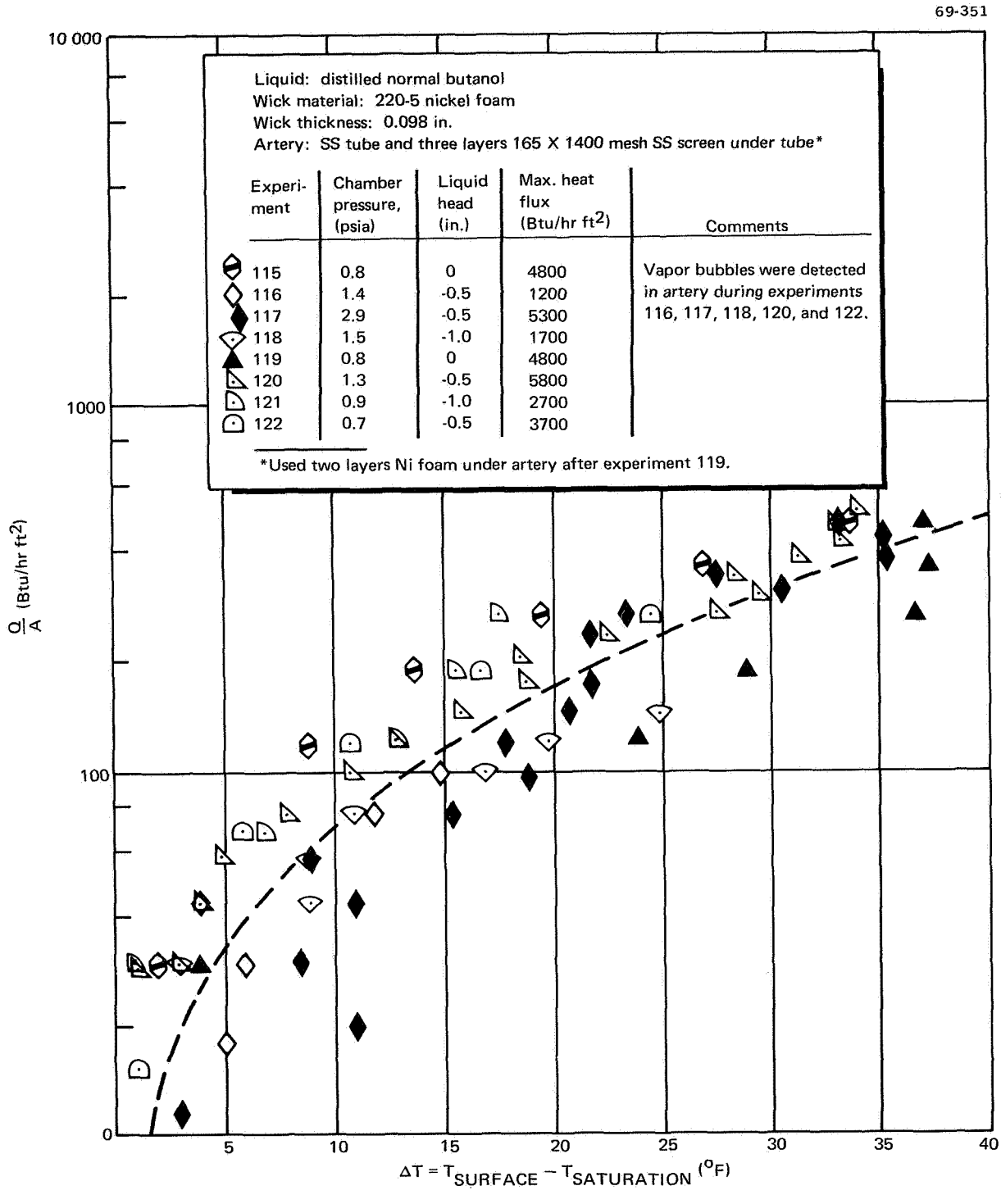

Figure 44. Experimental Results for Distilled Normal Butanol and 0.098-In. Nickel Foam

TABLE 8

SUMMARY OF MAXIMUM HEAT FLUXES FOR A WICK CONSISTING OF ONE LAYER OF 200 MESH STAINLESS STEEL SCREEN

Experiment	Fluid	Head (in.)	Vapor (°F)	Maximum heat flux (Btu/hr/ft^2)
1	Water	-1.90	80	1200
2	Methanol	0	76	300
3	Methanol	-0.25	78	190
4	Methanol	-0.5	79	75
5	Methanol	-0.15	76	190
6	Methanol	-0.70	76	95
7	Methanol	-1.00	76	87
8	Methanol	-0.40	80	220
123	Butanol	0	154	1760
124	Butanol	-0.5	150	1760
125	Butanol	-1.0	152	1220
126	Butanol	0	106	1460
127	Butanol	-0.5	104	1470
128	Butanol	-1.0	101	1220

In experiments 61 through 68, the maximum values given in the legend are considerably larger than the highest data points plotted because, at the higher fluxes, temperatures exceeded the capacity of the recording instruments; therefore, the higher equilibrium fluxes could not be plotted.

Table 9 summarizes the range of maximum heat fluxes obtained with each combination of fluid and wick. For all except certain tests with butanol. these values are considerably lower than those predicted for fluid flow within the wick without vapor bubbles. Fluid flow was calculated using the measured Kp and ΔP_c for the test wick and the manufacturer's permeability data for nickel foam vapor barrier strips. For some tests with butanol, a maximum heat flux of 1000 Btu/hr ft^2 was predicted from the flow resistance of the nickel foam strips. The maximum heat flux was the product of the fluid flow and the latent heat.

These findings agree with the observations of Costello and Redecker (ref. 7) who demonstrated, by boiling ethanol in wicks, that significantly reduced heat fluxes are obtained when proper venting is not allowed. They observed this effect even though some vapor vented from their wicks. They obtained maximum heat fluxes ranging up to 12 000 Btu/hr-ft^2--values similar to the ones obtained in these tests.

The effect of vapor blockage was also demonstrated by Kunz et al. (ref. 10). They observed that with vapor venting through the sides of the wicks, higher heat fluxes can be obtained. They also showed that if the wick is thin enough, vapor can vent through the top of the wick which further increases the burnout heat flux. Notice, however, that the high values of heat fluxes obtained by them includes the effects of liquid subcooling, a condition that

TABLE 9

SUMMARY OF MAXIMUM HEAT FLUXES FOR ZERO LIQUID HEAD

Wick	Fluid	Vapor temp (°F)	Q_B/A (Btu/hr ft^2)
0.098-in.-thick nickel foam (AmPorNik 220-5)	Methanol	79-99	100-1200
	Butanol	127-128	4800
		150-152	4300-4800
0.05-in.-thick nickel foam (AmPorNik 220-5) covered by 200 mesh screen	Water	100	2700
		160	6900
	Methanol	91	3100
		140	3100
	Butanol	107-109	510-1100
		160-162	500-2200
0.05-in.-thick nickel felt	Water	100-104	1500-8000
		197-210	15 000-21 000
	Methanol	155-169	800-7700
	Butanol	128	6200
		148-172	6000-11 000

does not occur in heat pipes. This is demonstrated in several of their experiments and particularly in their experiments 14 and 15 where heat fluxes as high as 30 000 Btu/hr-ft^2 were measured at $\Delta T_{sat}=0$. These large fluxes can only be a result of heat conduction or convection (if convection could exist in their wicks) and this contribution must be subtracted from the total heat flux curve to obtain the contribution from nucleate boiling (see, for instance, refs. 19 and 20). Heat conduction and natural convection (convection under proper condition) can occur in wicks as was observed in the DWDL studies.

Premature burnout in some of the experiments could have resulted from partial or total vapor blockage of the artery. Vapor bubbles were detected in the artery previous to burnout in experiments 61 through 64 (fig. 38), 100 (fig. 41) and 116, 117, 118, 120, and 122 (fig. 44). In experiment 100 (fig. 41), the artery was completely blocked and caused burnout. In the other experiments, bubbles probably contributed to burnout by reducing the flow through the artery.

Effects due to low operating pressures. - Maximum heat fluxes for the majority of the low-pressure experiments are less than 10 000 Btu/hr-ft^2. A reduction in the maximum heat flux with decreasing pressure should be expected if vapor blockage is the reason for burnout. It is an established fact that the size of vapor bubbles formed during nucleate boiling significantly increases with decreasing pressure. This effect is shown in figure 45 where the departure diameter of vapor bubbles formed in water, methanol, and n-butanol is given. The curves were calculated using Cole and Shulman's correlation (ref. 12) which correlates the data for many fluids including water

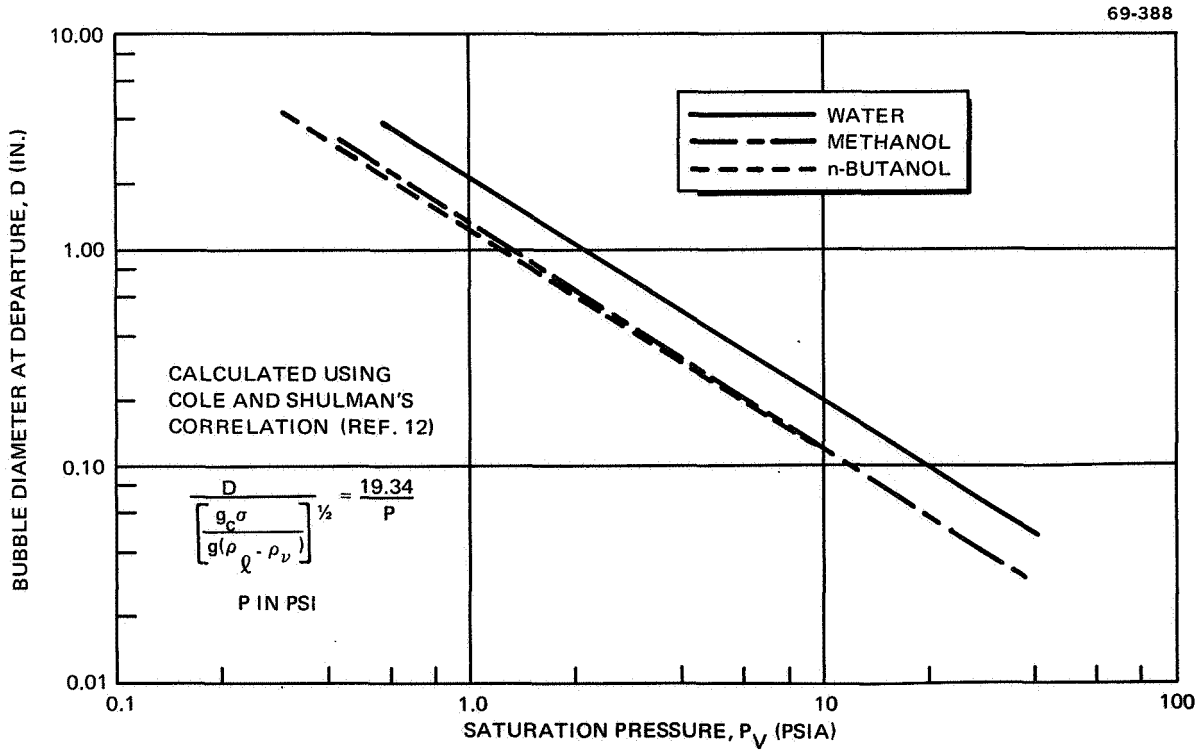

Figure 45. Variation of the Bubble Departure Diameter with Pressure for Fluids at their Saturation Temperature

and methanol. As shown, the departure diameters for these fluids increase by a factor of 10 to 30 times with a decrease in the pressure from atmospheric to the low values used in these tests.

The data in figure 45 were obtained for pool boiling. However, the same effect should occur for a heat transfer surface covered by a wick; in this case, the bubbles would probably spread over a large area contiguous to the surface (as opposed to large bubbles rising through the fluid in pool boiling). This effect would probably occur in the early stages of nucleate boiling and would cause burnout at very low heat fluxes, as was observed.

The high heat fluxes obtained by Kunz et al (ref. 10) were possibly due to good vapor venting, resulting from the fact that their experiments were conducted at atmospheric pressure and, perhaps, because the liquid was under subcooled conditions. High pressure would reduce the vapor bubble diameters to low values at 212°F (0.04 to 0.12 in. at 212°F in pool boiling) and, in addition, the diameters would be further decreased with subcooling. Van Stralen's (ref. 11) theory and experiments indicate that the diameters decrease according to

$$D_{subcool} = \left(\frac{\Delta T}{\Delta T + \Delta T^*}\right) D_{saturation} \qquad (15)$$

where $\Delta T = T_{surface} - T_{saturation}$

$\Delta T^* = T_{saturation} - T_{bulk}$

For instance, for $\Delta T = 10°F$ and $\Delta T^* = 100°F$ (Kunz's subcooling range from 137° to 0°F) the diameter would be reduced by a factor of 12, which, for pool boiling, would give vapor diameters on the order of 0.003 to 0.010 in. These very small bubbles would easily vent through the sides of the wicks used by Kunz. Subcooling was probably present in the upper region of their wicks since the data of Van Stralen (ref. 11) and Grant and Patten (ref. 21) predict that the thermal boundary layer at $\Delta T^* = 100°F$ should be around 0.003 in. which is about 1/30 the thickness of the wicks used by Kunz.

Note, however, that these numbers are for pool boiling and can only be used as trends that probably occur in boiling with wicks.

Mode of heat transfer. - The three modes of heat transfer that should be considered are: (1) heat conduction through the wick with evaporation at the top of the wick, (2) free convection in the wick with evaporation at the top of the wick, and (3) nucleate boiling at the heat transfer surface beneath the wick.

Experiments 36 (fig. 33), and 40 and 41 (fig. 34), indicate that conduction was the mode of heat transfer in these experiments prior to the onset of nucleate boiling (which occurred at $\Delta T = 10°F$ in experiment 41 and $\Delta T = 20°F$ in experiment 40). The nonboiling data in experiment 36 agrees with that predicted for conduction through a water film 0.061 in. thick (the thickness of the film for a flooded wick); and the nonboiling data in experiments

40 and 41 agree with that predicted for conduction through a water film 0.056 in. thick (the thickness for a wet wick in which the top of the liquid recedes below the 200 mesh screen). Apparently, thermal conductivity of the nickel foam wick did not have an effect on the conduction through the wick when filled with water. The open structure of the foam (fig. 46) is probably the reason for this observation. Heat fluxes for methanol and n-butanol in nickel foam were too large to be accounted for by heat conduction.

Heat conduction was the mode of heat transfer with water in nickel felt prior to the onset of nucleate boiling. The nonboiling data in figures 36, 38, and 40 agree with that predicted by heat conduction for a film with an apparent thermal conductivity of 1.4 Btu/hr-ft°F. This value was calculated using the expression given by Jakob (ref. 22):

$$\frac{1}{k_a} = \frac{1}{k_{Ni}} + \frac{\varepsilon}{3k_{H_2O}} \tag{16}$$

where

k_a = apparent thermal conductivity
k_{Ni} = thermal conductivity of Ni
k_{H_2O} = thermal conductivity of H_2O
ε = the wick porosity

This expression was derived for a porous plate with more or less plane gaps, assuming that one third of all the gaps extend perpendicular to the heat flow direction. Figure 46 reveals that the felt wicks could fit this description. Values used in equation (2) were k_{Ni} = 37 Btu/hr-ft °F, k_{H_2O} = 0.40 Btu/hr-ft °F, and ε = 0.84.

The criterion for the onset of free convection in a porous medium as given by Katto and Masuoka (ref. 23) indicates that free convection could have occurred with these fluids in the nickel foam wicks but not in the nickel felt wicks. The contribution to the heat transfer by free convection in a wick could not be calculated, but data in figures 31, 32, 43, and 44 indicate that free convection was probably the mode of heat transfer prior to nucleate boiling. Experiments 114 (fig. 43) and 115 through 122 (fig. 44) show this effect very clearly. Heat conduction alone cannot explain these high values.

Nucleate boiling occurred in all the experiments and was the cause for wick burnout (the exceptions are experiment 100, and possibly experiments 71, 72, and 82 in which burnouts are due to vapor blockage in the artery). Nucleate boiling is most evident in experiments 19, 31, 40, 41, 44, 56, 65, 67, 68, 112, and 113. Data for these experiments clearly show when nucleate boiling starts. This occurs when the heat flux curve departs from the conduction or convection curve and begins to rise very rapidly over a narrow range of ΔT (see, for instance, figs. 34 and 43).

14X

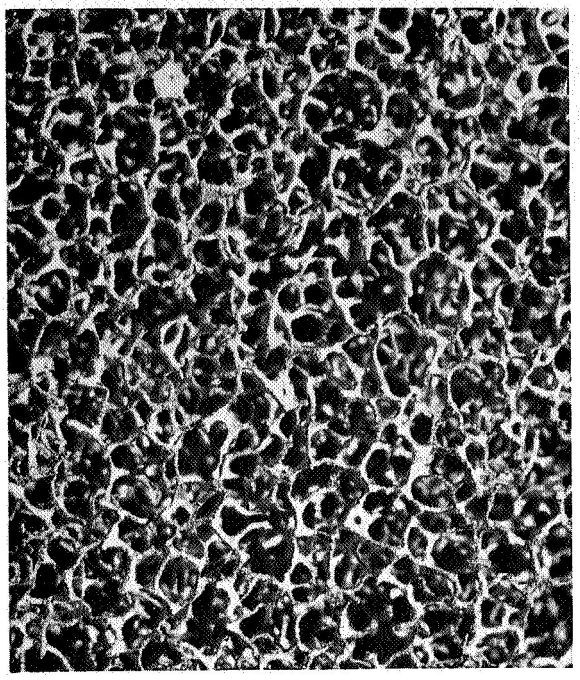

14X

100X

A. NICKEL FELT

100X

B. NICKEL FOAM

Figure 46. Structure of the Nickel Foam and Felt Wicks Used in the Evaporator Heat Flux Tests (Original Prints not Reduced for Publication)

The effects of surface conditioning. - The heat flux in nucleate boiling is a function of ΔT and (N/A), the number of nucleating sites per unit area (ref. 20). Unfortunately, (N/A) is a function of several variables (e. g. surface roughness, dissolved gases, corrosion, operating conditions, etc.) which are very difficult to control. Corty and Foust (ref. 24) first observed these effects in 1955 and since then several investigators have investigated the phenomenon.

The effects of conditioning were also observed in these studies. The hysteresis effect in which the heat flux forms an S-shaped curve was most apparent in experiments 40, 65, 67, and 68 (figs. 34 and 39). The effects of replacing slightly decomposed butanol is observed in experiment 31 (fig. 32), and the effects of chemically cleaning the wick and the heat transfer surface is observed in experiment 37 (fig. 33).

Conclusions

Heat flux data were taken with water, methanol, and n-butanol in nickel foam and nickel felt, at low- and high-saturation pressures.

Results of these tests show that without proper venting, the burnout heat fluxes are limited to 20 000 Btu/hr-ft^2 or less.

With low operating pressures, the burnout heat flux can be significantly decreased because of large volumes of vapor accumulating in the wick.

The heat flux due to heat conduction in nickel foam and nickel felt with water can be predicted analytically.

Heat transfer by free convection can occur in nickel foam, but not in the nickel felt used in these tests.

Variations in heat flux due to surface conditioning were observed.

Premature burnout can result from partial or total vapor blockage of the artery; thus, proper consideration must be given to preventing vapor from entering the artery.

DESIGN OF LOW-TEMPERATURE HEAT PIPES

Need for Low-Temperature Heat Pipes

The heat pipe is an especially attractive device for use on space vehicles because of its superior operation in zero-g fields. The temperature range of from -100° to +200° F is characteristic of the required operating temperatures of many spacecraft components. Thus, interest in heat pipes which can

operate in this range has developed rapidly in recent years. The purpose of this work was to develop data that will be useful in the design of heat pipes for low-temperature applications; this part of the report indicates the method of applying these data to heat pipe designs.

Design Factors

The first task which must be undertaken is to define the conditions to be designed for. Then, tradeoff study should be made to indicate whether a heat pipe system is most desirable, or whether some other method of heat transfer would be more effective. For example, the problem of cooling an earthbound system, with sufficient power available, might well use a pumped loop heat transfer network instead of a heat pipe.

The design of heat pipes for spacecraft applications can be simplified considerably if proper consideration is given early in the design phase. For example, a spin-stabilized spacecraft provides artifical gravity which can be useful in returning working fluid condensate to the evaporator, if the components which are to be thermally controlled are located in a favorable orientation in the gravity field.

Heat pipes can be an integral part of the spacecraft structure or a separate component that can be easily removed. Thus, structural considerations may be important in the heat pipe design.

In order to optimize a heat pipe design, the following parameters must be considered:

- Allowable weight
- Required temperature uniformity
- Maximum axial heat flux
- Maximum radial heat flux
- Operation in a gravity field

These must be considered simultaneously because they interact with one another. However, some general comments may be made about each of them.

Allowable weight. - The weight available for thermal control of a spacecraft is usually rigidly fixed. Thus, careful consideration of the container and wick material from a weight standpoint is very important. This is why aluminum is a particularly attractive choice for container material.

Required temperature uniformity. - The degree of temperature control is important, for it influences the selection of the wick and container materials. The primary temperature drop in most heat pipe systems occurs during passage of heat into and out of the pipe. Thus, thin container walls, thin wicks, and high thermal conductivity materials are desirable if the temperature control requirement is very stringent.

Maximum axial heat flux. - The maximum heat transfer capability of any heat pipe is fixed by the wick design, working fluid, and heat pipe size. A given heat load can be carried by a few large heat pipes or a greater number of smaller ones. A number of parameters, which will be mentioned later, influence this choice. The use of permeability and capillary pressure data such as were generated during the course of this program, will aid the designer in analyzing the effect of axial heat flux on overall system design.

Maximum radial heat flux. - The size of the heat pipe's evaporator region is a very important design consideration. If the radial heat flux exceeds a certain value, the pipe will burn out regardless of the magnitude of the total axial heat load. Results of evaporator heat flux experiments should aid the designer in the consideration of this limitation.

Operation in a gravity field. - Heat pipe operation may be aided or hindered by a gravity field, depending on the heat pipe orientation with respect to the field. Thus, consideration should be given to using the orientation which aids operation if this is consistent with other design constraints.

Design Aids

Following is a discussion of specific considerations that should be taken into account during the design of heat pipe systems.

Basic theory for prediction of maximum axial heat flux. - Even though several refinements of Cotter's theory of heat pipe operation have been developed in recent years, most of these are concerned with high-temperature, high-vapor-velocity heat pipes. For most low-temperature applications, equations (1) through (5) may be used to determine the maximum heat flux.

If the vapor flow area is small, the vapor density is low, or for some other reason ΔP_V is not negligible with respect to ΔP_L, it must be included in equation 1. There have been a number of refinements to Cotter's method for calculating ΔP_V (ref. 2) which should be useful. For example, Busse (ref. 25) has calculated the pressure drop in the vapor phase for any evaporation rate, rather than for the limit of very low or high evaporation rates which was the scope of the previous theory. Van Andel (ref. 26) has synthesized Busse's results and turbulent flow empirical data into a unified relationship that predicts the value of ΔP_V for any value of radial or axial heat flux. Another correction which should be made to Cotter's theory occurs in the event of large pressure recovery in the condenser. Ernst (ref. 27) has called attention to the fact that in such a case the point at which liquid pressure equals vapor pressure will move back to the beginning of the condenser.

When equations (2) through (5) are substituted into equation (1), the value of Q obtained is the maximum heat flux. However, equations (1) through (5) neglect the effect of nucleate boiling in the evaporator on maximum heat transfer capability; thus, they usually predict a value of maximum axial heat flux

higher than a value which can actually be achieved. However, the theory is useful for indicating trends and the relative merit of various wick and fluid systems. In addition, if the radial heat flux is low (nucleate boiling not occurring), equations (1) through (5) should accurately predict the maximum axial heat flux.

If equations (1) through (5) are combined (ΔP_V neglected), with $\ell_a = 0$ and the contact angle, θ, equal to zero, the following expression for Q_{max} is obtained:

$$Q_{max} = 4 \left[\frac{\sigma h_{fg}}{\nu_L} \right] \frac{K_p A_w g_c}{r_c \ell} - 2 \left[\frac{\rho_L h_{fg}}{\nu_L} \right] K_p A_w g \sin \alpha \tag{17}$$

where r_c is the effective value of capillary radius, such as is listed in table 3. Thus, r_c includes the effect of contact angle since it is calculated from measured values of ΔP_C assuming $\theta = 0$.

If the heat pipe is operating in a zero-g field, the second term disappears and the following expression results:

$$Q_{max} = 4 \left[\frac{\sigma h_{fg}}{\nu_L} \right] \frac{K_p A_w g_c}{r_c \ell} \tag{18}$$

The expression contains two factors: one dependent on fluid properties, and the other on properties of the wicking medium. To determine the relative merit of various fluids for heat pipe operation in a zero-g field, a quantity may be defined by:

$$(FOM)_0 = \frac{\sigma h_{fg}}{\nu_L} \tag{19}$$

This quantity is plotted in figure 47. The second factor contains K_p and r_c, which may not be independent of fluid properties, and this effect must be investigated. The value of r_c is a function of contact angle and may be significant, but for experimentally obtained values presented in table 3, r_c is relatively independent of fluid.

If the heat pipe must operate in an adverse gravity field, the second term becomes important, and a simple expression which can be broken into two independent factors for fluid and wick properties is no longer obtainable.

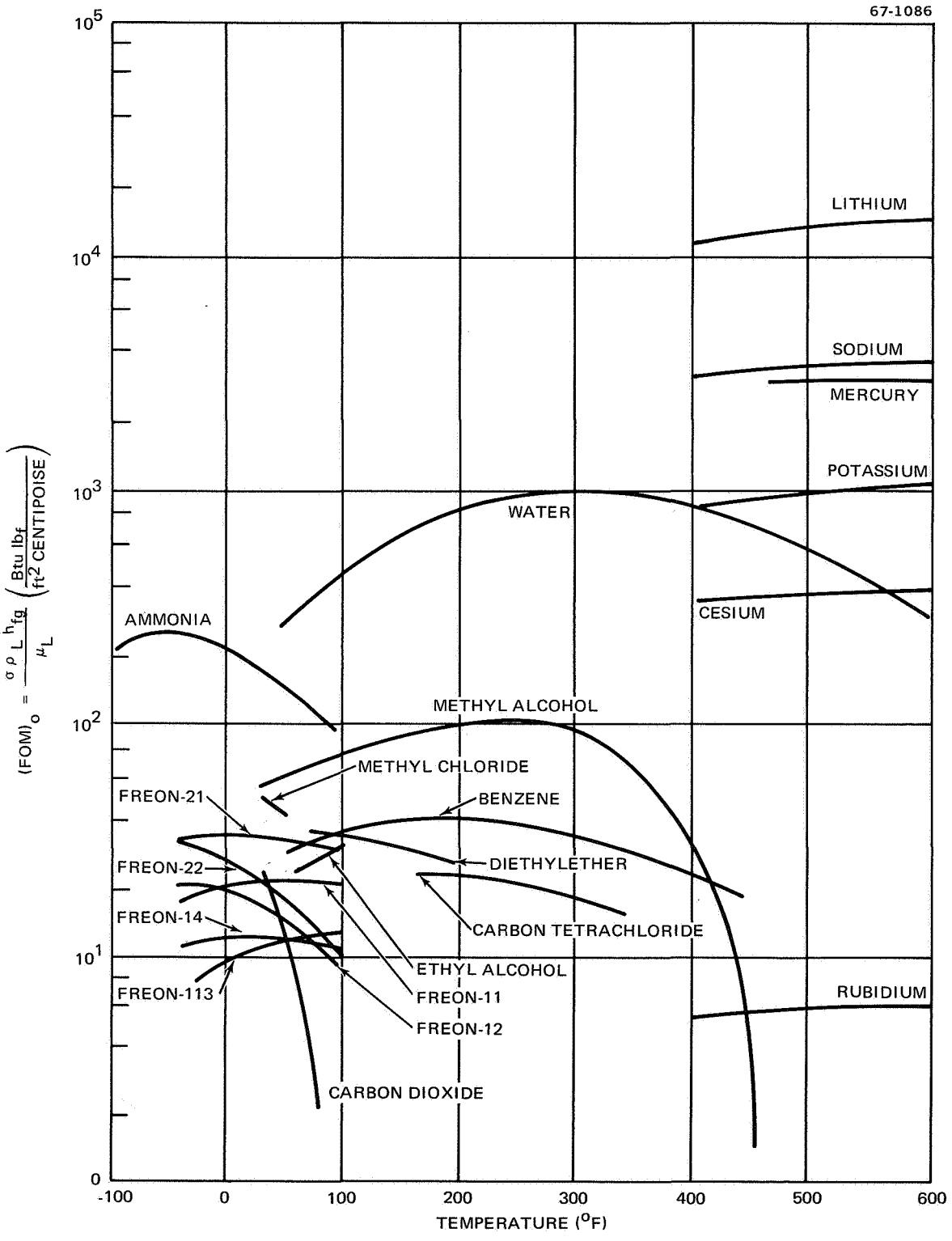

Figure 47. Zero-G Figure of Merit

However, another figure of merit may be defined which is useful in comparing the relative merits of fluids for operation in gravity fields. The fluid properties in the second term of equation (18) are

$$\frac{\rho_L \, h_{fg}}{\nu_L} = \frac{(FOM)_0}{\sigma/\rho} \tag{20}$$

Thus, a figure of merit for 1 g is defined as

$$(FOM)_1 = \sigma / \rho \tag{21}$$

This is plotted in figure 48 for various fluids. Since it is desirable to make the second term of equation (18) as small as possible, $(FOM)_0$ should be as large as possible for a given value of $(FOM)_1$. If a particular fluid has a higher value of $(FOM)_0$ and $(FOM)_1$ than do alternative choices for a particular gravity application, it would be the desirable fluid to use from the standpoint of maximum heat transfer capability. However, if a fluid does not have larger values of $(FOM)_0$ and $(FOM)_1$ than alternative choices, then equation (17), with the wick properties included, must be evaluated for each fluid.

Capillary pressure data. - Equations (18) and (19) contain r_c which must be determined by experiment. Table 3 contains values of these data ($D_c = 2r_c$) for several wicks and fluids. In addition, Kunz et al. (ref. 10) and Katzoff (ref. 14) have r_c data for several wicks. Our data indicate very little effect of fluid on r_c. Katzoff observed essentially the same fact, although Kunz did observe an appreciable difference between r_c for water and for Freon, indicating a difference in contact angle.

Permeability data. - The other experimentally determined constant which must be obtained for use in equation (17) is K_p. Values are tabulated for several wicks in tables 6 and 7. In addition, there are data for porous metal wicks presented in reference 10. Table 7 requires the use of equation (12) rather than 11 in the derivation of equation (17). An alternative approach is to multiply R by wick thickness in order to obtain an effective value of $1/K_p$.

For thin wicks, it may be desirable to include the effect of meniscus recession on the resistance of the wick. The resistance value will increase as a function of position when moving from condenser to evaporator. This is due to a large meniscus recession in the evaporator and the essentially flat surface in the condenser. As a first approximation, a linear increase in resistance may be assumed; an arithmetic average between the value for zero meniscus recession and a value of meniscus equal to r_c may be used. A value of r_c for the wick in question may be obtained from table 3 or similar sources. For example, from table 3, a value for r_c of approximately

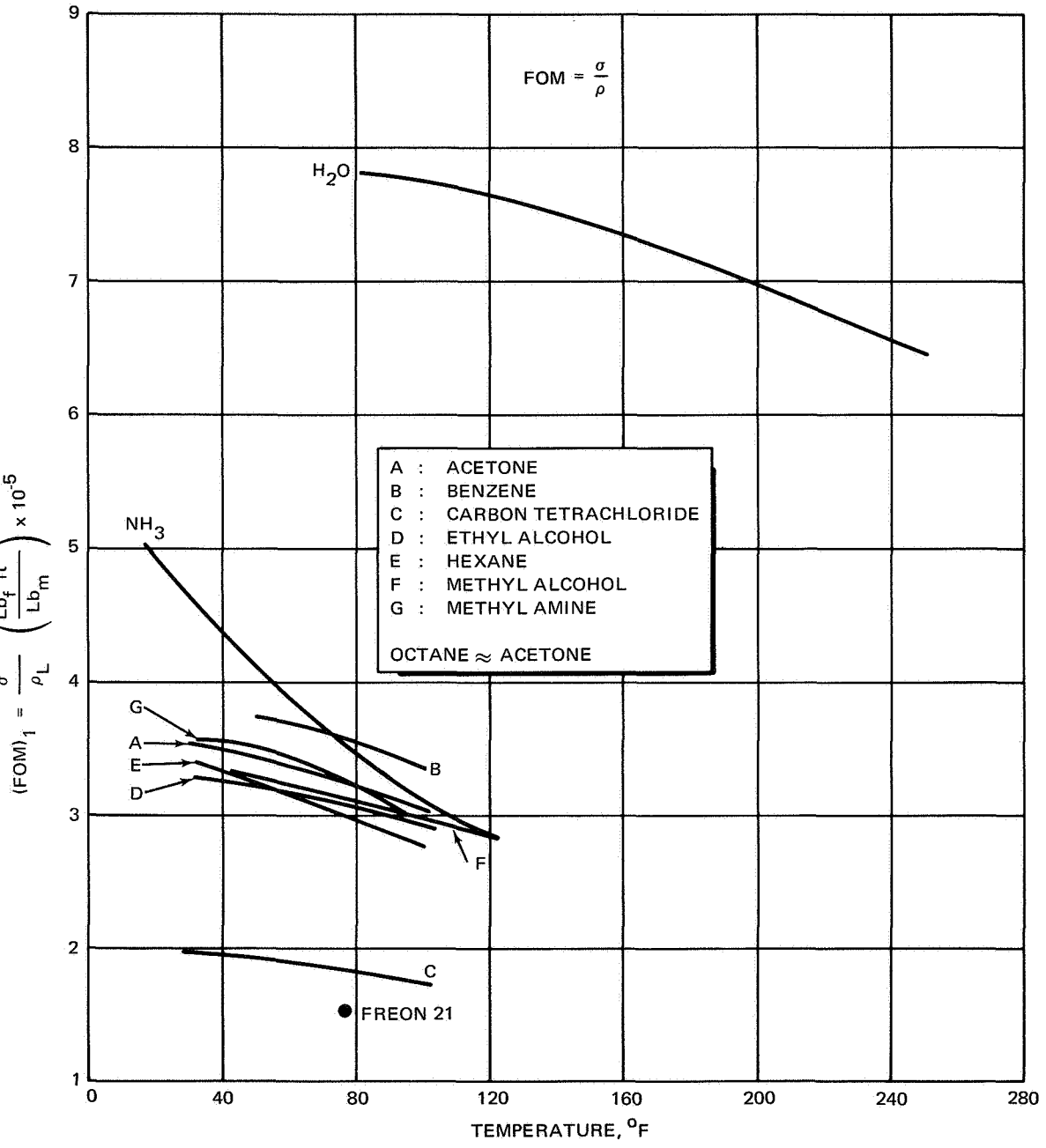

Figure 48. One-G Figure of Merit

0.0022 in. is obtained for 200 mesh stainless steel screen. From table 4 for a meniscus radius of 0.0022 in. for a single layer of 200 mesh screen, a value of R between 14 and 17 x 10^{12} ft^{-3} is obtained. An arithmetic average between the values for infinite radius and r = 0.0022 in. is approximately (4.4 + 15.5)/2 x 10^{12} = 9.9 x 10^{12} ft^{-3}. Therefore, a value of R = 9.9 x 10^{12} ft^{-3} or $1/K_p$ = 9.9 x 10^{12} (0.0049) /12 ft^{-2} would be used in equations (17) or (18) to determine the maximum axial heat flux for a single layer of 200 mesh screen.

Comparison of various wicks. - From equation 17, it can be seen that in the selection of a wick for a zero-g application, the most important parameter is the ratio, K_p/r_c. This quantity is shown in table 10 for wicks that have been tested on this program and by Kunz. The most desirable wicks of those tested appear to be the foam wicks tested by DWDL and the felt wicks tested by Kunz et al.

Maximum radial heat flux prediction. - Information contained in the previous section will permit design of a heat pipe in the absence of nucleate boiling. Vapor formation in the wick may change its permeability or even the effective capillary radius (for a liquid bypass wick configuration).

Data obtained during this program on maximum evaporator heat flux is most applicable for wicks that contain arteries. A summary of the maximum evaporative heat flux limits for various wick-fluid combinations at various temperatures is shown in table 8. A range of heat fluxes is shown for each condition. This range reflects the high sensitivity of wick conditioning on evaporative heat flux burnout. Evidences of the effect of surface conditioning observed in these experiments were changes in heat flux due to chemical cleaning, replacement of working fluid, and degassing of surface cavities with time. The maximum value represents a potentially realizable value which can be achieved with proper wick conditioning, although the exact requirement is still undefined.

Even though the data are most applicable for wicks using arteries, a similar burnout mechanism would occur for nonarterial wick configurations; that is, once incipient nucleate boiling occurs, the wick is susceptible to blockage. Thus, the values contained in table 4 should give an indication of the radial heat flux limitation of an isotropic wick configuration.

Compatibility information. - A crucial consideration in heat pipe design--one which may be the determining factor in the selection of fluid and container materials--is the mutual compatibility of these materials. For example, from its figure-of-merit values, water appears to be a desirable candidate, but generation of H_2 gas in the presence of aluminum and stainless steel has been observed by DWDL and others. Additional research is necessary on the purity or surface preparation required to prevent such reactions. In any event, thorough investigations of compatibility should be undertaken before a final design is fixed.

TABLE 10

COMPARISON OF K_p/r_c FOR VARIOUS WICKS

(Based on tests with water)

Wick	Experimenter	Porosity	K_p ft^2	r_c ft	K_p/r_c ft
Nickel sintered powder (M2)	Kunz	0.658	0.294×10^{-8}	0.20×10^{-3}	1.47×10^{-5}
Nickel sintered powder (M6)	Kunz	0.696	0.323×10^{-8}	0.27×10^{-3}	1.20×10^{-5}
AmPorCop 210-5 (foam)	DWDL	0.945	2.17×10^{-8}	0.75×10^{-3}	2.89×10^{-5}
AmPorCop 220-5 (foam)	DWDL	0.912	2.50×10^{-8}	0.79×10^{-3}	3.16×10^{-5}
AmPorNik 210-5 (foam)	DWDL	0.944	2.94×10^{-8}	0.75×10^{-3}	3.92×10^{-5}
AmPorNik 220-5 (foam)	DWDL	0.960	4.00×10^{-8}	0.75×10^{-3}	5.33×10^{-5}
Copper felt	DWDL	0.895	1.33×10^{-8}	0.75×10^{-3}	1.77×10^{-5}
Nickel felt	DWDL	0.891	0.556×10^{-8}	0.54×10^{-3}	1.03×10^{-5}
Nickel felt (H1)	Kunz	0.868	0.0472×10^{-8}	$<0.12\times10^{-3}$	$>0.39\times10^{-5}$
Nickel felt (H3)	Kunz	0.689	0.0163×10^{-8}	$<0.12\times10^{-3}$	$>0.14\times10^{-5}$
Nickel felt (H11)	Kunz	0.916	0.588×10^{-8}	0.31×10^{-3}	1.90×10^{-5}
Nickel felt (H13)	Kunz	0.822	1.25×10^{-8}	0.36×10^{-3}	3.47×10^{-5}
50 mesh nickel screen (M7)	Kunz	0.625	0.714×10^{-8}	1.00×10^{-3}	0.71×10^{-5}
100 mesh nickel screen (M8)	Kunz	0.679	0.164×10^{-8}	$<0.43\times10^{-3}$	$>0.38\times10^{-5}$
200 mesh nickel screen (M10)	Kunz	0.676	0.083×10^{-8}	0.21×10^{-3}	$>0.40\times10^{-5}$
200 mesh 1 layer (methanol test) ss screen	DWDL	-	0.056×10^{-8}	0.19×10^{-3}	0.29×10^{-5}

Considerations in Designing a Heat Pipe

The following is a summary of some of the factors which must be considered in designing a heat pipe.

Selection of container configuration. - A decision must be made as to whether a heat-pipe-fin or vapor chamber arrangement (an evacuated chamber lined with a wick and loaded with working fluid) should be used. In general, a vapor chamber is more isothermal than a multiple heat pipe and fin system. But reliability of a heat pipe system is significantly greater because a single leak (for example, a meteoroid puncture) can render a vapor chamber inoperative, whereas temperature distribution in a heat pipe system is only slightly degraded. The ease of fabrication of a particular configuration should also be considered.

Selection of container material. - Four factors are important in the selection of a container material:

1. Weight
2. Thermal conductivity
3. Compatibility with working fluid
4. Strength

The relative importance of these factors may vary for different applications. For example, if the vapor pressure of working fluid is low and the heat pipe does not have to act as a structural member, strength would be a minor consideration.

Selection of wick configuration. - The two most important factors in selecting a wick configuration are the required thermal performance and the required stability in a gravity field. For large axial heat flux in space, an artery configuration would probably be most desirable. If the heat pipe must be able to operate in a gravity field, however, an artery may not refill and an isotropic wick pipe may be the optimum design. The particular wicking material used will be determined by information such as is contained in table 10.

Selection of working fluid. - The selection should be based on information discussed previously and summarized as follows:

- Required heat transfer performance.
- Required operation in a gravity field.
- Compatibility.
- Required temperature range.

CONCLUSIONS AND RECOMMENDATIONS

The design of low-temperature heat pipes requires detailed data regarding wick permeability, capillary pore radius, and burnout heat flux. In addition, FOM data for the candidate working fluids are required in order to select appropriate fluids in the temperature range of interest.

Permeability, effective capillary pore radius, and burnout heat flux data applicable to low-temperature heat pipes were obtained experimentally for a number of wick-fluid combinations. Testing techniques and procedures which can be used to generate data appropriate for low-temperature heat pipe design were developed. Physical property data for a large number of working fluids was obtained from the literature and used to calculate FOM's.

Design Data

The transfer of heat in a heat pipe is limited by maximum axial heat flow and maximum radial heat flux. For low-temperature heat pipes, the most important limitation on maximum axial heat flow is the capillary pumping limit. This limit is a function of fluid properties and wick properties. The effect of fluid properties on maximum axial heat flow is given by either $(FOM)_0$ or $(FOM)_1$. $(FOM)_0$ is used for a zero-g application and $(FOM)_1$ is used for a 1-g application. Thus, a comparison of fluids for a particular application can be made by using the figure-of-merit data plotted in figures 47 and 48.

The effect of wick properties on maximum axial heat flow may be ascertained by considering the ratio of the permeability to the effective capillary pore radius, K_p/r_c, as well as the effective capillary pore radius itself. Consideration of K_p/r_c is adequate for heat pipe operation in a zero-g application, but both K_p/r_c and r_c must be considered for 1-g applications. The larger the value of K_p/r_c and the smaller the value of r_c, the greater the maximum heat transfer will be. In general, from the standpoint of K_p/r_c, foam wicks are most desirable, felts rank second, and screens are least desirable for the wicks tested in this program. The 200-mesh screen exhibited the smallest value of r_c of any of the wicks tested.

Experiments to measure the maximum radial heat flux that a wick can withstand before drying out indicate that water as a working fluid will withstand larger radial heat fluxes than methanol or butanol, with methanol being slightly better than butanol. In addition, felt wicks were found to sustain a larger radial heat flux than the foam wicks. The felts were less porous than the foams and so had a higher effective thermal conductivity when filled with the test fluid; it is desirable to use a wick which has a high effective thermal conductivity in order to increase the maximum radial heat flux.

Experimental Test Procedures

Values of r_c were obtained in the environment of the working fluid vapor and in air. Data tabulated in table 3 indicate that there is no significant difference between the data obtained from the two test procedures. Testing in air, however, is much simpler.

Three techniques for determining permeability were employed during the program. Relatively thick wicks were tested using a standard forced-flow permeability technique. These tests yielded information on thick wicks applicable to heat pipe design. In order to minimize wall effects, thin wicks were tested using a gravity flow technique. Meniscus recession and corner flow were found to have a significant effect on the measured permeability values. This test procedure is significantly more difficult than the forced flow permeability technique, but useful design data for thin wicks and the effect of meniscus recession were obtained once corner-flow effects were eliminated. Problems encountered with the pressure-sensing equipment used on the condenser flow test apparatus were never satisfactorily solved. As a result, permeability data obtained by this method is considered too costly and of questionable value in heat pipe design.

The maximum evaporator flux for several wicks fed by an artery was determined. Burnout was caused by vapor generation with subsequent blockage of the artery. Thus, an artery is susceptible to vapor blockage, and proper consideration must be given to this in heat pipe design. The maximum evaporative heat flux was found to be a very sensitive function of the amount of subcooling and the operating temperature. Therefore, it is imperative that evaporative heat flux tests be conducted only under the vapor of the fluid--not open to the atmosphere. It was observed that the maximum evaporative heat flux is a very sensitive function of wick conditioning. Further investigation of the effect of conditioning time and wick preparation is required in order to determine the effect on burnout flux limits.

An integrated thermal management system for a spacecraft will be made up of a variety of heat pipe configurations--each designed to perform a specific task in an optimum manner. Thermal problems for a single spacecraft can vary considerably. Such scientific areas as optical and electronic systems require not only isothermal surfaces, but temperature control as well. Other systems such as fuel cells will exhibit very high heat flux sources. Thermal distribution of solar loads generally requires heat pipes that can operate over very long distances. The successful uses of heat pipes can be realized if an orderly sequence of events is followed.

The events recommended are presented in a three-phase program: The first phase consists of acquiring the heat pipe operating data necessary for use in analytical prediction of heat pipe performance. Such data are essentially contained in this report for a limited combination of wicks and fluids.

The second phase consists of identifying the important operating characteristics of the heat pipe; and developing operation data pertinent to tradeoff considerations necessary for evaluation of the merits of a heat pipe system vs other thermal control techniques for a given problem. Such characteristics as the degree of isothermal operation attainable, and maximum heat transfer and heat pipe weight for varying operating temperature/fluid combinations should be quantified and displayed parametrically for use by the designer. Other characteristics such as radial flux and temperature control using inert gas pressure-sensitive systems for variable conductance design will also be useful.

The third and final phase is systems definition and integration of the heat pipe subsystem into a given spacecraft. This phase occurs when a specific program is identified as having a thermal environment that is unacceptable by passive means without employing some control technique.

In summary, design of a fully integrated heat pipe thermal management system for space vehicles involves a three-phase program of which the actual system design is the third phase. The program just completed is essentially the first phase--generation of basic low-temperature heat pipe data.

The second phase should be planned and initiated to provide design curves derived from the fabrication and testing of heat pipe configurations considered useful for spacecraft applications.

Donald W. Douglas Laboratories,
McDonnell Douglas Astronautics Company - Western Division,
Richland, Washington 99352, June 19, 1969.

Appendix A
CORNER FLOW PHENOMENA IN GRAVITY FLOW TESTS

The anomalies in the values of K_p, obtained using the gravity-flow test apparatus, are attributed to a corner flow phenomenon which is physically observable; this led to the addition of nonwetting Teflon-coated walls. In this appendix, corner flow will be treated in detail, and explanations of discrepancies observed in the data will be presented.

Determination of Height to Which a Liquid Can Rise on a Wetted Wall

The height to which a liquid will rise on a wetted wall is derived by Ferrell and Carnesale (ref. 28). The assumed model is depicted in figure A-1. The differential equation describing the pressure at the liquid surface at position, x, is

$$\frac{g}{g_c}\,\rho y(x) = \frac{\sigma}{r(x)} = \sigma\frac{d^2y/dx^2}{\left[1 + (dy/dx)^2\right]^{3/2}} \qquad \text{(A1)}$$

If a parameter γ is defined as

$$\gamma = 1/2\ g/g_c\ \rho/\sigma$$

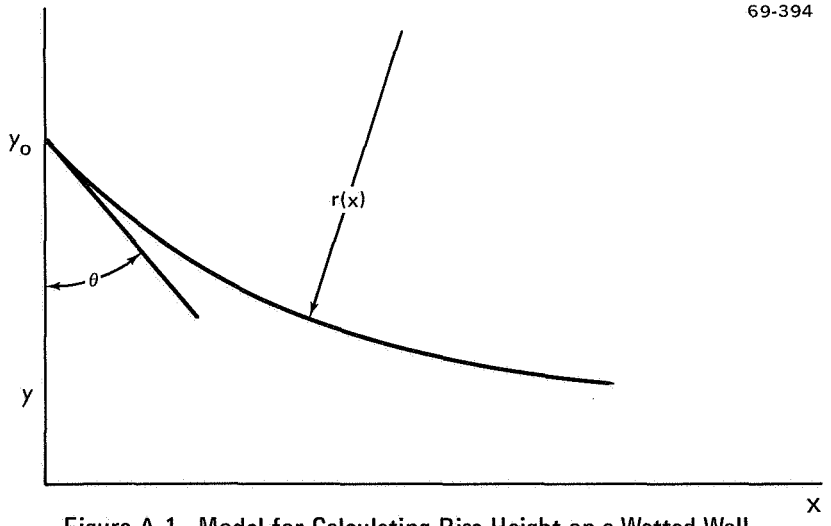

Figure A-1. Model for Calculating Rise Height on a Wetted Wall

the differential equation becomes

$$2\gamma y = \frac{d^2 y/dx^2}{\left[1 + (dy/dx)^2\right]^{3/2}} \tag{A2}$$

Let $\nearrow = dy/dx$, and equation (A2) becomes

$$2\gamma y\, dy = \frac{\nearrow d\nearrow}{\left[1 + \nearrow^2\right]^{3/2}} \tag{A3}$$

Equation (A3) may be integrated, recalling that $\nearrow = 0$ at $y = 0$. This integration yields

$$\gamma y^2 = 1 - \frac{1}{\sqrt{1 + \nearrow^2}} \tag{A4}$$

Equation (A4) may be solved for $\nearrow$, and by referring to figure A-1 for $x = 0$, the following equation may be written:

$$\nearrow_o = (dy/dx)_{x=0} = -\frac{\sqrt{\gamma}\, y_o}{(1 - \gamma y_o^2)} \sqrt{2 - \gamma y_o^2} = -\cot\theta \tag{A5}$$

Equation (A5), when solved for y_o, yields

$$y_o = \sqrt{\frac{1 - \sin\theta}{\gamma}} \tag{A6}$$

The value of γ for methanol at 75°F is 16 100 ft^{-2}. Thus, the value of $1/\sqrt{\gamma}$ in inches is

$$\frac{1}{\sqrt{\gamma}} = 0.095 \text{ in.}$$

The variation of y_o with contact angle for methanol is shown in table A-1.

Thus, for a contact angle of $\theta = 0$, the liquid will rise to a height of almost 0.100 in.; this is consistent with visual observations. Even for a contact angle of 45°, the height is still about 0.050 in. In the next paragraphs, it will be shown that 0.050 in. is a large enough rise to cause a significant error.

TABLE A-1

VARIATION OF LIQUID RISE HEIGHT WITH CONTACT ANGLE FOR METHANOL

θ	y_o(in.)
0	0.095
10	0.086
20	0.077
30	0.067
40	0.057
45	0.051
50	0.046
60	0.035
70	0.023
80	0.012
90	0

Effect of Flow in Corners on Determination of $\frac{1}{K_p}$

The effect of flow in the corner between the wick and the adjacent sidewall is a significant source of error in determining values of permeability, K_p, for thin wicks. The situation is depicted in figure A-2.

Flow can occur in either of two parallel paths: in the corner, or through the wick. The size of the fillet required to cause the observed difference between values of K_p for wetted and nonwetted sidewalls is not very large.

An expression for the pressure drop vs flow for a corner flow can be obtained by using the general statement of Poiseuilles law for flow in a pipe:

$$\frac{\Delta P}{\ell} = \frac{32\ \nu_L \dot{m}}{D_H^2\ Ag_c} \qquad \text{(A7)}$$

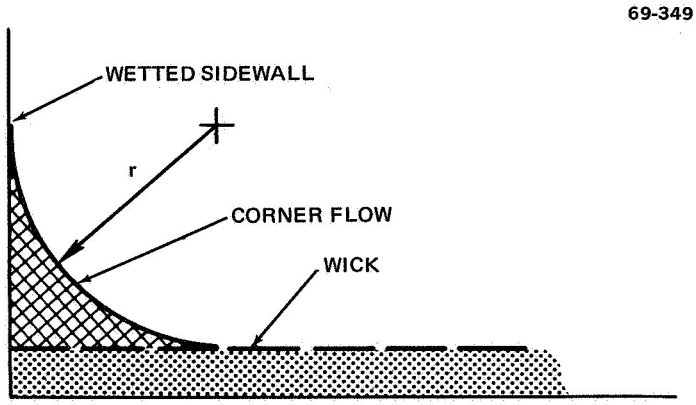

Figure A-2. Corner Flow with Wetted Sidewalls

where

D_H = hydraulic diameter = 4A/P

A = flow area

P = wetted perimeter

ν_L = kinematic viscosity

$\dot{m}$ = mass flow

$\Delta P/\ell$ = pressure gradient causing flow

g_c = universal gravitational constant

Referring to figure A-2, the values of A and P are

$$A = r(1 - \pi/4) = 0.215r^2 \tag{A8}$$

$$P = 2r \tag{A9}$$

where θ is assumed to be equal to zero, and r is equal to y_o. Thus,

$$D_H = \frac{4A}{P} = \frac{4(0.215)r^2}{2r} = 0.430r \tag{A10}$$

Permeability is defined as

$$K_p = \frac{\nu_L \dot{m}}{A(\Delta P/\ell)g_c} \tag{A11}$$

Combining equations (A7), (A10), and (A11),

$$K_{p_{corner}} = \frac{D_H^2}{32} = \frac{r^2}{173} \tag{A12}$$

For parallel flow paths, the overall flow conductance will be the sum of the individual conductances:

$$2(K_pA)_{corner} + (K_pA)_{wick} = (K_pA)_{total} \tag{A13}$$

Substituting equations (A8) and (A12) into (A13),

$$r^4 = 403 \left[(K_pA)_{total} - (K_pA)_{wick}\right] \tag{A14}$$

Note that since the value of K_p for the tests with wetted sidewalls was based on the area of the wick alone, $(K_pA)_{total}$ is just the value of K_p presented in figures 17, 18, 19, and 21, multiplied by A_{wick}. Since data are available for the same wicks tested in the apparatus with wettable walls and in the modified apparatus using nonwetting Teflon-coated walls, the value of r required to account for the discrepancies in the data can be calculated.

Calculations for both the screen and thicker porous metal wicks are presented in succeeding paragraphs.

Screen wick. - Typical values of $1/K_{pwetted}$ and $1/K_{pnonwetted}$ may be obtained from figures 18 and 19 for 1 layer of 200 mesh screen by multiplying R values by thickness. If values of $(1/K_p)_{wetted} = 0.4 \times 10^8$ ft^{-2} and $(1/K_p)_{nonwetted} = 15 \times 10^8$ ft^{-2} are used with the cross-sectional area of the wick approximately 0.005 in.^{2}, a value of r is obtained:

$$r = 0.048 \text{ in.} \tag{A15}$$

Thus, a radius of less than 1/16 in. would be enough to cause the observed differences between the tests with wetted and nonwetted walls for a screen wick.

Foam wick. - The gravity flow tests were conducted with the wetted wall present; the forced-flow tests were characteristic of the nonwetted wall, since there was no free surface present, and thus no fillet could be formed.

Therefore, if the values of $1/K_p$ from table 5 for AmPorCop 210-5 for both tests at a flow of 20×10^3 lb$_m$/hr-ft^2 are substituted into equation (A8).

$$\frac{r^4}{403} = \left(\frac{1}{0.19} - \frac{1}{0.46}\right) \times 10^{-8} \qquad \text{(A16)}$$

Therefore,

$$r = 8.25 \times 10^{-3} \text{ ft} = 0.10 \text{ in.}$$

A fillet of 0.1 in. radius will be enough to cause the observed discrepancies in the data. As was previously mentioned, a fluid rise of approximately 1/8 in. on the wetted walls was observed for some of the gravity flow tests. Such a rise has been shown to be reasonable. Thus, the flow in the corners for the wetted wall gravity flow test could cause the observed discrepancies.

Instability of Corner Flow

In some of the gravity flow tests with wetted walls, flow actually decreased as the slope angle increased, indicating a decrease in permeability. This may have been caused by one of two factors: during the change of slope angle, some gas may have been trapped in the wick; or the flow area of the fillet may have changed during the change of slope angle.

Caution was exercised to prevent the first factor from occurring by flooding the wick with an excess of liquid before the angle was changed, although blockage could have occurred in spite of such precautions.

The second factor may have occurred even though the flow area of the porous wick material did not appreciably change. A systematic decrease in the fillet cross-sectional flow area and a corresponding decrease in $(K_pA)_{total}$ takes place as the inclination angle is increased. This situation is depicted in figure A-3, where y_o is the height above the surface of the meniscus as calculated earlier in this appendix, and r is the radius of the fillet. If y_o is only a function of σ, ρ, and contact angle θ, r will decrease as α increases. This will cause a systematic increase in $1/K_p$.

This effect, however, does not explain the erratic behavior of the permeability data. Sudden changes in the fillet cross-sectional area, unassociated with change in α, are possible and could cause the behavior indicated by the data. Such a situation is depicted in figures A-4 and A-5. The situation depicted in figure A-4 has a relatively large-flow fillet, and the stable flow will be given by equation (A1) with $\rho g/g_c \sin \alpha = \Delta P/\Delta \ell$ and with the conductances, AK_p, added for parallel flows,

$$\dot{m} = \frac{\rho_g \sin\alpha}{\nu_L}\left[A_w K_{p_w} + 2(AK_p)_{corner}\right] \qquad \text{(A17)}$$

69-391

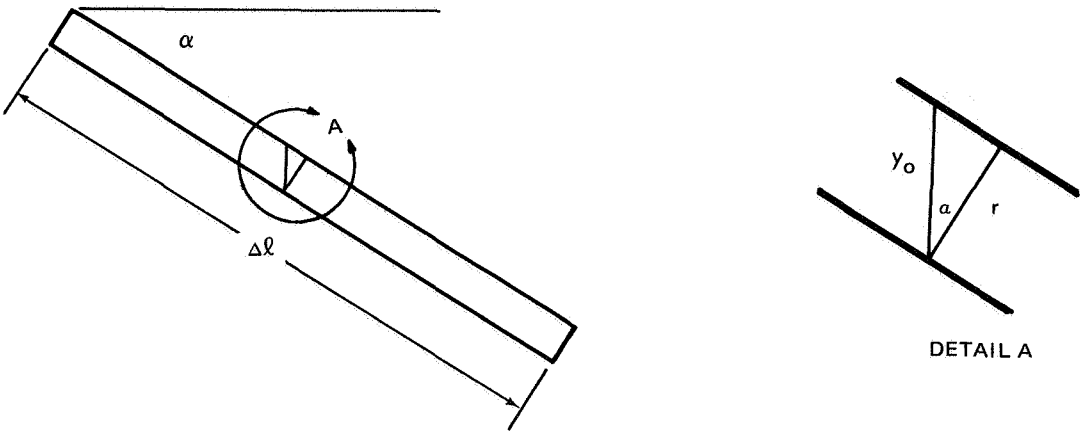

Figure A-3. Flow Angle Affect

69-392

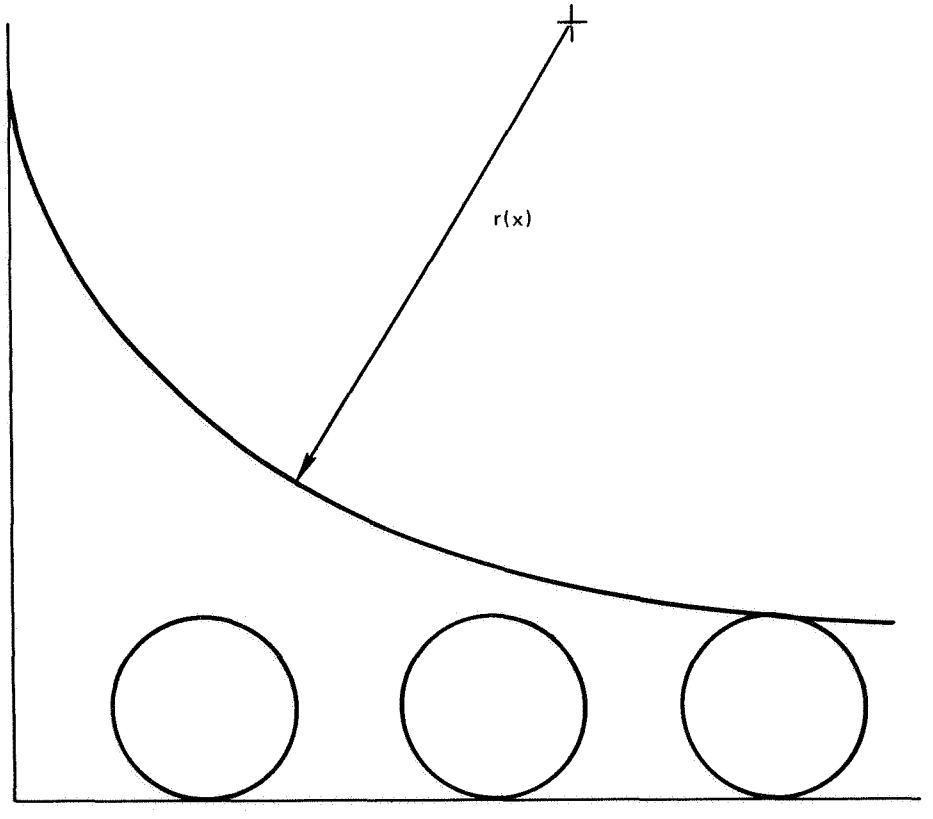

Figure A-4. Full Corner Meniscus

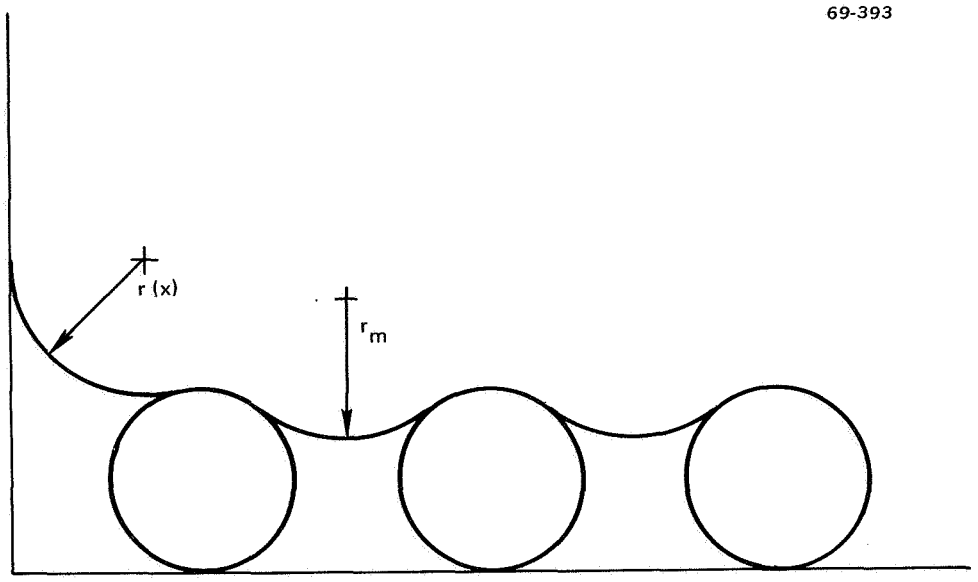

Figure A-5. Receded Corner Meniscus

But from the equation for the conductance of corner flow as a function of radius [equations (A8) and(A12)], the following expression is obtained:

$$\dot{m} = \frac{\rho_g \sin \alpha}{\nu_L} \left(A_w K_{p_w} + \frac{r^4}{403} \right) \tag{A18}$$

As has been demonstrated, effective conductance for the corner flow may be a great deal larger than that for the wick. Thus, the value of $\dot{m}$ for uniform flow (uniform pressure along the wick) may be a very strong function of r.

The value of r(x) is a function of r_m which, in figure A-3, is infinity. The value of r(x) must always be less than r_m, and it will increase as the distance from the wall increases; a change from the situation depicted in figure A-3 to that depicted in figure A-4 could occur if the flow is not properly adjusted. If the liquid level is allowed to recede below the surface of the wick, the fillet will drain until r(x) is again less than r_m. Thus, the erratic variation in the values of $1/K_p$ for the gravity-flow-wetted wall tests may be explained by a variation in r(x) as the slope angle is changed and the flow is readjusted.

Appendix B

WICK BONDING TECHNIQUES AND MANUFACTURERS

Vacuum Sintering of Wick Materials to Plate Substrates

A series of nickel foam, nickel felt, and copper foam wick materials were vacuum-sintered to plate substrates to determine temperatures and area loadings for obtaining satisfactory sintered bonds between the two members. Nickel felt, nickel foam, and copper foam had apparent densities of 10.9%, 5.6%, and 2.5% respectively. Results of these tests are listed in table B-1, and were used as a temperature-area loading guide for sintering wicks used in the gravity flow permeability and evaporator heat flux tests.

TABLE B-1
VACUUM SINTERING TESTS

Material	Substrate	Area loading (psi)	Temp (°F)	Time (minutes)	Bulk density increase (%)	Sintered bond strength
100 mesh stainless steel screen	Stainless steel	1.19	2250	30	0	Wick bulk
200 mesh stainless steel screen	Stainless steel	1.19	2250	30	0	Wick bulk
Ni foam	Stainless steel	0.124	2200	10	3	>Wick bulk
Ni foam	Stainless steel	0.124	1975	10	2	<Wick bulk
Ni felt	Stainless steel	0.124	2200	10	2	>Wick bulk
Ni felt	Stainless steel	0.124	1975	10	0	<Wick bulk
Cu foam	Cu	0.114	1750	10	0	>Bulk

The temperatures chosen were approximately 0.85 of the absolute melting point for rapid sintering, and specimens sintered at these temperatures--2200°F for nickel and 1750°F for copper--developed strong sintered bonds to the base plates. One specimen of nickel foam and one of nickel felt were sintered at 1975° ± 25°F. The area loadings and times were kept constant and the resultant sintered bonds with the base plates were satisfactory but less than the bulk strength of the wick materials.

The following list identifies the manufacturers of porous metals used for the DWDL tests.

Metal foams:

Astro Met Associates, Inc.
95 Barron Drive
Cincinnati, Ohio 45215

Clevite Corporation
Aerospace Division
540 E. 105
Cleveland, Ohio 44108

General Electric Co.
Metallurgical Products Dept.
Box 237, General Post Office
Detroit, Michigan 48238

Union Carbide Corporation
12900 Snow Road
Parma, Ohio

Metal felts:

Astro Met Associates, Inc.
95 Barron Drive
Cincinnati, Ohio 45215

Huyck Metals Company
45 Woodmont Road
Milford, Connecticut 06460

REFERENCES

1. Grover, G. M.; Cotter, T. P.; and Erickson, G. F.: Structures of Very High Thermal Conductance. J. Appl. Phys., Jun. 1964.

2. Cotter, T. P.: Theory of Heat Pipes. LA 3246 - MS(TID-4500) Mar. 26, 1965.

3. Cotter, T. P.: Heat Pipe Startup Dynamics. Proc. Thermionic Conversion Specialists Conference, Palo Alto, California. Oct. 30 - Nov. 1, 1967.

4. Levy, E. K.: Theoretical Investigation of Heat Pipes Operating at Low Vapor Pressures. Proc. ASME Aviation and Space Conference, Beverly Hills, California. Jun. 16 - 19, 1968.

5. Kemme, J. E.: High Performance Heat Pipes. Proc. Thermionic Conversion Specialists Conference, Palo Alto California. Oct. 30 - Nov. 1, 1967.

6. Bähr, A.; Burck, E.; and Hufschmidt, W.: Liquid Vapor Interaction and Evaporation in Heat Pipes. Proc. Second Int. Conf. on Thermionic Electric Power Generation, Stresa, 1968.

7. Costello, C. P.; and Redecker, E. R.: Boiling Heat Transfer and Maximum Heat Flux for a Surface with Coolant Supplied by Capillary Wicking. Chem. Engr. Progress Symp. Series, No. 41, 59, 1963. pp. 104-113.

8. Costello, C. P.; and Frea, W. J.: The Role of Capillary Wicking and Surface Deposits in the Attainment of High Pool Boiling Burnout Heat Fluxes. AIChE Journal, May 1964. pp. 393-398.

9. Reiss, F.; and Schretzmann, K.: Pressure Balance and Maximum Power Density at the Evaporation Gained from Heat Pipe Experiments. Proc. Second Internation Conference on Thermionic Electrical Power Generation, Stresa, 1968.

10. Kunz, H. R.; Langston, L. S.; Hilton, B. H.; Wyde, S. S.; and Nashick, G. H.: Vapor Chamber Fin Studies - Transport Properties and Boiling Characteristics of Wicks. NASA CR-812.

11. Van Stralen, S. J. D.: The Mechanism of Nucleate Boiling in Pure Liquids and in Binary Mixtures - Part IV Surface Boiling. Int. J. Heat & Mass Transfer, Vol. 10, pp. 1485-1498.

12. Cole, R.; and Shulman, H. L.: Bubble Departure Diameters at Subatmospheric Pressures. AIChE Chemical Engineering Progress Symp. Series (Los Angeles). No. 64, Vol. 62, 1966.

13. Schmidt, E.: Determination de la Perte de Charge dans des milieux Capillaires Susceptibles d'etre Utilizes dans des Caloducs. Centre d'Etudes Nucleaires de Grenoble, Note TT No. 265, 1967. (Summarized in Heat Pipe Research in Europe by C. A. Busse, Second International Conference on Thermionic Power Generation.)

14. Katzoff, S.: Heat Pipes and Vapor Chambers for Thermal Control of Spacecraft. AIAA Thermophysics Specialists Conference, New Orleans, Louisiana, Apr. 17-20, 1967.

15. Phillips, E. C.; and Holmgren, J. S.: Low Temperature Heat Pipe Research, DAC Report 60752P, Jul. 1968.

16. Anon.: Investigations of Foamed Metals for Launch and Space Vehicle Applications, Ipsen Industries, Inc., Rockford, Illinois, May 1966.

17. Anon.: Huyck Metals Company, Product Data Bulletins Series FM 300 and Series FM 400.

18. Scheidegger, A. E.: The Physics of Flow Through Porous Media. Revised Edition, Univ. of Toronto Press, 1960.

19. Bergles, A. E.; and Rohsenow, W. M.: The Determination of Forced-Convection Surface - Boiling Heat Transfer. Transactions of the ASME, Paper No. 63-HT-22, 1963.

20. Hall, I. S.; and Hatton, A. P.: The Influence of Surface Roughness and a Wetting Additive on Pool Boiling on Horizontal Rods. Proc. Inst. Mech. Engrs., Vol. 180, Pt 3c, p. 160, 1965-66.

21. Grant, I. D. R.; and Patten, T. D.: Thickness of the Thermal Layer at the Initiation of Nucleate Pool Boiling. Proc. Inst. Mech. Engrs. Vol. 180 Pt 3c, 1965-66.

22. Jakob, M.: Heat Transfer, Vol. I, John Wiley & Sons, 1964.

23. Katto, Y.; and Masuoka, T.: Criterion for the Onset of Convective Flow in a Fluid in a Porous Medium, Int. J. Heat Mass Transfer, Vol. 10, pp. 297-309, 1967.

24. Corty, C.; and Foust, A. S.: Surface Variables in Nucleate Boiling, Chem. Eng. Progress Sym. Series, Vol. 51, No. 17, p. 1 (1955).

25. Busse, C. A.: Pressure Drop in the Vapor Phase of Long Heat Pipes. Proc. Thermionic Conversion Specialist Conference. Oct. 30 - Nov. 1, 1967, Palo Alto, California.

26. Van Andel, E.: Heat Pipe Design Theory. Proc. Second Int. Conf. on Thermionic Electrical Power Generation, Stresa, 1968.

27. Ernst, D. M.: Evaluation of Theoretical Heat Pipe Performance Proc. Thermionic Conversion Specialists Conference, Palo Alto, California. Oct. 30 - Nov. 1, 1967.

28. Ferrell, J. K.; and Carnesale, A.: A Study of the Operating Characteristics of the Heat Pipe. Sixth Quarterly Progress Report USAEC Contract AT-(40-1) - 3411.